ஸ்ரீ சிவுவாச்சூர் மயூரகாளியம்மன் துணை சுவாமியே சரணம் ஐயப்பா வெற்றிவேல்முருகனுக்கு அரோகரா

Effects of interaction and topology in some condensed matter systems

A thesis submitted to the
Indian Institute of Technology Gandhinagar
for the award of the degree of

Doctor of Philosophy

by

Bharathiganesh D.
(Roll No. 19330005)

Under the guidance of

Prof. Navinder Singh
Professor
Theoretical Physics Division
Physical Research Laboratory, Ahmedabad, India

Department of Physics
Indian Institute of Technology Gandhinagar, India

August 2024

Dedicated to,

Amma, Appa, Athai and all others who have helped me all along.

Also to karrupar, kutti vellai, Periyavar, chinna anil, chinnavar and all others!

Department of Physics
Indian Institute of Technology Gandhinagar
Palaj, Gandhinagar, 382055, Gujarat, India

APPROVAL OF THE DOCTORAL STUDENT COMMITTEE

Date: 10/06/2025

Certified that the thesis entitled "**Effects of Interaction and Topology in some Condensed Matter Systems**", can be submitted by **Bharathiganesh D.** to the **Indian Institute of Technology Gandhinagar**, for the award of the degree of *Doctor of Philosophy*. The student has successfully presented his pre-thesis seminar on 19/07/2024.

Dr. Ketan Patel (Member, DSC) Assistant Professor Theoretical Physics Division PRL Ahmedabad	**Dr. Paramita Dutta** (Member, DSC) Assistant Professor Theoretical Physics Division PRL Ahmedabad	**Dr. K Durga Prasad** (Member, DSC) Assistant Professor Planetary Sciences Division PRL Ahmedabad

Prof. Navinder Singh
(Supervisor)
Professor
Theoretical Physics Division
PRL Ahmedabad

CERTIFICATE

This is to certify that the thesis entitled "**Effects of Interaction and Topology in some Condensed Matter Systems**", submitted by **Bharathiganesh D.** to **Indian Institute of Technology Gandhinagar**, is a record of bona fide research work under my supervision and guidance, and I consider it worthy of consideration for the award of the degree of *Doctor of Philosophy* of the Institute.

Date:
Place:

Prof. Navinder Singh
Professor
Theoretical Physics Division
Physical Research Laboratory Ahmedabad
Gujarat, India

DECLARATION

I certify that

a. the work contained in the thesis is original and has been done by myself under the general supervision of my supervisor.

b. the work has not been submitted to any other institute for any degree or diploma.

c. I have followed the guidelines provided by the institute in writing the thesis.

d. I have conformed to the norms and guidelines given in the ethical code of conduct of the institute.

e. Whenever I have used materials (data, theoretical analysis, and text) from other sources, I have given due credit to them by citing them in the text of the thesis and giving their details in the references.

f. Whenever I have quoted written materials from other sources, I have put them under quotation marks and given due credit to the sources by citing them and giving required details in the references.

Date:
Place:

Bharathiganesh D.
Roll No.: 19330005

Acknowledgments

"Sadāśiva samārambhām, śankarāchārya madhhyamām, asmad ācārya paryantam, vande guru paramparām!"

There has been a lot of support from various known and unknown sources that has helped me in the course of my PhD. First and foremost, I should thank my father and mother along with my aunt for supporting me in my choice to pursue a PhD and all the challenges there after.

I should thank my supervisor Prof. Navinder Singh for making my PhD experience not just joyful and memorable but more importantly making me learn to work in active research areas of condensed matter physics. He also supported me to grow independently and not to be afraid of failures that one may encounter in research.

I should thank Dr. Paramita Dutta for supporting me like her own student and helping me each time without a bit of hesitation. I should thank my other DSC members, Dr. Ketan Patel and Dr. Durga Prasad too for helping me out in all times of need. Especially Dr. Ketan Patel who kept me informed and prepared to face all the deadlines related to PhD. Special thanks also to Prof. Hiranmaya Mishra who was in my DSC before he retired from PRL. My deepest gratitude to Prof. Dilip Angom for his unmatched teaching of Statistical Mechanics. I consider it as an honor to be be able to attend his lectures.

Thanks also to Prof. Namit Mahajan and Prof. Shrubabati Goswami for helping me with moral support whenever I face some academic or non-academic issues.

I should thank Prof. T A Rajesh and Prof. Ramachandran for guiding me in my summer project.

I should also thank the amazing teachers from my school and college who have shaped my thinking and my interest overall. First and foremost I begin with Murugavel sir, whose extraordinary teaching of physics in high school motivated me to pursue physics further. I should also thank Jayajyothi sir for his unparalleled teaching of mathematics, which made my journey in theoretical physics comfortable. I should also thank Ankayarkanni madam, Sathheshkumar sir, Geethalatha madam, Gunasekaran sir, Jayashree madam, Geetha Srivatsava madam, Krishnambal madam, Sujata madam, Bhagirati madam, Shanmugam sir to name a few. Thanks also to Prof. Pawan Kumar and Prof. Saleem who always helped me in NIT Rourkela.

I should thank my colleagues Ritvik, Saurabh and Supriya for helping me out with things a daily basis and making my life smoother. I should also thank Jayashree madam for all her support in PRL. Thanks also to Ambareesh anna and his family for all their

love.

I should thank Dr. Nicolas Rougerie, for all his guidance and mentoring all along. I am deeply indebted for him, as he introduced me to this beautiful field of theoretical condensed matter physics.

Finally I recall the dakṣiṇāmūrtī stōtram by ādī śankarāchārya:

"viśvaṃ darpaṇa-dṛśyamāna-nagarī tulyaṃ nijāntargataṃ
paśyannātmani māyayā bahirivōdbhūtaṃ yathā nidrayā |
yassākṣātkurutē prabhōdhasamayē svātmānamē vādvayaṃ
tasmai śrīgurumūrtayē nama idaṃ śrī dakṣiṇāmūrtayē||"

where he says that all of the Creation is itself a mirror. My special thanks to that mirror which in the colloquial language is referred to as "Aaina" on whom my life has been a reflection.

hara hara śankara, jaya jaya śankara, Māhā Periyavā padamē śaranam!

Date:
Place:

Bharathiganesh D.
Roll No.: 18330023

***agnimīḷe purohitaṁ yajñasya devam ṛtvijaṁ hotāraṁ ratna dhātamam*||**
ṛg veda 1.1.1.

"I praise Agni, who is the Purohita of the yagna, who is a Deva, a Ritwik, a Hota and the bestower of wealth."

***adhyavōchadadhivaktā prathamō daivyō bhiṣak*|**
***ahīgścha sarvāmjambhayan-thsarvāścha yātudhānyaḥ* ||**
śri rudram, kṛṣṇa yajurvēdīya taittirīya saṃhitā

kūṭru āyinavāṟu vilakkagilīr; koḍumai pala seydana nān aṟiyēn; ēṭrāy aḍikkē iravum pagalum piriyādu vaṇaṅguvan eppoḷudum; tōṭrādu en vayiṭrin agambaḍiyē kuḍarōḍu tuḍakki muḍakki iḍa āṭrēn aḍiyēn, adigaik keḍila vīraṭṭānattu uṟai ammānē.
Tirunāvukkarasar tēvāram - padigam 4.1 - tiru adigai vīraṭṭānam

Abstract

One of the central goals of condensed matter physics is characterising different phases in which complex states of matter exists. These can be broadly classified as characterising different phases in the presence of interaction in the system and characterising the phases in the presence of non-trivial topology. The objective of the thesis is to study the effects of interaction and topology in two paradigmatic condensed matter systems, itinerant magnetism and Su-Schrieffer-Heeger (SSH) model like systems with dimerised hopping respectively. Accordingly, this thesis is divided into two parts, Part I and Part II, with the first part dealing with itinerant magnetism and correlation effects and the second part with topology, SSH model and its generalisations.

Part I deals with the Self-Consistent Renormalisation (SCR) theory of itinerant electron magnetism. It is one of the most accurate description of itinerant electron magnetism. It's remarkable success in explaining weak and nearly itinerant ferromagnets made it a litmus test to verify the itinerant nature of magnetism in a material. In the second chapter of the thesis, we discuss in detail this powerful formalism followed by a discussion on the algorithm of the numerical codes that we have developed to calculate the static susceptibility and Curie temperature using SCR theory.

$CaMn_2Al_{10}$ is a recently synthesised compound with several exotic features. According to the conventional wisdom based on the Mn-Mn distance in Mn based magnetic system, if the Mn-Mn distance is greater than 2.7 Å then the material should be a local magnet with a large magnetic moment. Intuitively this is understandable as larger Mn-Mn distance in real space means lower bandwidth in the momentum space leading to localisation of the electron in atomic sites. However $CaMn_2Al_{10}$ shows several signatures of itinerant magnetism even though Mn-Mn distance in this system is greater than the cut-off value of 2.7 Å. This makes it an excellent candidate to be studied through the lens of SCR theory and this study is discussed in the third chapter. We calculate the static susceptibility of $CaMn_2Al_{10}$ using the SCR theory and compare it with ex-

perimental data. We find that there is very good agreement between the theoretical calculations and experimental data. Based on the fit of theoretical calculation to experimental data, we extract the value of the Hubbard interaction parameter U to be 0.3136 eV. We use this value of U to perform DFT+U calculations to determine the reasons for the origin of itinerant magnetism in $CaMn_2Al_{10}$. We find that it is the strong hybridisation between Mn-3d and Al-3p orbitals that leads to itinerant magnetism in $CaMn_2Al_{10}$.

Part II deals with the topological aspects of condensed matter systems. The Su-Schrieffer-Heeger model is a paradigmatic model in one dimension that is simple in formulation but is conceptually rich. All the major principles in topological condensed matter like bulk invariants, boundary invariants, Bulk-Boundary correspondence can be understood via the SSH model. But as mentioned before it is very simple and thus the possibilities for newer phases in the conventional SSH model are low. We change the geometry of bulk in the SSH model with various one-dimensional and quasi-one-dimensional manifolds. This is not possible within the conventional SSH model. Hence, in chapter 4, we formulate the SSH model with two additional degrees of freedom and new set of rules that govern the hopping. With this more general version of the SSH model which we term the SSH model with any bulk or in short SAB model, we can study SSH like models with several non-trivial bulks. Some of these bulks have twists and branching in them bringing in new possibilities not possible in the conventional SSH model. We have studied the three band, four band and six band SAB models. All these models in some particular configuration called the "non-orientable" configuration, host a non-degenerate or doubly degenerate flat band exactly at the particle-hole symmetry level. We have calculated the eigenvalues and eigenvectors for these models with both periodic boundary conditions and open boundary conditions. We have also calculated topological invariants like Zak phase and number of zero energy edge states along with localisation measures like the inverse participation ratio (IPR). We have also given some plausible experimental platforms to realise different SAB models and verify our theoretical predictions.

When there are topological zero energy edge states in the system, they are generally robust to disorder and enjoy protection by symmetries of the system. However this may

not be true for the zero energy states that are localised in the bulk and arise due to the geometry of the lattice. In chapter 5 we verify the robustness of the zero energy states for chiral symmetry preserving and breaking disorders. We find that if the flat band is non-degenerate and the disorder is chiral symmetry preserving then the zero energy states are robust to large amount of disorders. However, when the flat band is doubly degenerate or the chiral symmetry is broken, the zero energy states disperse and acquire a finite bandwidth. They close the gap for a critical disorder strength indicating a localisation to delocalisation transition in the system at this critical disorder strength which is a very novel phenomenon.

Keywords — Itinerant magnetism , Hubbard model, Stoner model, RPA model, SCR theory, $CaMn_2Al_{10}$, SSH model, SAB model, Flat bands, chiral symmetry, disorder, Insulator to Metal transition

Table of Contents

List of Figures

"Arise, awake and stop not till the goal is reached.".

Swami Vivekananda

1

Introduction

This chapter provides a detailed introduction to the effects of interaction and non-trivial topology in condensed matter systems. We begin with an introduction to the Hubbard model and itinerant magnetism, followed by a discussion on the various theories of itinerant magnetism. We follow this with a brief introduction to the concept of topology. We conclude with a discussion on the basic principles of topological condensed matter physics.

Physics in my humble understanding is the branch of science that deals with discovering and understanding those laws of nature that govern the material realm of existence and many at times applying that knowledge in the service of humanity. The laws that govern this aspect of nature can be broadly classified in to three categories,

1. Those well suited for describing the smallest scale in which matter is known to exist, such as electrons, protons, neutrons, etc.
2. Those well suited for describing the largest scale in which matter is known to exist, such as cluster of galaxies, black holes, etc.
3. Those well suited for describing the complex states of matter, like condensed matter systems, etc.

However, there is no denying that the final goal is to formulate the unified set of physical laws well suited for describing matter in all the above three forms.

At this point, I should quickly announce that in the course of thesis, we will be contemplating only on the third kind of laws and formalism associated with them. Even the term *"laws governing complex states of matter"* is a broad umbrella term under which various physical phenomena with completely diverse origins can be placed. Our discussion will be restricted to only condensed matter systems also popularly known as solid state systems.

There is a multitude of opinions on ***"what is the central theme of condensed matter physics?"***, but the most plausible and appealing answer to the above question in my opinion is ***"characterising different phases of the complex states in which matter exists"***. In the course of this thesis we will characterise the phases of some condensed matter systems in the presence of two effects:

1. Interaction and

2. Topology.

We will be discussing two paradigms of condensed matter systems, the first involving itinerant magnetism[1], where effects of only interaction are present and the second relating to the Su-Schrieffer-Heeger model[2], where only the effects of topology are present (when we say effects of topology, we mean presence of non-trivial topology). However, we should clarify that there are systems where the effects of both interaction and topology play a leading role in dictating the physics of the system. The following graphic is a web of condensed mater in my humble opinion:

A web depicting different domains of condensed matter physics and one of its central theme

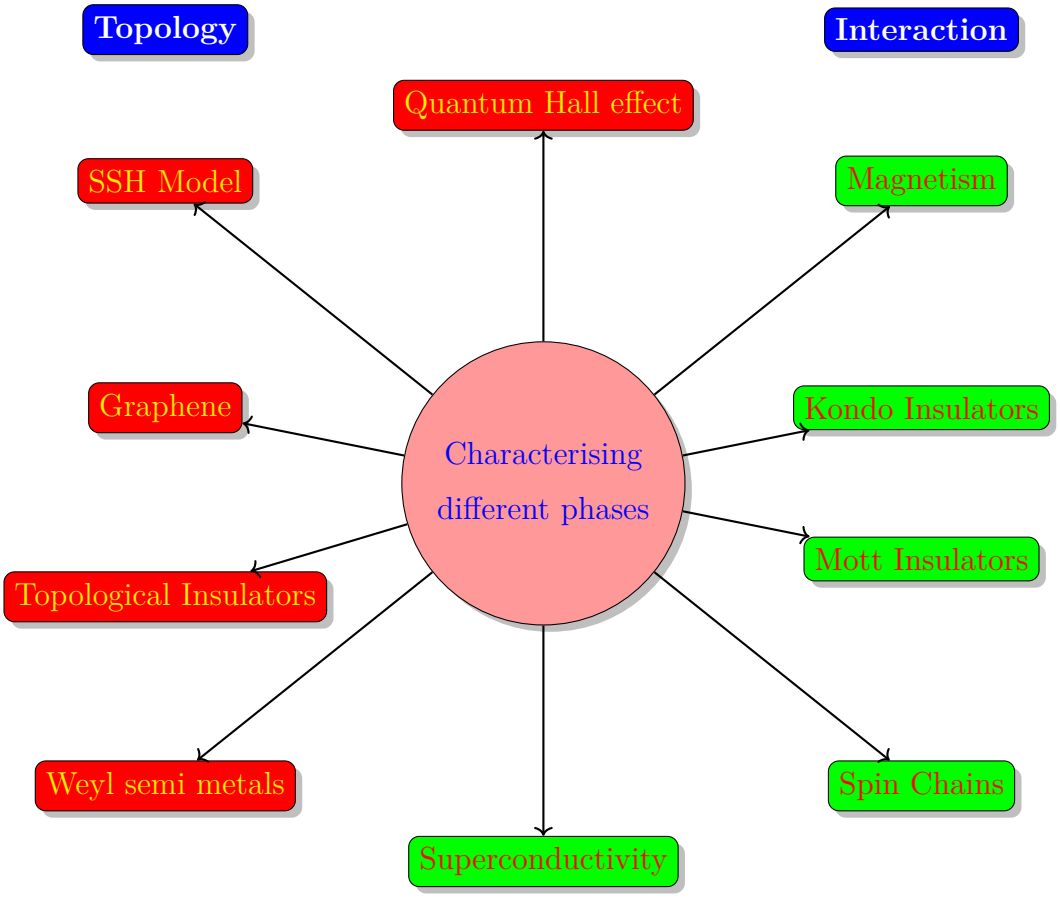

In the above graphic we have illustrated that one of the central theme of condensed matter physics is the characterisation of different phases. Also highlighted are some of the domains within the realm of condensed matter physics and the important effect their physical properties depend upon. Some of them are governed by both effects like the case of quantum Hall effect[3] and these are placed in between the two categories.

We will now shift our attention to theories that describe the physics of condensed matter systems. Theories describing the physics of condensed matter systems can be classified in to two categories:

1. Free theories which assume that electrons do not interact with each other,
2. Interacting theories which take in to effect, the interaction of electrons.

Band theory of solids, the pinnacle of free theories was and still continues to enjoy a remarkable success in explaining the physical properties of a variety of materials. The quantum mechanical explanation for the classification of materials in to insulators, conductors and semi-conductors was given by band theory.

However the arrival of topological band theory changed the landscape of free band theories forever[4, 5]. It lead to the emergence of a new field of condensed matter physics called ***"topological quantum matter"***. The emergence of the field of topological quantum matter has been met with pomp and splendor and it is not limited only to the rich mathematical framework it relies on but also to the promising applications it holds in domains like quantum computation[6].

To illustrate the complexity that the effects of interactions bring in to condensed matter physics, we will give a small illustration. We assume that there exists a fictitious multi dimensional space. If the free theories hold one dimension in this fictitious space, Interacting theories bring many new dimensions to it. Any theory that considers interaction is called an interacting theory. Depending on the

nature of the interaction and the nature of the quasi-particles that are interacting, there are a plethora of interacting theories.

In the course of this thesis, we will be discussing the effects of interaction based on the Hubbard model[7]. The Hubbard model as will be explained later is a very simplified treatment of electronic interactions but at the same time is known to produce accurate results. This makes it a very powerful model to study systems with electronic interactions.

1.1 The Hubbard Model

The Hubbard model is one of the most successful models in terms of explaining the role of interactions in a many body condensed matter system[7]. We will begin with the most general Hamiltonian describing an interacting system of electrons. We will then consider various approximations and simplify this Hamiltonian to obtain the Hubbard Hamiltonian.

Tight-binding models are used to describe electrons that are tightly bound to the atomic sites and can only hop from one atomic site to other by quantum mechanical tunneling with an hopping amplitude[8].

The general many electron tight binding Hamiltonian with effects of interaction is given as follows:

$$H = \sum_{ij\sigma} T_{ij} a^{\dagger}_{i\sigma} a_{j\sigma} + \frac{1}{2} \sum_{ijkl\sigma\sigma'} U_{ijkl} a^{\dagger}_{i\sigma} a^{\dagger}_{j\sigma'} a_{l\sigma'} a_{k\sigma}, \tag{1.1}$$

with T_{ij} the co-efficient of the kinetic energy term and U_{ijkl} the co-efficient of the potential energy term. Notice that co-efficient T_{ij} is a function of both sites i and j and co-efficient U_{ijkl} is a function of i, j, k and l. This Hamiltonian is very general but it turns out it is impossible to be solved for reasonable system sizes.

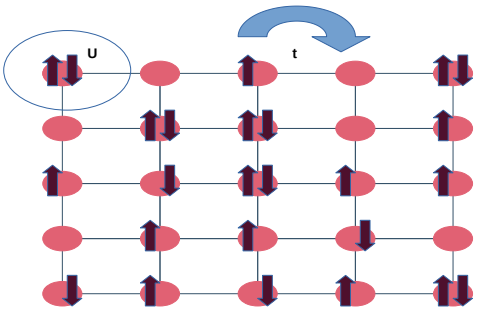

Figure 1.1: Pictorial depiction of the Hubbard model with tunneling amplitude to move from one site to its neighboring site as t and the on-site interaction energy as U.

The important assumption in the Hubbard model is that there is a huge amount of screening in the lattice and because of that the electron feels the repulsion only due to the electron at the same atomic site in which the electron is present and is not affected by the repulsion of other electrons in the material. This is to say it considers only on-site interaction. However by Pauli's exclusion principle for two electrons to be at the same site, their spins should be different.

Hence the Hubbard model simplifies the general Hamiltonian in Equation 1.1 to a much simpler form given as:

$$H = \sum_{ij\sigma} T_{ij} a^{\dagger}_{i\sigma} a_{j\sigma} + \frac{U}{2} \sum_{i} n_{i\uparrow} n_{i\downarrow}, \tag{1.2}$$

where $n_{i\uparrow}(n_{i\downarrow})$ is the number operator given as $a^{\dagger}_{i\uparrow} a_{i\uparrow}$ $(a^{\dagger}_{i\downarrow} a_{i\downarrow})$ and gives the number of up (down) electrons in the site i.

The Hubbard Hamiltonian in Equation 1.2, is no doubt more simpler to solve than the one in Equation 1.1 but is not straight forward or simple. Even to solve this model, there has to be several approximations made to arrive at a meaningful solution. The Hubbard model is depicted pictorially in Figure 1.1.

As mentioned before we will study models of itinerant magnetism based on the Hubbard model. Before starting with this study, we will give a brief introduction

to magnetism in general followed by an introduction to itinerant magnetism in section 1.2. This will be followed with discussions on the various approximations that can be made to solve the Hubbard model in subsection 1.2.1, subsection 1.2.2 and subsection 1.2.3. The pros and cons of each of these approximations and the accuracy of the results obtain with these approximations will also be discussed.

1.2 Magnetism

Magnetism is a phenomena that has been known to mankind from the ancient times[9, 10]. From the calculated geometric construction of temples with magnets resulting in the idol of deities levitating in that magnetic field, to the use of magnets in compass by sailors to navigate across seas, magnetism has been a point of interest for a very long time.

Pierre Curie and Pierre Weiss gave the first classical theories of magnetism in the early 19th century[11, 12]. Curie and Weiss had derived the expression for the static susceptibility (which is a measure of response of a material to an applied constant magnetic field) assuming local magnetic moments and an internal field ($H = H_{ext} + \lambda\, H_{int}$)[13]. They were successful in some sense. To understand their success we need to define the two defining features of a magnetic material:

1. Curie temperature: The temperature below which the magnetic moments in the material get ordered. This can also be said as the temperature at which the material transitions from the paramagnetic state (state without magnetic order) to the ferromagnetic state (ordered state).
2. Curie-Weiss behavior: Curie-Weiss behavior of a material simply implies it obeys Curie-Weiss law. Curie-Weiss law states that the susceptibility of a material is inversely proportional to temperature. In other words the plot of inverse of susceptibility as a function of temperature above the Curie temperature is a straight line.

.

The Curie-Weiss behavior is an experimental fact that was observed before. Curie and Weiss were able to theoretically calculate the expression for susceptibility and show its inverse dependence on temperature. However their theory has several issues like the unreasonably high values required for the constant λ which dented its success.

However the theory was given a final blow with the advent of quantum mechanics which changed our understanding of magnetism forever. Niels Bohr, one of the founding fathers of quantum mechanics, showed that magnetism is inherently a quantum mechanical phenomenon and lacks a classical counterpart[14, 15]. The statement of the theorem as mentioned by Van Vleck is as follows: "At any finite temperature, and in all finite applied electrical or magnetic fields, the net magnetization of a collection of electrons in thermal equilibrium vanishes identically". The Bohr-Van Leeuwen theorem made it essential to completely discard the classical theories of magnetism and develop quantum mechanical theories of magnetism to understand the phenomena of magnetism correctly.

Magnetism can be classified in to two types based on the nature of electrons whose magnetic moments align giving rise to magnetism.

1. If the electrons responsible for magnetism are localised at atomic orbitals in a particular site, the magnetism arising from these electrons is called localised magnetism. This phenomena of localised magnetism has been relatively well understood through the Heisenberg model of magnetism[16].

2. If the electrons that align to give rise to magnetism are not localised at atomic orbitals at each site and can move from one site to another, that form of magnetism is called itinerant magnetism[17].

Stoner came up with the first and most simple description of such a form of magnetism called the Stoner model[17]. This model considers that the electrons in a material interact with the mean field which is a resultant average field arising due to the presence of all the electrons. However in such an approach one naturally loses out on the effect of the correlation of electrons which gets averaged out. The Stoner model is discussed in detail in subsection 1.2.1

Izuyama, Kim and Kubo formulated the theory of itinerant magnetism to explain the data obtained from neutron diffraction experiments[18]. They had gone beyond the mean field approximation for such a calculation employing the Random Phase Approximation (RPA). The RPA model is explained in detail in subsection 1.2.2. They were successful in explaining neutron diffraction data but RPA theory in the static limit reduced to the Stoner model and hence could not correctly estimate the Curie Weiss temperature and paramagnetic susceptibility. The need for a theory to accurately explain itinerant magnetism still remained elusive.

It is in this juncture that Moriya and Kawabata formulated the Self-Consistent Renormalisation theory of itinerant electron Ferromagnetism[1, 19]. We will discuss each of these theories sequentially along with their merits and drawbacks in the following discussions.

1.2.1 Stoner Model

We present here a simple derivation of the Stoner model at zero temperature. The objective here is not derive the results rigorously but to illustrate the results of the Stoner model and to compare it with results obtained from other models.

We first derive the Stoner condition for itinerant magnetism which is a criteria to find whether a material is an itinerant magnet or not. We will follow this with the expression for susceptibility in Stoner model.

Stoner Condition

The Stoner model employs a mean field approximation. In mean field approximation an electron feels the net effect of the field of all other electrons. With this

assumption the potential energy term in Equation 1.2 becomes:

$$U \sum_i n_{i\uparrow} n_{i\downarrow} = U\, N_\uparrow\, N_\downarrow, \tag{1.3}$$

where $N_\uparrow(N_\downarrow)$ is the total number of up (down) electrons in the system.

If we assume that the potential energy of the system comes only from the exchange energy and denote by U_{eff} the coefficient of the Hubbard interaction, we get the following relation,

$$H_{exch} = U_{eff}\, N_\uparrow\, N_\downarrow = U_{eff}(N - N_\downarrow)N_\downarrow. \tag{1.4}$$

It is clear from Equation 1.4 that H_{exch} has a maximum when $N_\downarrow = \frac{N}{2}$ with a value $U_{eff}\,\frac{N^2}{4}$ and its value is zero when $N_\downarrow = 0$ or $N_\downarrow = N$.

If we set the maximum of H_{exch} as the zero reference and denote that energy as ΔE_{eff} defined as:

$$\Delta E_{eff} = U_{eff}(N - N_\downarrow)N_\downarrow - U_{eff}\,\frac{N^2}{4} \tag{1.5}$$

Now let us assume a deformation in the Fermi level of energy $\Delta << \varepsilon_F$ where ε_F is the Fermi energy. It is equivalent to say that $p\,N$ electrons in the down spin state have migrated to the up spin state. Initially we had $\frac{N}{2}$ electrons in up spin and the same number of electrons in the down spin state.

Now we have $\frac{N}{2} + p\,N$ electrons in the up spin and $\frac{N}{2} - p\,N$ in the down spin state. However, the total number of electrons $N_\uparrow + N_\downarrow$ remains conserved. It is easy to show from Equation 1.5 that the exchange energy in terms of $p\,N$ is:

$$\Delta E_{exch} = -U_{eff}\, p^2\, N^2. \tag{1.6}$$

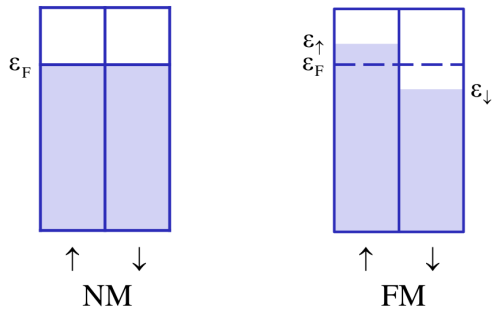

Figure 1.2: If the deformation of Δ amount of energy around the Fermi level causes net increase in energy the material remains as a normal metal (left), but if there is net decrease in energy it becomes a ferromagnet (right).

Let us now calculate the increase in kinetic energy due to this migration,

$$\Delta K.E. = \int_0^{+\Delta} d\varepsilon\, \varepsilon\, \rho_\uparrow(\varepsilon) - \int_{-\Delta}^{0} d\varepsilon\, \varepsilon\, \rho_\downarrow(\varepsilon). \tag{1.7}$$

But since we assumed the disturbance Δ to be very small compared to ε, the density of states for both the spin configurations remain the same and is nearly equal to:

$$\rho_\uparrow(\varepsilon) \simeq \rho_\downarrow(\varepsilon) \simeq \rho_{total} \tag{1.8}$$

where ρ_{total} is the value of density of states at the Fermi level.

The increase in kinetic energy due to the migration from Equation 1.7 is thus given as:

$$\Delta K.E. = \rho_\uparrow(\varepsilon_F)\, \Delta^2 \tag{1.9}$$

From Equation 1.9 it is clear that $\Delta K.E. > 0$. We also have:

$$N_\uparrow - N_\downarrow = 2\, p\, N = \int_{-\Delta}^{+\Delta} d\varepsilon\, \rho_\uparrow(\varepsilon) = 2\, \rho_\uparrow(\varepsilon_F)\, \Delta. \tag{1.10}$$

this implies,

$$\Delta = \frac{p\, N}{\rho_\downarrow(\varepsilon_F)}. \tag{1.11}$$

Substituting Equation 1.11 in Equation 1.9, we get the increase in kinetic energy

in terms of p and N as:

$$\Delta K.E. = \frac{(p\,n)^2}{\rho_\uparrow(\varepsilon_F)}. \tag{1.12}$$

The total energy can be written now with the help of Equation 1.6 and Equation 1.12 as:

$$\Delta E_{total} = -U_{eff}(p\,n)^2 + \frac{(p\,n)^2}{\rho_\uparrow(\varepsilon_F)} = \frac{(p\,n)^2}{\rho_\uparrow(\varepsilon_F)}(1 - U_{eff}\,\rho_\uparrow(\varepsilon_F)). \tag{1.13}$$

Thus the total change in energy is negative if $U_{eff}\,\rho_\uparrow(\varepsilon_F) > 1$. This is the celebrated Stoner condition for itinerant magnetism. This is illustrated in Figure 1.2.

Susceptibility in the Stoner model

Susceptibility is the measure of response of the system to an external magnetic field. With an applied magnetic field H, the total energy of the system (ΔE_T) becomes:

$$\begin{aligned}\Delta E_T &= \Delta E_{K.E.} + \Delta E_{exch} + \Delta E_{mag} \\ &= \frac{(p\,n)^2}{\rho_\uparrow(\varepsilon_F)} - U_{eff}(p\,n)^2 - \mu_B(2\,n\,p)H.\end{aligned} \tag{1.14}$$

The equilibrium condition is:

$$\frac{d\Delta E_T}{dp} = 0, \tag{1.15}$$

which implies,

$$\frac{2\,p\,n^2}{\rho_\uparrow(\varepsilon_F)} - 2\,U_{eff}\,p\,n^2 - 2\,\mu_B\,n\,H. \tag{1.16}$$

Rearranging Equation 1.16, we get:

$$p\,n = \frac{\mu_B\,\rho_\uparrow(\varepsilon_F)}{1 - U_{eff}\,\rho_\uparrow(\varepsilon_F)}\,H. \tag{1.17}$$

But $M = 2\,\mu_B\,p\,n$, this implies:

$$M = \frac{\mu_B^2\,\rho_\uparrow(\varepsilon_F)}{1 - U_{eff}\,\rho_{total}(\varepsilon_F)}\,H, \tag{1.18}$$

which simplifies to,

$$\chi_{Stoner} = \frac{\chi_{Pauli}}{1 - \frac{1}{2}U_{eff}\,\rho_\uparrow(\varepsilon_F)} \tag{1.19}$$

Equation 1.19 is the expression for susceptibility in the Stoner model. It is to note that $\frac{1}{1-\frac{1}{2}U_{eff}\,\rho_\uparrow(\varepsilon_F)}$ is called the Stoner enhancement factor. It turns out that this expression for susceptibility of itinerant magnetism is very inaccurate and needs modification[20]. The Curie temperature can be calculated from Equation 1.19, because the inverse of susceptibility goes to zero at the Curie temperature. The estimated Curie temperature is nearly an order of magnitude higher than the experimental measured value[1, 13].

This can be expected as the Stoner model considers a mean field treatment where the effects of correlations have been washed away (that is only exchange effect is taken in to account). It turns out that it is necessary to consider the effects of electronic correlations and they affect the ground state of the magnetic system.

1.2.2 Random Phase Approximation Theory

As mentioned before Izuyama, Kim and Kubo went beyond the Stoner model by employing a Random Phase Approximation (RPA) to solve the Hubbard model[18]. In their new approach they went beyond the static susceptibility obtained in the Stoner model and they could derive the expression for dynamical susceptibility, With the expression for dynamical susceptibility derived from RPA theory, they argued that the neutron diffraction data could be explained through itinerant magnetism too. But as shown in Appendix A, in the zero frequency ($\omega \to 0$) and long wavelength ($q \to 0$) limit (static limit), the expression for dynamical susceptibility in the RPA model reduces to the static susceptibility value equivalent to that of

the one obtained from Stoner theory.

Our objective in this subsection is to derive the expressions for transverse dynamical susceptibility in RPA model. This is important as later when we perform the calculations of the Self-Consistent Renormalisation theory, we will be employing a modified Random Phase Approximation and will be requiring these expressions of transverse dynamical susceptibilities in the RPA model as the inputs to begin the calculation with.

In the RPA model, the dynamical susceptibility is given by the Fourier transform of the response function (the retarded Green function) defined with respect to spin densities. We follow the equation of motion approach. Let us consider the spin density operator defined as:

$$S(\mathbf{r}) = \psi^{\dagger}(\mathbf{r})\,\sigma\,\psi(\mathbf{r}), \tag{1.20}$$

where σ are the Pauli matrices, ψ and $\psi^{\dagger}$ are field operators which are given as:

$$\psi = \sum_{k} \phi_k(\mathbf{r})\, a_k, \tag{1.21}$$

$$\psi^{\dagger} = \sum_{k} \phi_k^{*}(\mathbf{r})\, a_k^{\dagger}. \tag{1.22}$$

Also, the generalized dynamical susceptibility is given by the expression:

$$\chi_{BA}(\omega) = \frac{i}{\hbar}\int_0^{\infty} dt\, e^{i\omega t - \epsilon t}\, \langle [B(t), A] \rangle\,. \tag{1.23}$$

Let us define the operators $B(t)$ and A as follows,

$$\begin{aligned} B(t) &= S_\alpha\left(\mathbf{r},t\right), \\ A &= S_\beta(\mathbf{r}'). \end{aligned} \tag{1.24}$$

The dynamical magnetic susceptibility can now be written as:

$$\chi_{\alpha,\beta}(\mathbf{r}-\mathbf{r}',\omega) = \frac{i}{\hbar}\int_0^\infty dt\, e^{i\omega t-\epsilon t}\,\left\langle\left[S_\alpha\left(\mathbf{r},t\right),S_\beta(\mathbf{r}')\right]\right\rangle. \tag{1.25}$$

Fourier transform of the above equation can be written as,

$$\chi_{\alpha,\beta}(k,\omega) = \frac{i}{\hbar}\int_0^\infty dt\, e^{i\omega t-\epsilon t}\int_{-\infty}^\infty d^3(\mathbf{r}-\mathbf{r}')\, e^{-i\mathbf{k}\cdot(\mathbf{r}-\mathbf{r}')}\,\left\langle\left[S_\alpha\left(\mathbf{r},t\right),S_\beta(\mathbf{r}')\right]\right\rangle, \tag{1.26}$$

making the following transformation $\mathbf{r}-\mathbf{r}'\to\mathbf{R}$ and $\mathbf{r}\to\mathbf{r}'+\mathbf{R}$ we get,

$$\chi_{\alpha,\beta}(k,\omega) = \frac{i}{\hbar}\int_0^\infty dt\, e^{i\omega t-\epsilon t}\int_{-\infty}^\infty d^3\mathbf{R}\, e^{-ik\cdot\mathbf{R}}\,\left\langle\left[S_\alpha\left(\mathbf{r}'+\mathbf{R},t\right),S_\beta(\mathbf{r}')\right]\right\rangle. \tag{1.27}$$

Further, since $\left\langle\left[S_\alpha\left(\mathbf{r}'+\mathbf{R},t\right),S_\beta(\mathbf{r}')\right]\right\rangle$ in terms of $\mathbf{k}$ can be written using the transformation: $S_\alpha(\mathbf{r}) = \sum_k e^{i\mathbf{k}\cdot\mathbf{r}}S_\alpha(\mathbf{k})$

$$\begin{aligned} \chi_{\alpha,\beta}(k,\omega) &= \frac{i}{\hbar}\int_0^\infty dt\, e^{i\omega t-\epsilon t}\int_{-\infty}^\infty d^3\mathbf{R}\, e^{-i\mathbf{k}\cdot\mathbf{R}}\sum_{K_1} e^{i\mathbf{K_1}\cdot(\mathbf{r}'+\mathbf{R})}\sum_{K_2} e^{i\mathbf{K_2}\cdot\mathbf{r}'} \\ &\quad \left\langle\left[S_\alpha\left(K_1,t\right),S_\beta(\mathbf{K_2})\right]\right\rangle \\ &= \frac{i}{\hbar}\int_0^\infty dt\, e^{i\omega t-\epsilon t}\int_{-\infty}^\infty d^3\mathbf{R}\, e^{-i\mathbf{k}\cdot\mathbf{R}}\sum_{K_1,K_2} e^{i(\mathbf{K_1}+\mathbf{K_2})\cdot\mathbf{r}'}e^{i\mathbf{K_1}\cdot\mathbf{R}} \\ &\quad \left\langle\left[S_\alpha\left(K_1,t\right),S_\beta(\mathbf{K_2})\right]\right\rangle. \end{aligned} \tag{1.28}$$

To make this equation independent of $\mathbf{r}'$, consider $e^{i(\mathbf{K_1}+\mathbf{K_2})\cdot\mathbf{r}'} = 1$, which implies $(\mathbf{K_1}+\mathbf{K_2})\cdot\mathbf{r}' = n\pi$, for $n=0 \implies \mathbf{K_1} = -\mathbf{K_2}$. Therefore the above equation takes the form:

$$\begin{aligned}\chi_{\alpha,\beta}(k,\omega) &= \frac{i}{\hbar}\int_0^\infty dt\, e^{i\omega t-\epsilon t}\int_{-\infty}^{\infty} d^3\mathbf{R}\, e^{-i\mathbf{k}\cdot\mathbf{R}}\, e^{i\mathbf{K_1}\cdot\mathbf{R}}\left\langle\left[S_\alpha\left(\mathbf{K}_1,t\right),S_\beta(-\mathbf{K_1})\right]\right\rangle \\ &= \frac{i}{\hbar}\int_0^\infty dt\, e^{i\omega t-\epsilon t}\int_{-\infty}^{\infty} d^3\mathbf{R}\, e^{i(\mathbf{K_1}-\mathbf{k})\cdot\mathbf{R}}\,\left\langle\left[S_\alpha\left(\mathbf{K}_1,t\right),S_\beta(-\mathbf{K_1})\right]\right\rangle .\end{aligned} \tag{1.29}$$

From definition of the δ-function we get,

$$\int_{-\infty}^{\infty} d^3\mathbf{R}\, e^{i(\mathbf{K_1}-\mathbf{k})\cdot\mathbf{R}} = \delta_{\mathbf{K}_1,k}, \tag{1.30}$$

implies

$$\chi_{\alpha,\beta}(k,\omega) = \frac{i}{\hbar}\int_0^\infty dt\, e^{i\omega t-\epsilon t}\,\left\langle\left[S_\alpha\left(k,t\right),S_\beta(-k)\right]\right\rangle . \tag{1.31}$$

Approximate calculation of the reduced susceptibility in RPA model

We will now calculate χ_{-+} component of the dynamical susceptibility,defined as:

$$\begin{aligned}\chi_{-+}(\boldsymbol{q},\omega) =& \frac{i}{\hbar}\int_0^\infty e^{-i\omega t}\left\langle[S_-(\boldsymbol{q},t),S_+(-\boldsymbol{q})]\right\rangle dt \\ =& \int_{-\infty}^{\infty} e^{-i\omega t}\langle\langle S_-(\boldsymbol{q},\mathrm{t});S_+(-\boldsymbol{q})\rangle\rangle dt\end{aligned} \tag{1.32}$$

where S_{-+} is given as

$$S_-(\boldsymbol{q},t) = \sum_{\boldsymbol{k}} a^*_{\boldsymbol{k}+\boldsymbol{q}\downarrow}(t)a_{\boldsymbol{k}\uparrow}(t) \tag{1.33}$$

$$S_+(-\boldsymbol{q}) = \sum_{\boldsymbol{k}} a^*_{\boldsymbol{k}\uparrow}a_{\boldsymbol{k}+\boldsymbol{q}\downarrow} \tag{1.34}$$

for simplicity we introduce the following notation

$$\vartheta_k(\boldsymbol{q},t) \equiv a^*_{k+q\downarrow}(t)a_{k\uparrow}(t), \tag{1.35}$$

and rewrite Equation 1.33 as

$$S_{-}(\boldsymbol{q},t)=\sum_{\boldsymbol{k}}\vartheta_{\boldsymbol{k}}(\boldsymbol{q},t). \tag{1.36}$$

Defining the retarded Green function as,

$$\langle\langle\widetilde{\sigma}_{-}(\boldsymbol{q},t);S_{+}(\boldsymbol{q})\rangle\rangle=\sum_{\boldsymbol{k}}\langle\langle\vartheta_{\boldsymbol{k}}(\boldsymbol{q},t);S_{+}(-\boldsymbol{q})\rangle\rangle, \tag{1.37}$$

which can determined by applying the Equation of motion (EOM) approach. By using the conventional definition of the retarded Green function, the R.H.S of the above equation takes the form as:

$$\iota\hbar\frac{d}{dt}\langle\langle\vartheta_{k}(\boldsymbol{q},t);S_{+}(-\boldsymbol{q})\rangle\rangle=-\delta(t)\langle[\vartheta_{k}(\boldsymbol{q},t),S_{+}(-\boldsymbol{q})]\rangle+\langle\langle[\vartheta_{k}(\boldsymbol{q},t),\mathcal{H}]\,;S_{+}(-\boldsymbol{q})\rangle\rangle, \tag{1.38}$$

here $\mathcal{H}$ is the Hamiltonian of the system of interest and is given as

$$\mathcal{H}=\mathcal{H}_{0}+\mathcal{H}_{c} \tag{1.39}$$

$$\mathcal{H}_{0}=\sum_{\boldsymbol{k\mu}}\epsilon(k)n_{k\mu} \tag{1.40}$$

$$\mathcal{H}_{c}=\frac{1}{2}U_{eff}\sum_{\kappa}^{'}\sum_{\boldsymbol{k}\mu}\sum_{l\nu}a^{\dagger}_{\boldsymbol{k}+\kappa,\mu}a_{k\mu}a^{\dagger}_{l,\nu}a_{l+\kappa,\nu} \tag{1.41}$$

where

$$n_{k\mu}=a^{*}_{k\mu}a_{k\mu} \tag{1.42}$$

Now we will calculate the commutators that are involved in solving the EOM in Equation 1.38:

$$[\vartheta_k(\boldsymbol{q}), S_+(-\boldsymbol{q})] = a^\dagger_{k+q\downarrow} a_{k+q\downarrow} + a^\dagger_{k\uparrow} a_{k\uparrow} = n_{k+q\downarrow} - n_{k\uparrow}. \tag{1.43}$$

$$[\vartheta_k(\boldsymbol{q}), \mathcal{H}_0] = \varepsilon(\boldsymbol{k}) a^\dagger_\downarrow a_\uparrow - \varepsilon(\boldsymbol{k}+\boldsymbol{q}) a^\dagger_{k+q\downarrow} a_{k\uparrow} = (\varepsilon(\boldsymbol{k}) - \varepsilon(\boldsymbol{k}+\boldsymbol{q}))\, \vartheta_k(\boldsymbol{q}) \tag{1.44}$$

The commutator $[\vartheta_k(\boldsymbol{q}), \mathcal{H}_c]$ has so many complex terms, thus a complete treatment that involves all the terms is futile. We will consider only those terms that can be transformed in to the form $\vartheta_l(\boldsymbol{q}) n_{m\mu}$ and ignore the rest. This corresponds to employing the Random Phase Approximation (RPA).

With the above approximation, the expression for $[\vartheta_k(\boldsymbol{q}), \mathcal{H}_c]$ can be simplified by considering only terms of the type

$$[\vartheta_k(\boldsymbol{q}), \mathcal{H}_c] \simeq U_{eff} \sum_{q'} \{\vartheta_{k+q'}(\boldsymbol{q})\, (-n_{k+q\downarrow} + n_{k\uparrow}) + \vartheta_k(\boldsymbol{q})\, (-n_{k+\kappa,\uparrow} + n_{k+q+k,\downarrow})\} \tag{1.45}$$

The first term on right hand side of Equation 1.45, gives the ladder type interaction between electron and hole by which the effects of correlations is taken in to account. This is diagrammatically shown in Figure 1.3. The second term corresponds to exchange self energy correction to each one particle state and it takes care of the molecular field acting on the electron.

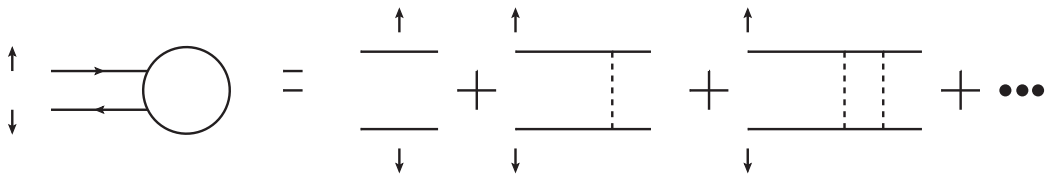

Figure 1.3: Ladder diagrams contributing to $\chi_{+-}(q, \omega)$.

Also, in the same approximation (RPA),

$$\begin{aligned} \langle\langle n_{k,\mu} \vartheta_i(\boldsymbol{q}, t); S_+(-\boldsymbol{q})\rangle\rangle &\cong \langle n_{k,\mu}\rangle \langle\langle \vartheta_l(\boldsymbol{q}, t); S_+(-\boldsymbol{q})\rangle\rangle \\ &= f_{k\mu} \langle\langle \vartheta_\iota(\boldsymbol{q}, t); S_+(-\boldsymbol{q})\rangle\rangle \end{aligned} \tag{1.46}$$

EOM is now reduced to a simpler form as

$$\begin{aligned} \iota\hbar\frac{d}{dt}\langle\vartheta_k(\boldsymbol{q},t);S_+(-\boldsymbol{q})\rangle &= -\delta(t)\left(f_{k+\boldsymbol{q}\downarrow}-f_{k\uparrow}\right)+\left(\tilde{\varepsilon}_\uparrow(\boldsymbol{k})-\tilde{\varepsilon}_\downarrow(\boldsymbol{k}+\boldsymbol{q})\right) \\ &\quad \langle\langle\vartheta_k(\boldsymbol{q},t);S_+(-\boldsymbol{q})\rangle\rangle+U_{eff}\left(f_{k\uparrow}-f_{k+q\downarrow}\right) \\ &\quad \sum_\kappa\left\langle\langle\vartheta_{k+k}(\boldsymbol{q},t);S'_+(-\boldsymbol{q})\rangle\right\rangle \end{aligned} \tag{1.47}$$

where

$$\widetilde{\varepsilon}_\mu(\boldsymbol{k})\equiv\varepsilon(\boldsymbol{k})-U_{eff}\sum_\kappa{}' f_{k+\kappa,\mu} \tag{1.48}$$

Therefore the EOM is further transformed to its Fourier transform as

$$\begin{aligned} &\{-\hbar\omega+\tilde{\varepsilon}_\downarrow(\boldsymbol{k}+\boldsymbol{q})-\tilde{\varepsilon}_\uparrow(\boldsymbol{k})\}\langle\langle\vartheta_{\boldsymbol{k}}(\boldsymbol{q},\omega);S_+(-\boldsymbol{q})\rangle\rangle \\ &\quad =-\left(f_{\boldsymbol{k}+\boldsymbol{q}\downarrow}-f_{\boldsymbol{k}\uparrow}\right)+U_{eff}\left(f_{\boldsymbol{k}\uparrow}-f_{\boldsymbol{k}+\boldsymbol{q}\downarrow}\right)\textstyle\sum_{\boldsymbol{k}}\langle\langle\vartheta_{\boldsymbol{k}+\kappa}(\boldsymbol{q},\omega);S_+(-\boldsymbol{q})\rangle\rangle \end{aligned} \tag{1.49}$$

dividing both sides of the expression by $(-\hbar\omega+\tilde{\varepsilon}_\downarrow(\boldsymbol{k}+\boldsymbol{q})-\tilde{\varepsilon}_\uparrow(\boldsymbol{k})$ and then summing over all wave numbers we obtain the solution as

$$\chi_{-+}(\boldsymbol{q},\omega)=\sum_{\boldsymbol{k}}\langle\vartheta_{\boldsymbol{k}}(\boldsymbol{q},\omega);S(-\boldsymbol{q})\rangle=\frac{\Gamma_{-+}(\boldsymbol{q},\boldsymbol{\omega})}{1-U_{eff}\Gamma_{-+}(\boldsymbol{q},\omega)}, \tag{1.50}$$

where $\Gamma_{-+}(\boldsymbol{q},\boldsymbol{\omega})$ is the definition of Lindhard function and is defined as

$$\Gamma_{-+}(\boldsymbol{q},\omega)=\sum_k\frac{f_{k\uparrow}-f_{k+q\uparrow}}{\varepsilon_\downarrow(\boldsymbol{k}+\boldsymbol{q})-\varepsilon_\uparrow(\boldsymbol{k})-\hbar\omega} \tag{1.51}$$

If we put $1-U_{eff}\Gamma_{-+}(\boldsymbol{q},\omega)=0$ in Equation 1.50 then $\chi^{-1}_{-+}(\boldsymbol{q},\omega)\to 0$ which indicates a phase transition happening in the system. In the RPA, the χ_{zz} is calculated through the following way, where z is the direction of the spontaneous magnetization. Therefore $S_z(\boldsymbol{q},t)$ in Equation 1.32 is written as:

$$S_z(\boldsymbol{q},t)=\frac{1}{2}\{\sum_k\vartheta_{k\uparrow}(\boldsymbol{q},t)-\sum_k\vartheta_{k\downarrow}(\boldsymbol{q},t)\} \tag{1.52}$$

where

$$\vartheta_{k\sigma}(\boldsymbol{q},t) = a^{*}_{k+q\sigma}(t)a_{k\sigma}(t) \tag{1.53}$$

hence the Green function associated with $\chi^{'}_{zz}$ takes the form

$$\langle\langle S_z(\boldsymbol{q},t); S_z(-\boldsymbol{q})\rangle\rangle = \frac{1}{2}\{G_{\uparrow}(\boldsymbol{q},t) - G_{\downarrow}(\boldsymbol{q},t)\} \tag{1.54}$$

with

$$G_{\sigma}(\boldsymbol{q},t) = \sum_{k}\langle\langle \vartheta_{k\sigma}(\boldsymbol{q},t); S_z(-\boldsymbol{q})\rangle\rangle \tag{1.55}$$

In RPA, we put the following

$$[\vartheta_{k\sigma}(\boldsymbol{q}), \mathcal{H}_c] = U_{eff}(\eta_{\boldsymbol{k}+\boldsymbol{q},\sigma} - \eta_{\boldsymbol{k},\sigma})\sum_{l}\vartheta_{l,-\sigma}(\boldsymbol{q}) \tag{1.56}$$

here $-\sigma$ corresponds to the anti-parallel spin state of σ. Further the EOM is now obtained as

$$\begin{aligned} i\hbar\frac{d}{dt}\langle\langle \vartheta_{k\sigma}(\boldsymbol{q},t); S_z(-\boldsymbol{q})\rangle\rangle &= -\frac{1}{2}\delta(t)\left(f_{k+q,\sigma} - f_{k,\sigma}\right)\eta_{\sigma} + \{\varepsilon(\boldsymbol{k}) - \varepsilon(\boldsymbol{k}+\boldsymbol{q})\} \\ &\langle\langle \vartheta_{\boldsymbol{k},\sigma}(\boldsymbol{q},t); S_z(-\boldsymbol{q})\rangle\rangle + U_{eff}\left(f_{\boldsymbol{k}+\boldsymbol{q},\sigma} - f_{\boldsymbol{k},\sigma}\right)\sum_{\boldsymbol{l}}\langle\langle \vartheta_{\boldsymbol{l},-\sigma}(\boldsymbol{q},t); S_z(-\boldsymbol{q})\rangle\rangle \end{aligned} \tag{1.57}$$

by doing the Fourier transform of the above equation we find

$$\begin{aligned} &\{-\hbar\omega + \varepsilon(\boldsymbol{k}+\boldsymbol{q}) - \varepsilon(\boldsymbol{k})\}\langle\langle \vartheta_{k\sigma}(\boldsymbol{q},\omega); S_z(-\boldsymbol{q})\rangle\rangle \\ &= -\tfrac{1}{2}\left(f_{k+\boldsymbol{q},\sigma} - f_{\boldsymbol{k},\sigma}\right)\eta_{\sigma} + U_{eff}\left(f_{\boldsymbol{k}+\boldsymbol{q},\sigma} - f_{\boldsymbol{k},\sigma}\right)\textstyle\sum_{\boldsymbol{l}}\langle\langle \vartheta_{\ell,-\sigma}(\boldsymbol{q},\omega); S_z(-\boldsymbol{q})\rangle\rangle \end{aligned} \tag{1.58}$$

this is a coupled equation between the spin-up and spin-down electrons. Dividing both the sides by the factor which appears in the L.H.S of this equation and then summing over k's, one easily arrives at

$$\begin{aligned} &\textstyle\sum_{\boldsymbol{k}}\langle\langle \vartheta_{\boldsymbol{k}}(\boldsymbol{q},\omega); S(-\boldsymbol{q})\rangle\rangle = \frac{1}{2}\sum_{k}\frac{f_{k\uparrow} - f_{k+q\uparrow}}{\varepsilon_{\downarrow}(\boldsymbol{k}+\boldsymbol{q}) - \varepsilon_{\uparrow}(\boldsymbol{k}) - \hbar\omega} \\ &+U_{eff}\textstyle\sum_{k}\frac{f_{k\uparrow} - f_{k+q\uparrow}}{\varepsilon_{\downarrow}(\boldsymbol{k}+\boldsymbol{q}) - \varepsilon_{\uparrow}(\boldsymbol{k}) - \hbar\omega} \times \sum_{\boldsymbol{l}}\langle\langle \vartheta_{\ell,-\sigma}(\boldsymbol{q},\omega); S_z(-\boldsymbol{q})\rangle\rangle \end{aligned} \tag{1.59}$$

this implies

$$G_\sigma(\boldsymbol{q},\omega) = \Gamma_\sigma(q,\omega)\{\frac{1}{2}\eta_\sigma - U_{eff}G_{-\sigma}(q,\omega)\} \tag{1.60}$$

where $G_\sigma(q,\omega)$ is Fourier transform of $G_\sigma(q,t)$ given in Equation 1.55

and

$$\Gamma_\sigma(\boldsymbol{q},\omega) = \sum_k \frac{f_{k\sigma} - f_{k+q\sigma}}{\varepsilon(\boldsymbol{k}+\boldsymbol{q}) - \varepsilon(\boldsymbol{k}) - \hbar\omega}. \tag{1.61}$$

Therefore $G_\sigma(q,\omega)$ can be written in terms of the $\Gamma_\sigma(q,\omega)$ as

$$G_\sigma(\boldsymbol{q},\omega) = \frac{1}{2}\eta_\sigma \frac{\Gamma_\sigma(\boldsymbol{q},\omega)\{1 + U_{eff}\Gamma_{-\sigma}(q,\omega)\}}{1 - U_{eff}^2\Gamma_{-\sigma}(q,\omega)\Gamma_\sigma(q,\omega)}. \tag{1.62}$$

Now, from Equation 1.54 and Equation 1.32 $\chi_{zz}(\boldsymbol{q},\omega)$ can be obtained as

$$\chi_{zz}(\boldsymbol{q},\omega) = \frac{1}{4}\frac{\Gamma_\downarrow(\boldsymbol{q},\boldsymbol{\omega}) + \Gamma_\uparrow(\boldsymbol{q},\boldsymbol{\omega}) + 2U_{eff}\Gamma_\downarrow(\boldsymbol{q},\omega)\Gamma_\uparrow(\boldsymbol{q},\boldsymbol{\omega})}{1 - U_{eff}^2\Gamma_\uparrow(\boldsymbol{q},\omega)\Gamma_\downarrow(\boldsymbol{q},\omega)} \tag{1.63}$$

And this is the required expression for longitudinal susceptibility[13, 18].

1.2.3 Self Consistent Renormalisation Theory

In the last two sub sections we have derived the expression for the susceptibility in Stoner model and the RPA model. The expression for static susceptibility was obtained in the Stoner model. The Stoner model gave a criteria for the emergence of itinerant magnetism in a system called the Stoner condition. However, the expression for susceptibility obtained in the Stoner model is very crude and it turns out that it is very inaccurate when compared with experimental data for Curie temperature and susceptibility as a function of temperature.

The RPA model went a step further and calculated the Dynamical susceptibility of itinerant magnets. This is remarkable because through the calculation of dynamical susceptibility one can calculate the magnetic structure factor and

compare it with the neutron diffraction data.Before the RPA theory of itinerant magnetism was given there was a strong belief that the neutron diffraction data can only be explained using localised magnetism and the RPA model established that this data can be explained through itinerant magnetism too.

However as shown in Appendix A, in the long wavelength ($q \to 0$) and zero frequency ($\omega \to 0$) limit, the RPA expression for the susceptibility is the same as the one predicted by the Stoner model[13]. Hence the RPA expression is incorrect at the long wavelength ($q \to 0$) and zero frequency ($\omega \to 0$) limit and needs to be corrected. It is also important to note that RPA is a weak coupling approximation and it becomes ineffective when the value of the Hubbard interaction U is large. Additionally in RPA, the summing is over the ladder diagrams and hence in systems where exchange diagrams also contribute significantly, RPA becomes inapplicable[21].

T. Moriya and A. Kawabata adjusted the RPA expression at the ($q \to 0$) and ($\omega \to 0$) limit[1]. They did this by employing a modified Random phase approximation as the expression from conventional RPA is incorrect at the static limit. They modified the expression for susceptibility obtained from RPA by adding an additional temperature dependent parameter $\lambda(T)$ in the denominator. They then proceed to calculate the exact value of the susceptibility at the static limit employing a self-consistent scheme of calculation. Since the effects of electronic correlations at the static limit are taken in to account by a self-consistent scheme, hence the name Self-Consistent Renormalisation theory.

We will discuss the Self-Consistent Renormalisation theory of itinerant electron magnetism in detail in chapter 2.

1.3 Topology in Condensed Matter Physics

Band theory of electrons in solids has been a cornerstone in terms of its remarkable success in explaining the various physical properties of electrons in solid state systems[22]. The advent of topological band theory took it newer, uncharted territories.

As mentioned before one of the central goals of condensed matter physics is to characterise different phases of matter. At the same time it is also important to understand the phase transitions that occur due to the transition of the system from one phase to the other phase and the changes accompanied with such transitions.

Phase transitions in quantum systems were understood through spontaneous breaking of symmetries. Such transitions were in fact key to understand certain quantum phenomena like magnetism and superconductivity. Celebrated Physicist Lev Landau had introduced his theory of phase transitions through the introduction of an order parameter to explain such phase transitions[23].

However the introduction of topological order was a paradigmatic shift in the theory of phase transitions. Quantum Hall effect is one of the first examples of system which does not break any symmetries and has physical properties like the quantised Hall conductance which are insensitive to smooth changes in system parameters and do not change unless the system undergoes a quantum phase transition.

These quantum phase transitions in general do not require breaking of any symmetry. In fact, as we will see later, symmetry plays an important role in protecting the topological order of the system and breaking of the symmetries may lead to the change in the structure or complete loss of the topological order.

We will give a detailed introduction to the effects of topology in condensed matter systems in this section. We will begin with a brief introduction to the mathematical concept of topology in subsection 1.3.1. We will then discuss the application of the principles of topology to band theory and its consequences in subsection 1.3.2. We proceed then to the topological invariants which enable us to identify topological phase transitions and characterise topological phases in subsection 1.3.3. We will conclude this section with a discussion on the Bulk-Boundary correspondence in subsection 1.3.4 which is regarded as a very important concept in the context of topological condensed matter physics.

1.3.1 Topology

Topology is a branch of mathematics that deals with studying the properties of spaces or objects that are invariant under continuous transformations[24].

Often it has been described through the topological equivalence of two objects. The strict mathematical definition for two objects, say A and B to be topologically equivalent is there should exist a homeomorphism between these two objects. Homeomorphism is the condition that a continuous bijection and its inverse which is also continuous should exist between the two objects[24]. This makes homeomorphism a structure preserving map which preserves the topology of the space being considered and a lack of homeomorphism between two spaces indicates that they have different topology.

This can be explained with an example of a line segment and a circle. Suppose we map every point in the line segment to the circle through a function f, where the function, f is one to one and onto. It follows from the definition of f that it is a continuous function and making it a continuous bijection. However the inverse of f is discontinuous making the line and the circle not topologically equivalent. This is pictorially depicted in Figure 1.4.

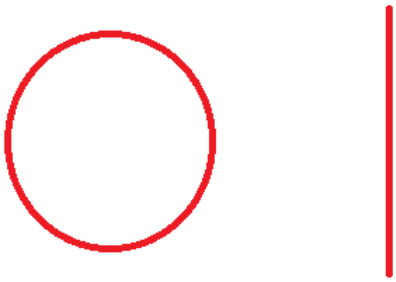

Figure 1.4: A circle and a line are topologically not equivalent.

A simpler definition from a physical perspective for topological equivalence is two objects are topologically equivalent if one can be deformed in to the other without poking holes are gluing certain parts with others. Simple example is that of a sphere and torus. The sphere cannot be deformed in to a torus without making a hole in it, making the sphere and torus topologically not equivalent. At the same time a sphere can be smoothly deformed in to a disk.

This can be understood more rigorously by associating an invariant with the objects and in this case it is the genus, which is essentially the number of holes. The genus associated with the sphere and the disk is zero and the one associated with the torus is one. Since the value of genus can take only integer values, objects with one genus cannot be smoothly deformed in to object with another genus[4]. This is illustrated in Figure 1.5.

Another topological invariant that is associated with surfaces is the Euler characteristic (χ). It is defined through the Gauss-Bonnet theorem as the integral of the Gaussian curvature (K) over a surface (S),

$$\chi = \int_S K \, dA \tag{1.64}$$

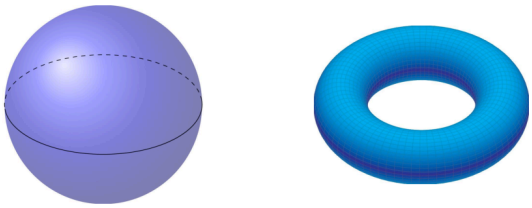

Figure 1.5: A sphere and a torus are not topologically equivalent.
[Source: arXiv:2201.07276]

Since the circle has constant curvature of $K = (1/R^2)$, the value of χ for the circle is:

$$\chi = 2. \tag{1.65}$$

From Equation 1.64, we see that the Euler characteristic takes only integer values and is related to the solid topological invariant genus as:

$$\chi = 2 - 2g. \tag{1.66}$$

Thus we see through Equation 1.66 that a relation exists between the solid and surface topological invariants and change in one of them will lead to the corresponding change in the other. This is called the Bulk-Boundary correspondence and as we will see later, it is at the heart of topological condensed matter physics.

The field of topology is very interesting and is an area of active research in mathematics. It is definitely impossible to give a complete flavor of it in a short discussion. However, considering the scope of this thesis, we end our discussion on topology here. The objective of this section was to familiarise the reader with abstract mathematical objects and concepts that would come handy later. We believe the introduction to topology presented here is self contained and good enough for understanding the effects of topology in condensed matter physics which we will take up in the coming sub-sections.

1.3.2 Topological Band Theory

The band theory of electrons is one of the most successful attempts made to understand solids. It explains the reason for certain materials to be insulators is the presence of band gap in these materials. This band gap separates the ground state from all the excited states, thus prohibiting the transport of an electron in the material, making it an insulator. This was the end of the picture for a while until the principles of topology where applied to band insulators. Before proceeding further we have to define the principle of adiabatic continuity as follows:

"The principle of adiabatic continuity states that if the system is in its ground state and the system parameters in the Hamiltonian are changed very slowly, the system continues to remain in the ground state of the changing Hamiltonian, given the ground state is gapped from other excited states"

The principle of adiabatic continuity then prompts us to define a geometric phase that would be picked up over a complete cycle. The concept of geometric phase existed before and was first pointed out by S. Pancharatnam in the context of interference of light in the year 1956[25]. It was later by Michael Berry in 1984[26] to quantum systems.

The principle of adiabatic continuity can be understood with the example of a particle in an one dimensional infinite square well. If the system is initially in the ground state $\left(\sqrt{\frac{2}{a}}cos(\frac{\pi x}{a})\right)$ and the width of the well is a and the width of the well is very slowly changed to $2a$, the particle will be in the ground state of the one dimensional infinite well with width $2a$, i.e. $\left(\sqrt{\frac{1}{a}}cos(\frac{\pi x}{2a})\right)$.

Now coming back to our discussion on band insulators, let us consider an insulator, (I_1) with band gap Δ and obviously $\Delta > 0$ for an insulator. Suppose we change the system parameters in the Hamiltonian very slowly and reach another insulator (I_2). Inspired from the definition of the topological equivalence discussed

in subsection 1.3.1, we can define that the insulators I_1 and I_2 are topologically equivalent if the value of the band gap has always been sufficiently greater than zero such that the system has always been in its ground state. If not then I_1 and I_2 are not topologically equivalent[4, 27].

It is interesting to note that if the insulators I_1 and I_2 are not topologically equivalent then, when the system parameters of the Hamiltonian are slowly varied to reach from I_1 to I_2 there exists some configuration of system parameters where the band gap vanishes. This is to say that the path from one insulator to the other is separated by a conducting state and one cannot reach from one insulator to another insulator which is topologically not equivalent to the first insulator without traversing this conducting state.

For simpler understanding if we compare the case of insulators with that physical objects the presence of conducting state in the insulators is the equivalent of making a cut or gluing a part in a physical object. This is to say that adiabatically continuing a Hamiltonian is similar the mathematical concept of continuous deformation of an object.

1.3.3 Topological Invariants

In the last subsection we have defined the principle of topological equivalence in the context of band insulators. The next logical step is to define topological invariants with which we can characterise these insulators based on their topology.

Since we are discussing band insulators, if we also assume the material that is being considered is crystalline then the translational symmetry allows us to label the states by their crystal momentum, k. From Bloch theorem these states are of the form:

$$|\psi(k)\rangle = e^{i\,k.r}\,|u(k)\rangle\,, \tag{1.67}$$

where $|u(k)\rangle$ are the periodic part of the Bloch wave function. We can immediately notice the intrinsic phase ambiguity of quantum mechanical wave functions, i.e. the inner products of the form $\langle u(k)|u(k)\rangle$ are gauge invariant under the following transformation:

$$|u(k)\rangle \rightarrow e^{i\,\phi(k)}\,|u(k)\rangle\,. \tag{1.68}$$

This prompts us to define the Pancharatnam-Berry phase (γ) for any closed loop (C) in the k space as:

$$\gamma = \oint_C dk\,\frac{\langle u(k)| - i\,\nabla\,|u(k)\rangle}{\langle u(k)\rangle\,u(k)}. \tag{1.69}$$

If we perform the following gauge transformation:

$$|\tilde{u}(k)\rangle = e^{-i\,\beta(k)}\,|u(k)\rangle\,, \tag{1.70}$$

and we calculate Pancharatnam-Berry phase for $|\tilde{u}(k)\rangle$ with its definition given in Equation 1.69, we get:

$$\tilde{\gamma} = \gamma + 2\pi\,m. \tag{1.71}$$

This implies the Pancharatnam-Berry phase is invariant under the gauge transformation Equation 1.70 up to a modulo 2π.

Before moving further, we would like to pause here and discuss the connection between the abstract mathematical objects discussed in subsection 1.3.1 and the physical quantities that we are discussing here. If we rewrite Equation 1.69 as:

$$\gamma = \oint_c A\,\cdot\,dk \tag{1.72}$$

where, A in Equation 1.72 is the Berry connection. Applying the Stokes theo-

rem to Equation 1.72, we get:

$$\gamma = \oint_c A \cdot dk = \int_S \nabla \times A \cdot dS = \int_S \mathcal{F} \cdot ds, \tag{1.73}$$

where $\mathcal{F} = \nabla \times A$ is the Berry curvature. If we observe Equation 1.64 and Equation 1.73, we find they are very similar (up to a 2π factor). Equation 1.64 is the expression for Euler characteristic and Equation 1.73 is for the Berry phase. Similarly in the place of Gaussian curvature in Equation 1.64, we have the Berry curvature in Equation 1.73.

If the system is one dimension then the Pancharatnam-Berry phase is called the Zak phase[28]. If the dimension of the system is two it is the Chern number. The Zak phase and the Chern number[29] are important topological invariants in one dimension and two dimensions respectively. Change in their value indicates a topological phase transition in the system.

Since their definition depends on the crystal momentum, k they are only defined for an infinite system or finite system with periodic boundary conditions. This makes them the bulk topological invariants.

Similar to the bulk topological invariants there exists boundary topological invariants which are defined only when the system size is finite i.e., when we employ open boundary conditions. The number of zero energy edge states and the number and the number of conducting edge modes are examples of boundary topological invariants in one and two dimension respectively.

1.3.4 Bulk-Boundary Correspondence

The validity of the Bulk-Boundary correspondence in the topological band insulators that we have discussed so far is at the heart of topological condensed matter physics[30].

In subsection 1.3.1, we saw the existence of Bulk-Boundary correspondence between the solid invariant genus and the surface invariant Euler characteristic[24]. A change in the genus automatically leads to a change in the Euler characteristic via the relation Equation 1.66.

Similarly in the case of the Su-Schrieffer-Heeger (SSH) model[2] (for a detailed introduction to SSH model, refer to chapter 4) which is an one dimensional gaped system, the Zak phase is the bulk invariant and the number of zero energy edge modes is the boundary invariant. If we change the system parameters in the Hamiltonian such that we cross the band closing point, the value of the Zak phase changes. In the finite bulk case this leads to the emergence (or disappearance) of zero energy edge states validating the existence of Bulk-Boundary correspondence in this system.

Similarly in the case two dimensions, take the example of the integer quantum Hall effect. A change in the value of the Chern number leads to the change in the number of conducting surface states validating the Bulk-Boundary correspondence[29].

With these examples it is clear that the Bulk-Boundary correspondence is valid for the topological classification of gaped systems that we have introduced in this section. In this thesis we will be interested in studying the effects of topology in SSH like dimer models in one and quasi-one dimension.

1.4 An overview of the thesis

In this thesis, we have studied the effects of interaction and topology in some condensed matter systems. The effects of interaction were studied through the Self-Consistent Renormalisation theory of itinerant magnetism. We find out that the ferromagnetic ordering in itinerant magnets is because of the Hubbard interaction and the electronic correlations play an important role in determining the physical quantities like Curie temperature. We study an hands on example by studying the case of itinerant magnetism in the unconventional material, $CaMn_2Al_{10}$.

We then formulate the Su-Schrieffer-Heeger model with any bulk (SAB model), to study topological systems in one and quasi one dimension with twists and branching. We also study the effects of disorder in the SAB model.

The first chapter is a general introduction to the effects of interaction and topology in characterising the phase of condensed matter systems. We introduce the Hubbard model, followed by an introduction to itinerant magnetism and the models of itinerant magnetism like Stoner model and RPA model and the need for the SCR theory of itinerant magnetism. This is followed by an introduction to topology and the field of topological band theory.

In the second chapter we introduce the complete formalism of the SCR theory. This is followed by the discussion of the algorithm of the numerical code that we have developed to calculate static susceptibility from the SCR theory. We conclude this chapter by showing some results from our numerical codes which are in agreement with already available literature to bench mark the validity of our results.

The third chapter is a presentation of results obtained by studying the case of itinerant magnetism in $CaMn_2Al_{10}$ through the SCR theory of itinerant mag-

netism. $CaMn_2Al_{10}$ being an unconventional, Mn based magnetic system in disagreement with the conventional wisdom for the type of magnetism based on the Mn-Mn distance was a well suited candidate to be studied by SCR theory. We present our calculations of static susceptibility through SCR theory and show that it is in excellent agreement with experimental results. Our DFT and DFT+U calculations point to the origin of itinerant nature of magnetism as the hybridisation between Mn and Al orbitals.

In the fourth chapter we formulate the new model based on the SSH model that we named as the Su-Schrieffer-Heeger model with any bulk (SAB model). We study the properties of various SAB models like three band, four band and six band SAB models. We find that these SAB models exhibit several exotic features like the simultaneous presence of both dispersive topological bands and flat bands in the same system. This leads to a large number of zero energy states localised in the bulk along with the zero energy edge states. Along with the eigenvalues and eigenvectors with different boundary conditions, we calculated topological invariants like Zak phase and localisation measures like inverse participation ratio. We end this chapter with possible experimental platforms on which our theoretical results can be verified.

In the fifth chapter, we study the robustness of the zero energy modes in the SAB model to chiral symmetry preserving and breaking disorders. We find that the major factors that affect the robustness of the zero energy states is the degeneracy of the flat band and the breaking or preserving of the chiral symmetry. We find that if the flat band is non-degenerate and the disorder preserves chiral symmetry, the zero energy states are robust to large disorders. In all other cases the zero energy cases acquire a finite bandwidth and close the band gap for a critical disorder strength, resulting in a localisation to delocalisation transition which is very rare.

We conclude by summarising and discussing the results obtained in the course

of this thesis in chapter six.

Part I

Itinerant magnetism and correlation effects

"An equation for me has no meaning, unless it expresses a thought of God."

Srinivasa Ramanujan

2

The Self-Consistent Renormalisation theory of itinerant electron magnetism

This chapter is dedicated to the clear and complete review of the formalism of the Self-Consistent Renormalisation (SCR) theory of itinerant electron magnetism formulated by T.Moriya and A.Kawabata. We will first review in detail the formalism of the SCR theory. Following this we will discuss in detail the algorithm of the computer codes, that we have developed to numerically obtain the value of static susceptibility through the calculations of the SCR theory. We will conclude by showing some calculations performed through these codes.

The phenomena of itinerant magnetism is very interesting owing to the fact that there are several unique features that are possible only in this form of magnetism unlike the localised magnetism[31]. The non-saturation of magnetisation for very high fields and the very low values of magnetic moment per atom are a few to quote among several such unique physical properties[32]. However, despite several attempts a comprehensive theory of itinerant magnetism remained elusive. Be it the mean field approximation based Stoner-Slater theory[17, 33] given by Stoner or the Random phase approximation based RPA model given by Izuyama, Kim and Kubo[18], the theories of itinerant magnetism could explain some of the aspects of itinerant magnetism but they couldn't quantitatively explain several other features[20, 34]. Of all the glaring issues in these theories were the overestimation of Curie temperature and lack of Curie-Weiss behavior in the inverse susceptibility as a function of temperature plot[1, 34].

Due to enhanced correlations in itinerant systems [35–52] ferromagnetic (FM) instabilities and [17, 33] and spin density wave (SDW) [53, 54] instabilities arise. At absolute zero ordering the spin fluctuations[55–57] with pronounced quantum character play an significant role in the measurement of quantities like magnetic susceptibility, specific heat, resistivity etc.

It is this juncture T.Moriya and A.Kawabata introduced the Self-Consistent Renormalisation theory of itinerant electron magnetism[1, 20, 34]. The remarkable success of this theory was in its ability to predict the physical quantities of interest accurately in the quantitative sense and not limited to only qualitative description[19–21, 34, 55–61]. The theory self-consistently takes in to account the effects of electronic correlations not taken in to account in the mean field description of Stoner and hence the name Self-Consistent Renormalisation (SCR) theory.

In this chapter we will begin with the complete review of the formalism of the SCR theory in section 2.1. We will then discuss in detail the algorithm of numerical codes that we have developed to obtain the static susceptibility as a function of temperature for an itinerant magnet in section 2.2. We will discuss

some results obtained by us using these numerical codes in section 2.3. We will conclude this chapter with a summary of the discussions in section 2.4.

2.1 The Self-Consistent Renormalisation theory of itinerant magnetism

In this section we will give a complete review of the formalism of the Self-Consistent Renormalisation (SCR) theory[13]. The essence of the SCR theory is in obtaining the expression for the inverse susceptibility which is made possible through the equations of the SCR theory. After obtaining this equations it remains only to solve these equations self-consistently.

We will begin this section describing the procedure to obtain an exact expression for susceptibility based on the one band Hubbard model Hamiltonian in subsection 2.1.1. This exact expression cannot be solved directly and to make this solvable, we will then introduce a modified Random Phase Approximation in subsection 2.1.2.

2.1.1 A general formula for the magnetic susceptibility

Our starting point is the one band Hubbard Hamiltonian. The Hubbard model considers only the on-site interactions and is a simple but an effective model to study systems with interacting electrons. The Hamiltonian of the one band Hubbard model is as follows:

$$H = \sum_{ij\sigma} T_{ij} a^{\dagger}_{i\sigma} a_{j\sigma} + \frac{U}{2} \sum_{i} n_{i\uparrow} n_{i\downarrow} \tag{2.1}$$

If we do the Fourier transformation of Equation 2.1 and diagonalise the Kinetic energy term with Bloch states owing to the translational symmetry in the system, we get the following equation,

$$H = H_0 + H'(U) \tag{2.2}$$

where,

$$H_0 = \sum_{k,\sigma} \varepsilon_k a^\dagger_{k\sigma} a_{k\sigma}, \tag{2.3}$$

is the free part of the Hamiltonian and

$$H'(U) = U \sum_{k,k',q} a^\dagger_{k+q\uparrow} a^\dagger_{k'-q\downarrow} a_{k'\downarrow} a_{k\uparrow}, \tag{2.4}$$

is the interacting part of the Hamiltonian. The spin raising and lowering operators are defined as follows:

$$\mathcal{S}_+(q) = \sum_k a^\dagger_{k+q\uparrow} a_{k\downarrow}; \qquad \mathcal{S}_-(q) = \sum_k a^\dagger_{k+q\downarrow} a_{k\uparrow}.$$

The interacting part can also be equivalently represented through the spin raising and lowering operators as:

$$H'(U) = \frac{1}{2}\mathcal{U}\mathcal{N} - \frac{1}{2}U \sum_q \left\{\mathcal{S}_+(q), \mathcal{S}_-(-q)\right\}, \tag{2.5}$$

where $\mathcal{N}$ is the total number of electrons, $\mathcal{U} = \mathcal{N}_0 U$ is the intra-atomic exchange energy, $\mathcal{N}_0$ is the number of atoms in the crystal and $\{\,,\}$ stands for the anti-commutator.

It is simple to verify the equivalence of Equation 2.4 and Equation 2.5. Starting from Equation 2.5 and writing spin raising $\mathcal{S}_+(q)$ and lowering $\mathcal{S}_-(q)$ operator in terms of creation and annihilation operators and with a little bit of algebra, we subsequently reach at Equation 2.4.

Next, the magnetic susceptibility in the unit of Bohr Magneton square (μ_B^2) is given as:

$$\chi = \left[\left(\frac{\delta^2 F(M)}{\delta M^2} \right)^{-1} \right]_{M=M^*}, \tag{2.6}$$

where, M is the magnetization, M^* is the saturation value of magnetization and $F(M)$ is the total free energy as a function of M *i.e.*, $M = N_\downarrow - N_\uparrow$ and $N = N_\downarrow + N_\uparrow$.

The partition function of the system in the presence of magnetic field is given as:

$$Z(H) = Tr \left[exp \left(\frac{-[\mathcal{H} + H M_z]}{K_B T} \right) \right], \tag{2.7}$$

where H is the magnetic field applied along the z-axis, $\mathcal{H}$ is the Hamiltonian of the system of interest and M_z is the component of magnetization along H. Therefore, the expression for free energy of the system is (from here on unless mentioned explicitly, the value of $K_B = 1$):

$$F(H) = -T \, ln \, Z(H). \tag{2.8}$$

Further, the free energy can be expressed as a function of M through the Laplace transformation to get the following expression:

$$Z(M) = \frac{1}{2\pi i} \int_{-i\infty-\epsilon}^{+i\infty+\epsilon} d\left(\frac{H}{T}\right) exp\left(\left(-\frac{H}{T} \right) M \right) Z(H). \tag{2.9}$$

Now with the definition, $F(M) = -T \, ln \, Z(M)$, for the free energy value for a given value of M, we have the relations:

$$\frac{F(M)}{T} = -lnZ(M); \qquad Z(M) = exp\left(-\frac{F(M)}{T}\right). \tag{2.10}$$

Therefore from Equation 2.9 and Equation 2.10 we get the following relation:

$$exp\left(-\frac{F(M)}{T}\right) = \frac{1}{2\pi iT}\int_{-i\infty-\epsilon}^{+i\infty+\epsilon} d(H)\, exp\left(\left(-\frac{1}{T}\right)[HM + F(H)]\right). \tag{2.11}$$

Now with the help of the saddle point approximation we get,

$$M = M^* = -\frac{\delta F(H)}{\delta H}, \tag{2.12}$$

where M^* is the equilibrium value of the magnetisation M. From Equation 2.12 (saddle point integral), we get the following:

$$F(M^*) = F(H) + HM^*. \tag{2.13}$$

Physically this means that the free energy $F(M)$ can be estimated by means of calculating the free energy under an applied magnetic field H which gives rise to the magnetization of M and then subtracting the contribution to the energy due to external field *i.e.*, $-HM^*$.

Further we express $F(M)$ as follows:

$$F(M) = F_0(M) + \int_0^U \frac{dU}{U}\left\langle \mathcal{H}'(U)\right\rangle_{M,U}, \tag{2.14}$$

where, the first term $F_0(M)$ corresponds to the free energy contribution of free electrons and the second term corresponds to the free energy coming from interactions. Equation 2.14 can be further decomposed in to:

$$F(M) = F_0(M) + \underbrace{F^U_{HF}(M) + \Delta F^U(M)}_{F^U(M)}. \tag{2.15}$$

In Equation 2.15 we have expressed the total free energy of the magnetic system in terms of magnetization as the sum of free energy terms due to free electrons, free energy contributed by the Hartree-Fock Approximation (HFA) term (Mean Field Contribution) and the term solely contributed by the correlation effects. The HFA term is of linear order while the correlation term is found to be of second order in nature.

From Equation 2.6 it is evident that the second order differentiation of $F(M)$ with respect to magnetization gives us χ^{-1}. The terms $(F^U_{HF}(M) + \Delta F^U(M))$ are the contributions to free energy from the interactions and together form the interaction term, $F^U(M)$ in Equation 2.14.

The expression for the contribution to the free energy solely from the effects of electronic correlations ($\Delta F^U(M)$) is given as:

$$\Delta F^U(M) = -\frac{1}{2}\sum_q \int_0^U \mathrm{d}U \left\{ \left\langle [S_+(q), S_-(-q)]_+ \right\rangle_{M,U} - \left\langle [S_+(q), S_-(-q)]_+ \right\rangle_{M,0} \right\}. \tag{2.16}$$

Now employing the fluctuation-dissipation theorem to express Equation 2.16 in terms of the dynamical susceptibilities, we get the following expression:

$$\Delta F^U(M) = -\frac{1}{2\pi}\int_{-\infty}^{+\infty} d\omega \coth\left(\frac{1}{2}\beta\omega\right) \mathrm{Im} \int_0^U dt \sum_q \left[\chi^{+-}_{M,U}(q,\omega) - \chi^{+-}_{M,0}(q,\omega)\right], \tag{2.17}$$

where $\chi^{+-}_{M,U}(q,\omega)$ in Equation 2.17 are the transversal dynamic susceptibilities under fixed values of M and U and are given by the expression:

$$\chi^{+-}_{M,U}(q,\omega) = i\int_0^\infty dt e^{i\omega t}\langle[S_+(q,t), S_-(-q)]\rangle_{M,U}\,. \tag{2.18}$$

After obtaining the expression for the renormalised free energy in Equation 2.17, that contains the additional contributions coming from the electronic correlations, we recall Equation 2.6 to obtain the expression for the susceptibility to be:

$$\chi = \frac{\chi_0}{1 - \frac{1}{2}U\chi_0 + \lambda(T)}, \tag{2.19}$$

where the temperature dependent parameter $\lambda(T)$ which brings in to account the effects of electronic correlations is given as:

$$\lambda(T) = \frac{1}{2\pi}\int_{-\infty}^{+\infty} d\omega \coth\left(\frac{1}{2}\beta\omega\right) g(\omega), \tag{2.20}$$

and the expression for $g(\omega)$ also termed as the spin fluctuation function is:

$$g(\omega) = -\chi_0 \,\mathrm{Im}\,\frac{\partial^2}{\partial M^2}\left(\int_0^\infty dU \sum_q \left[\chi^{+-}_{M,U}(q,\omega) - \chi^{+-}_{M,0}(q,\omega)\right]\right). \tag{2.21}$$

Equation 2.15 is an exact expression for the free energy, implying that Equation 2.19 along with Equation 2.20 and Equation 2.21 is an exact expression for finding the value of susceptibility. However the problem is Equation 2.21 requires the value of transversal dynamical susceptibilities as an input to proceed with the calculations and they are not available before hand.

In a sense we started of with the quest to find an expression for static susceptibility but obtained an expression which requires the dynamical susceptibilities

as inputs to proceed with the calculations. This conundrum is nicely illustrated in the following graphic.

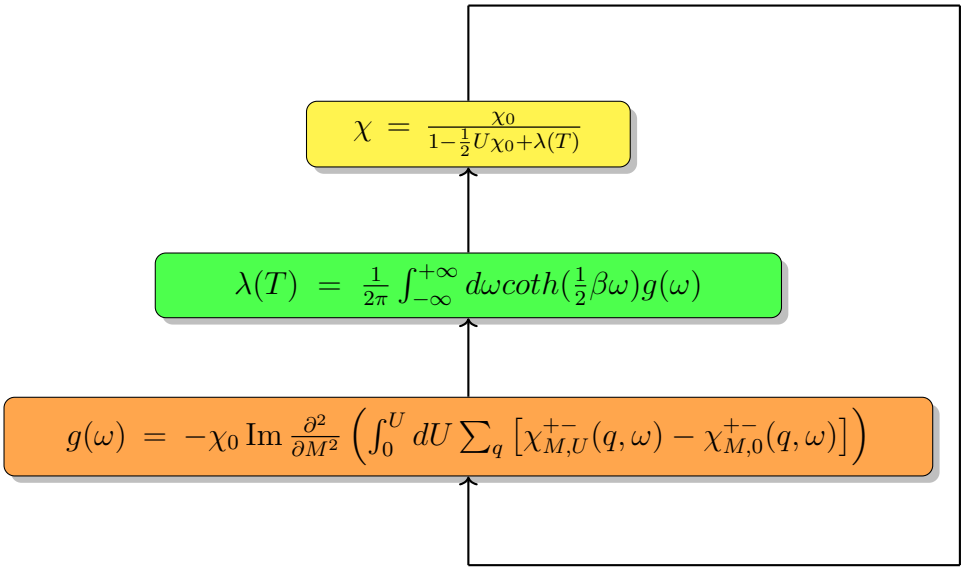

From the above graphic it is clear that the expression for static susceptibility χ requires the expression for $\lambda(T)$, which in turn requires the expression for $g(\omega)$ which depends on the transverse dynamical susceptibility, which is equivalent to asking for the values of susceptibility after starting to find one.

To resolve this conundrum we discuss the modified Random Phase Approximation in the next subsection 2.1.2.

2.1.2 Modified Random Phase Approximation

In subsection 2.1.1 the exact expression for susceptibility and the impossibility of solving it was discussed. The first hunch that follows is to substitute the expression for dynamical susceptibilities obtained in the RPA model. The problem in doing that is that the longer wavelength and zero frequency value of the dynamical susceptibility in the RPA model does not agree with the uniform susceptibility that we are calculating. This is because as discussed earlier and as shown in Appendix A, it coincides with the expression of the Stoner model in this limit due

to the lack of effects of electronic correlations which plays a crucial role. This is explained in detail in [13]. Hence this procedure would be incorrect to follow.

This inconsistency however, can be rectified by using a modified Random Phase approximation. A convenient feature of this approximation is that the value of magnetization M is kept constant, if we keep the longitudinal molecular field B to be constant for varying values of U. We will elaborate more on this procedure in this subsection.

As mentioned before the first logical direction to proceed will be to substitute the transversal dynamical susceptibilities values obtained from RPA model in Equation 3.4. The transversal dynamical susceptibilities under a fixed longitudinal molecular field B by using a random phase approximation is obtained as:

$$\chi^{+-}(q,\omega) = \frac{\chi_0^{+-}(q,\omega)}{\left[1 - U\chi_0^{+-}(q,\omega)\right]}. \tag{2.22}$$

Substituting Equation 2.22 in Equation 2.21, we get the following expression:

$$g(\omega) = -\xi\alpha^2(4\pi)^{-1}\,\mathrm{Im}\int \mathrm{d}q\{f_0(\partial^2 f_0/\partial B^2)(1-\alpha f_0)^{-1} + \partial f_0/\partial B)^2 (1-\alpha f_0)^{-2}\}, \tag{2.23}$$

with

$$\left.\begin{aligned} f_0 = f_0(q,\omega+\mathrm{is}) = \chi_0^{+-}(q,\omega+\mathrm{is})/(\chi_0/2) \\ \xi = (k_\mathrm{F}^3/2\pi^2\varepsilon_\mathrm{F}\chi_0)\,, \quad \alpha = U\chi_0/2 \end{aligned}\right\}, \tag{2.24}$$

where ζ equals to 1 for the electron gas model at $T = 0$ K and k_F (ϵ_F) is the Fermi wave-vector (Fermi-energy).

The expression Equation 2.23 for $g(\omega)$ is incorrect as we have obtained it directly from the RPA model.

Thus there needs to be some modification to the expression for $g(\omega)$ in order to obtain the correct value of susceptibility in the static limit. For this a modified random phase approximation is employed which will adjust the RPA susceptibility at $q = \omega = 0$. This modification is realised by replacing $(1-\alpha)/\alpha$ in Equation 2.23 by:

$$\delta = \chi_0/\alpha\chi = 2/U\chi = (1 - \alpha + \lambda)/\alpha. \tag{2.25}$$

A closer look at Equation 2.25 reveals that the modification performed here is indeed the same thing that we did to the expression of static susceptibility of the Stoner model shown in Equation 2.19. This makes it suitable to term δ as the inverse susceptibility. With the above modification Equation 2.23 becomes:

$$g(\omega) = -\xi(4\pi)^{-1} Im \int \mathrm{d}q\{\alpha f_0 \left(\partial^2 f_0/\partial B^2\right) (\delta + 1 - f_0)^{-1} + (\partial f_0/\partial B)^2(\delta + 1 - f_0)^{-2}\}. \tag{2.26}$$

One can thus obtain the magnetic susceptibility by solving the three equations Equation 2.20, Equation 2.25 and Equation 2.26 self consistently for the three variables δ, α and $g(\omega)$.

The value of Curie temperature can also be obtained through this method. The value of inverse susceptibility is zero at the Curie temperature which implies the value of δ is also zero. This leads us to the expression to determine the Curie temperature (T_c):

$$1 - \alpha\left(T_\mathrm{c}\right) + \lambda\left(0, T_\mathrm{c}\right) = 0 \tag{2.27}$$

where δ-dependence of $\lambda(0, T_c)$ comes from $g(\omega)$.

Before concluding this section we should make a few comments:

- The method discussed above based on solving the equations of SCR theory self-consistently through a modified Random Phase Approximation is one of the most accurate method available until now to calculate static susceptibility of itinerant magnets.
- This method is not only limited to the calculation of static susceptibility but enables one to calculate the Curie temperature of the system too. As the value of susceptibility diverges at the Curie temperature, the value of inverse susceptibility approaches zero. Hence by finding the temperature value where the inverse susceptibility becomes zero in the above method, one can calculate the Curie temperature. The SCR theory was very successful in calculating the susceptibility and Curie temperature of $ZrZn_2$, which was one of the first known weak itinerant magnet[20, 34].
- This method of modified random phase approximation has also been used for the calculation of transversal dynamical susceptibilities and Curie temperature for heavy Fermion like materials [62, 63].

We have now arrived at three equations that can be solved self-consistently to obtain the Curie temperature and static susceptibility of a itinerant magnet numerically. We will now discuss the algorithm of the numerical codes developed by us to calculate the same in section 2.2.

2.2 Algorithm for numerical calculation of susceptibility

In this section we will discuss in detail the algorithm based on which we developed our numerical codes to obtain the values of static susceptibility and Curie temperature through the SCR theory. Before discussing the algorithm we will discuss the pre-requisites to begin with the numerical calculation in subsection 2.2.1. Once

we have everything ready, we will outline how to numerically calculate the static susceptibility in subsection 2.2.2.

2.2.1 Pre-requisites for numerical calculation of susceptibility in SCR theory

From the discussions in the previous sections it is clear that the quantity $g(\omega)$ is central to the calculations that we wish to undertake. We will discuss in detail its calculations and the nuances involved thereof in this subsection. The expression for $g(\omega)$ given in Equation 2.26 is:

$$g(\omega) = -\xi(4\pi)^{-1} Im \int \mathrm{d}q \{\alpha f_0 \left(\partial^2 f_0/\partial B^2\right) (\delta + 1 - f_0)^{-1} + (\partial f_0/\partial B)^2 (\delta + 1 - f_0)^{-2}\}. \tag{2.28}$$

Expanding it further by writing $f_0(q,\omega)$ in terms of its real and imaginary parts:

$$f_0(q,\omega) = f_0'(q,\omega) + i f_0''(q,\omega), \tag{2.29}$$

we get the following expression for $g(\omega)$,

$$\begin{aligned} g(\omega) = -\int \mathrm{d}q\, q^2 [E(q,\omega)\{\alpha(1+\delta)[f_0''(\partial^2 f_0'/\partial B^2) + f_0'(\partial^2 f_0''/\partial B^2)] \\ -\alpha[(f_0')^2 + (f_0'')^2](\partial^2 f_0''/\partial B^2)\} + 2[E(q,\omega)]^2\{[(\delta + 1 - f_0')^2 - \\ (f_0'')^2](\partial f_0'/\partial B)(\partial f_0''/\partial B) + (\delta + 1 - f_0')\, f_0''[(\partial f_0'/\partial B)^2 - (\partial f_0''/\partial B)^2]\}], \end{aligned} \tag{2.30}$$

where,

$$E(q,\omega) = \left[(\delta + 1 - f_0')^2 + (f_0'')^2\right]^{-1}. \tag{2.31}$$

It is clear from Equation 2.30 that to proceed further with the calculations of $g(\omega)$, we require the expressions for $f_0'(q,\omega)$, $[\partial f_0'(q,\omega)/\partial B]_{B=0}$, $[\partial^2 f_0(q,\omega)/\partial B^2]_{B=0}$ and $f_0''(q,\omega)$, $[\partial^2 f_0''(q,\omega)/\partial B^2]_{B=0}$, $[\partial f_0''(q,\omega)/\partial B]_{B=0}$. These are already available in the literature.

Important expressions for the real and imaginary parts of the free electron model are as follows:

Real parts i.e., $f_0'(q,\omega)$ and its derivatives are given by the following expressions:

$$\begin{aligned} f_0'(q,\omega) = (1/2) - \left\{\left[q^4 - (4-2\omega)q^2 + \omega^2\right]/16q^3\right\} \\ \log\left|(q+q_1)(q+q_2)/(q-q_1)(q-q_2)\right| - \left\{\left[q^4 - (4+2\omega)q^2 + \omega^2\right]/16q^3\right\} \\ \log\left|(q+q_0)(q+q_3)/(q-q_0)(q-q_3)\right|, \end{aligned} \tag{2.32}$$

$$[\partial f_0'(q,\omega)/\partial B]_{B=0} = \left(\omega/4q^3\right)\sum_{m=0}^{3}\log\left|(q+q_m)/(q-q_m)\right|, \tag{2.33}$$

$$\begin{aligned} \left[\partial^2 f_0(q,\omega)/\partial B^2\right]_{B=0} = \left(1/2q^2\right)\left\{\left[q^4 - (4-\omega)q^2 + 4\omega\right]\right. \\ \left(q^2 - {q_1}^2\right)^{-1}\left(q^2 - q_2^2\right)^{-1} + \left[q^4 - (4+\omega)q^2 \quad - 4\omega\right] \\ \left.\left(q^2 - q_0^2\right)^{-1}\left(q^2 - {q_3}^2\right)^{-1} - q^{-1}\left[1 + \left(q^2/4\right)\right]\sum_{m=0}^{3}\log\left|(q+q_m)/(q-q_m)\right|\right\}. \end{aligned} \tag{2.34}$$

Imaginary parts i.e., $f_0''(q,\omega)$ and its derivatives are given by the following expres-

sions:

$$f_0''(q,\omega) = (\pi/4)(\omega/q)\theta\left(q-q_1\right)\theta\left(q_2-q\right) \quad + \left(\pi/16q^3\right)\left(q^2-q_0^2\right)\left({q_3}^2-q^2\right)$$
$$\left[\theta\left(q-q_0\right)\theta\left(q_3-q\right)-\theta\left(q-q_1\right)\theta\left(q_2-q\right)\right]$$
$$= \left(\pi/16q^3\right)\left[\left(q^2-q_0^2\right)\left(q_3^2-q^2\right)\theta\left(q-q_0\right)\theta\left(q_3-q\right)\right.$$
$$\left.-\left(q^2-{q_1}^2\right)\left({q_2}^2-q^2\right)\theta\left(q-q_1\right)\theta\left(q_2-q\right)\right], \tag{2.35}$$

$$\left[\partial {f_0}''(q,\omega)/\partial B\right]_{B=0} = (\pi/4)\left(\omega/q^3\right)\left[\theta\left(q-q_0\right)\left(q_3-q\right)-\theta\left(q-q_1\right)\theta\left(q_2-q\right)\right], \tag{2.36}$$

$$\left[\partial^2 {f_0}''(q,\omega)/\partial B^2\right]_{B=0} = -\left(\pi/2q^3\right)\left[1+\left(q^2/4\right)\right]\left[\theta\left(q-q_0\right)\theta\left(q_3-q\right)-\right.$$
$$\left.\theta\left(q-q_1\right)\theta\left(q_2-q\right)\right] \quad + \left(\pi/8q^2\right)\left\{(1+\omega)^{-1/2}\left[{q_0}^2\delta\left(q-q_3\right)+{q_3}^2\delta\left(q+q_0\right)\right]\right.$$
$$\left.-(1-\omega)^{-1/2}\left[{q_2}^2\delta\left(q-q_1\right)+{q_1}^2\delta\left(q-q_2\right)\right]\right\}, \tag{2.37}$$

where

$$\left.\begin{matrix} q_1 \\ q_2 \end{matrix}\right\} = 1 \mp (1-\omega)^{1/2}$$

$$\left.\begin{matrix} q_0 \\ q_3 \end{matrix}\right\} = 1 \mp (1+\omega)^{1/2}$$

$$s = \omega/q$$

$$F(x) = (1/2)\left\{1+\left[\left(1-x^2\right)/2x\right]\log|(1+x)/(1-x)|\right\}$$

The above expressions for real and imaginary parts of $f_0(q,\omega)$ and its derivatives are given in [1] and is given for the free electron model at zero temperature. With all the above expressions we can calculate the value of $g(\omega)$ as a function of ω for a given value of δ. The plots of $g(\omega)$ as a function of ω for different values of δ is given in section 2.3 for the reader's perusal.

2.2.2 Algorithm for numerical calculation static susceptibility through SCR theory

After being able to calculate the function $g(\omega)$ for any given δ, we now have everything that is needed to calculate the value of static susceptibility self-consistently through numerical methods.

Schematic diagram of the algorithm to calculate the static susceptibility from the SCR theory

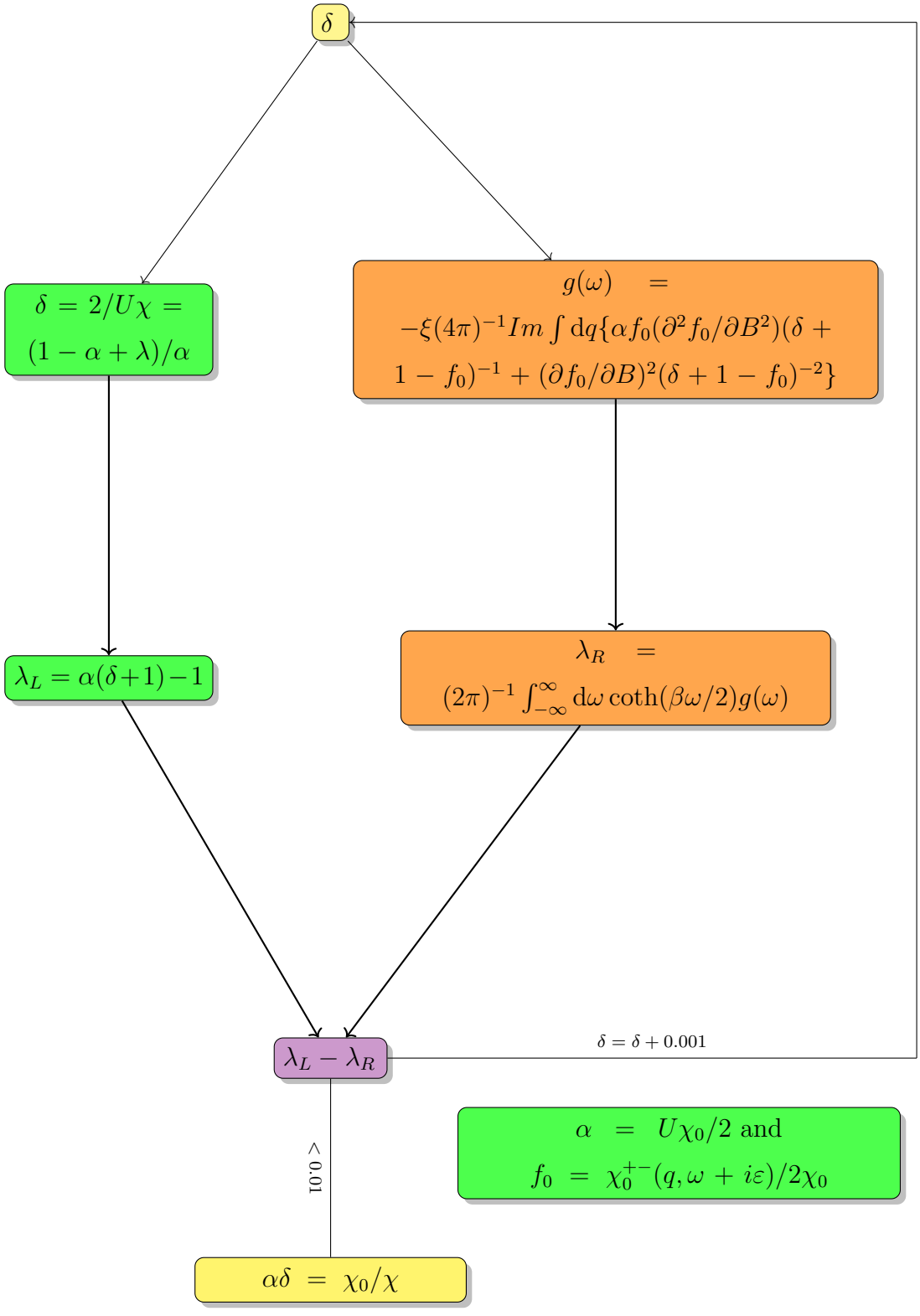

The algorithm to calculate the static susceptibility is as follows:

1. We should start with an optimum value of δ to begin the calculation with. If in case there can be no initial guesses made for the value of δ start with the value $\delta = 0$.

2. For the value of δ assumed calculate the corresponding $g(\omega)$. This is possible thanks to the discussions in subsection 3.3.1.

3. From the calculated $g(\omega)$, calculate the function λ_R using Equation 2.19. Notice the temperature dependence of λ in Equation 2.19. Begin with a single initial temperature value to perform the calculations (Note that the temperature here is in reduced unit of T/T_F, T_F is the Fermi temperature).

4. Invert equation Equation 2.25, to obtain λ for a given value of δ.

5. Now using this inverted equation, for the same chosen value of δ, calculate λ_L.

6. If the difference: $|\lambda_L - \lambda_R|$ is less than certain tolerance value, the chosen value of δ is the correct value of δ predicted by the SCR theory. We have set the tolerance value to be 0.01.

7. If $|\lambda_L - \lambda_R|$ is greater than certain tolerance value, increment the value of δ by a small number and repeat the process from step 2 to step 5 again. We have incremented the value of δ by 0.001 to repeat the calculation every time.

8. Keep repeating the process by incrementing δ again and again until $|\lambda_L - \lambda_R|$ converges within the tolerance value. The δ value for which it converges is the value of δ predicted by SCR theory.

9. Change the value of temperature and repeat step 1 to step 8 for the newly chosen value of temperature.

10. Calculate δ for various values of temperature

11. From the value of δ obtained for various temperatures plot the inverse susceptibility as a function of temperature.

The above mentioned algorithm is also shown in a schematic form for reference. Through this algorithm the value of static susceptibility of various itinerant magnets can be calculated through SCR theory. We have obtained some results to verify that the results obtained from our numerical calculations are indeed correct. We will discuss these results in section 2.3.

More technical comments on the algorithm will be given in Appendix B and we suggest the interested reader to refer the same.

2.3 Results and discussions

In this section we will discuss some results obtained through our numerical implementation of SCR theory.

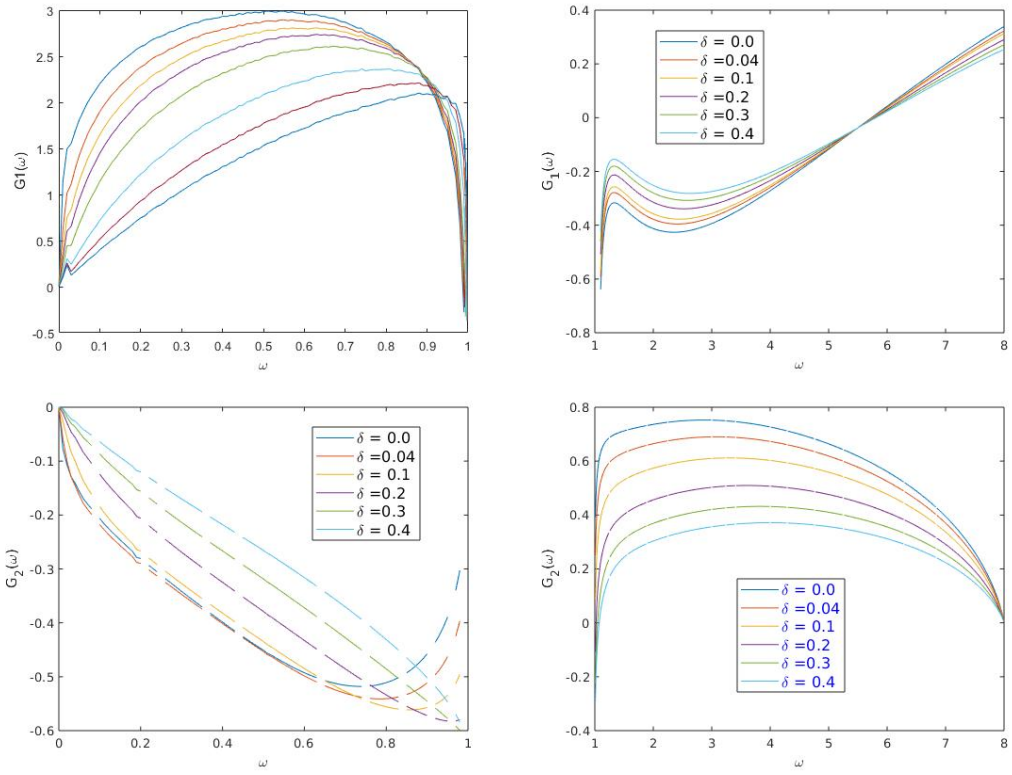

Figure 2.1: $G_1(\omega)$ (top panel) and $G_2(\omega)$ (bottom panel) as a function of ω.

First let us present our calculations for the value of $g(\omega)$ as a function of ω for

any given value of δ. $g(\omega)$ can be split in to two functions, given as:

$$g(\omega) = \alpha\, G_1(\omega) + G_2(\omega) \tag{2.38}$$

Hence it is sufficient to know the values of $G_1(\omega)$ and $G_2(\omega)$ to find the value of $g(\omega)$. The values of $G_1(\omega)$ and $G_2(\omega)$ as a function of ω are given in Figure 2.1.

After obtaining $g(\omega)$ as a function of ω for a given value of δ, we can then calculate the value of inverse susceptibility as a function of temperature for various interaction strengths α. This is shown in Figure 2.2.

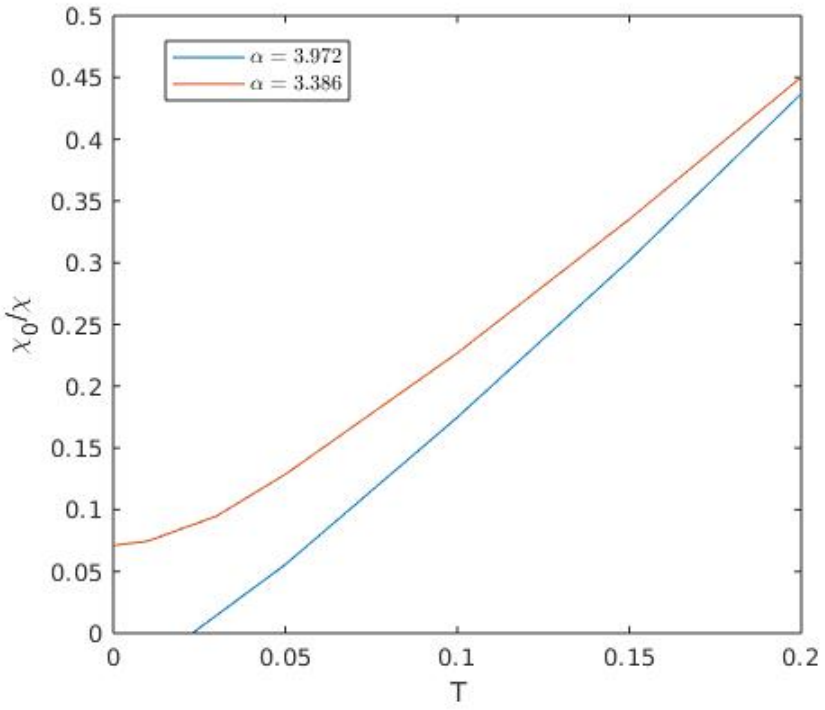

Figure 2.2: Inverse susceptibility (χ_0/χ) as a function of temperature (T/T_F) for two values of interaction strength (α).

In this way using the numerical code developed by us we can calculate the static susceptibility corresponding to various strength of interaction parameter through the SCR theory.

From Figure 2.2, it is clear that the value of the inverse paramagnetic susceptibility obtained from the SCR theory varies (almost) linearly with temperature.

This behavior is in fact the experimentally observed behavior of paramagnetic susceptibility. The temperature at which the value of inverse paramagnetic susceptibility reaches zero is where the paramagnetic susceptibility diverges and is the Curie temperature. Hence we can also calculate the Curie temperature from the above calculation. For weak itinerant magnets like $ZrZn_2$, the value of the Curie temperature obtained from SCR theory is close to the experimentally observed value.

The original formulation of SCR theory discussed in [1], can be applied to only certain values of the cut-off parameter q_c (up to $q_c = 2$). Our algorithm is very general from the original formulation because in our algorithm we can calculate for arbitrarily large q_c. This will be handy for problems where the value of α will be high.

2.4 Summary

In this chapter we started with a detailed introduction to the formalism of the Self-Consistent Renormalisation (SCR) theory in section 2.1 . We started with an one band Hubbard Hamiltonian and derived an exact expression for susceptibility that can in principle be obtained by solving a set of three equations subsection 2.1.1. However, since these equations can only be solved self-consistently, we introduce a modified Random Phase Approximation for the same subsection 2.1.2. We then discussed the pre-requisites for the numerical calculations in subsection 2.2.1. After this we discussed in detail the algorithm of the numerical codes that we designed to solve the equations of SCR theory self-consistently and obtain the value of inverse static susceptibility in subsection 2.2.2. We presented the results that we obtained through our numerical calculations in section 2.3.

After having developed the codes for calculating the static susceptibility and Curie temperature through SCR theory, we wish to test it hands on in an actual physical system. We have chosen $CaMn_2Al_{10}$ for such a study due to several exotic

and novel physical properties the system exhibits. We will discuss this study in detail in chapter 3.

"Creativity is contagious pass it on".

Albert Einstein

3

Self-Consistent Renormalisation (SCR) theory studies of itinerant magnetism in $CaMn_2Al_{10}$

The compound $CaMn_2Al_{10}$ exhibits anomalous magnetic behavior not in accordance with the conventional wisdom of magnetism relating to Mn-Mn distance in Mn based Magnetic systems. According to the conventional wisdom, if the Mn-Mn distance is greater than 2.7 Å, then the system exhibits localised form of magnetism. We study the static susceptibility of this system, $CaMn_2Al_{10}$ through the SCR theory and prove that magnetism in the case of $CaMn_2Al_{10}$ is indeed of itinerant nature. We calculate the value of Hubbard interaction parameter (U), by fitting the experimental data with the numerical calculations of SCR theory and classify it as an intermediately correlated system. We also perform DFT and DFT+U studies, with the value of U obtained from SCR theory, to pin point the origin of the anomalous magnetic behavior of $CaMn_2Al_{10}$ is in the hybridisation of Mn 3d orbitals with Al 3s orbitals in this system.

The recently synthesised Manganese (Mn) based magnetic system $CaMn_2Al_{10}$ has been of considerable interest. The wide range of interests in this system ranges from its potential to be a lower dimensional system with strong quantum fluctuations and to be an itinerant magnet with a low Curie temperature ($\sim$ 3 K). However the central piece in all the puzzles that these interests stem from is *"the character of magnetism in $CaMn_2Al_{10}$"*. According to the conventional wisdom, if the Mn-Mn distance is greater than 2.7 Å, then the system exhibits localised form of magnetism. This system has been conjectured to be an itinerant magnet based on some of the experimental observations. However the system should be a local magnet based on the conventional wisdom relating to the nature of magnetism in a Mn based system and the Mn-Mn distance in that system. If the itinerant nature in $CaMn_2Al_{10}$ can be proved and understood rigorously through a theoretical framework, it would lay the foundation for further studies on this system to shed more light on its exotic properties.

In this chapter we will try to unravel the nature of magnetism in $CaMn_2Al_{10}$ through the powerful Self-Consistent Renormalisation (SCR) theory. The SCR theory has been a well tested and proven theory for a variety of weak itinerant ferromagnets. Its predictions are very accurate that applicability of SCR theory to a material acts as an litmus test to determine the itinerant character of magnetism in that material. Hence we will determine the applicability of SCR theory to $CaMn_2Al_{10}$ to decide on the character of magnetism in that system. We will also undertake some first principle studies (DFT and DFT+U) to decipher the origin of magnetism in $CaMn_2Al_{10}$.

3.1 Conventional wisdom of Mn-Mn distance in Mn based systems and exceptional behavior of $CaMn_2Al_{10}$

In this section we will discuss the conventional wisdom relating to the nature of magnetism in Mn based magnetic systems and the nature of magnetism predicted by this rule for $CaMn_2Al_{10}$. We will begin with a brief review of localised and

itinerant pictures of magnetism and the key differences between these pictures in subsection 3.1.1. This would set the foundation for our further discussion on the conventional wisdom relating to the Mn-Mn distance and the form of magnetism in subsection 3.1.2. We will conclude this section with the applicability of this rule in $CaMn_2Al_{10}$ in subsection 3.1.3.

3.1.1 Magnetism: local picture vs itinerant picture

Magnetism can broadly be classified in to two types based on the mobility of the electrons whose magnetic moments align giving rise to the magnetic character of the system. If we term these electrons as magnetic electrons the following two scenario arises:

1. The magnetic electrons are localised at the respective atomic sites and are immobile. The magnetism emerging from such electrons is called **localised magnetism**. The Heisenberg model is best suited for studying the materials exhibiting this form of magnetism.
2. The magnetic electrons are mobile and can move from one site in the lattice to another site. This form of magnetism is called **itinerant magnetism**. In itinerant magnetism the magnetic electrons are also the conduction electrons in the material. SCR theory is by far the best available approach to study the materials exhibiting this form of magnetism.

After defining the two forms of magnetism it is important to differentiate between these two forms of magnetism. In this direction we make the following comments.

- **Magnetisation:**
    1. **Local magnetism:** The value of magnetisation saturates for the case of local magnets for lower values of temperature and higher values of magnetic field.

2. **Itinerant Magnetism:** The value of magnetisation does not saturate for the case itinerant magnets for lower values of temperature and higher values of applied magnetic field that are practically possible (around 10 Tesla)[64].

This can be understood as in the case of itinerant magnetism, even in very high applied magnetic fields the spins can easily flip and become parallel to the magnetic field. In fact the increase of magnetisation with increase of magnetic field in very high magnetic field is called the high field susceptibility (χ_{hf}) and is a characteristic feature of itinerant magnetism. This is not true to for local magnets as all the local spins saturate for a finite applied magnetic field and it is next to impossible to flip any spin further.

- **Electronic contribution to specific heat:**

1. **Local magnetism:** The electronic contribution to specific heat above the Curie temperature is nearly zero for the case of local magnets.
2. **Itinerant Magnetism:** The electronic contribution to specific heat above the Curie temperature is is finite for the case of itinerant magnets.

This can be attributed to the fact that the magnetic electrons can contribute to the specific heat only in the ordered phase for the case of local magnets. However in the case of itinerant magnets the magnetic electrons are also the conduction electrons. Hence even above the Curie temperature their contribution to specific heat remains finite.

- **The value of the Curie-Weiss moment:**

1. **Local magnetism:** The value of the Curie-Weiss moment per magnetic atom (μ_{CW}) obtained from the plot of inverse of susceptibility as a function of temperature can take only certain values. This is because the number of electrons localised at a site is always an integer which restricts the values μ_{CW} can take.
2. **Itinerant Magnetism:** The value of the Curie-Weiss moment per magnetic atom (μ_{CW}) obtained from the plot of inverse of susceptibility as

a function of temperature can take any values and can even be less than one.

The value of μ_{CW} is given as: $\mu_{CW} = \sqrt{n(n+2)}\,\mu_B$, where μ_B refers to Bohr magnetons. The value of n in case of local magnets is restricted to only integer values ($n \in \mathbb{Z}$) as the number of electrons localised at a particular atomic site has to be an integer. Hence the value of μ_{CW} is also restricted to particular values corresponding to the integer values of n. However for the case of itinerant magnets, the electrons are mobile and the average occupancy at each site is not required to be an integer and is almost always not. This allows the value of μ_{CW} to take any values. The average occupancy per site can also be less than one allowing μ_{CW} to take values even less than one[65, 66].

The final point relating to the value of μ_{CW} is of immense importance in our study and is also a very important experimental signature in conjecturing $CaMn_2Al_{10}$ to be an itinerant magnet. After understanding in detail the characteristic differences between the local and itinerant forms of magnetism, we can now proceed to the discussion on the conventional wisdom based on the Mn-Mn distance argument in Mn based magnetic systems.

3.1.2 Conventional wisdom in Mn based Magnetic systems

Manganese compounds in general are known for their strong magnetic character stemming from the Hund's coupling. This is evident even in elemental Mn which has a complex crystal structure and phase diagram which is a consequence of two competing tendencies. (a) to maximise the Mn-Mn distance consequently increasing the magnetic moment according to Hund's coupling and (b) to minimise Mn-Mn distance to increase the metallic bond strength but subsequently quenching the magnetic moments.

This dichotomy in Manganese compounds is visible as in the cases when the Coulomb interaction is very strong the Mn compounds are robust insulators as

in LaMnPO and $CaMn_2SB_2$ or in the cases when the Mn orbitals are strongly hybridised with conduction electrons leading to a much lesser magnetic moment as in MnSi. Much of the Mn compounds fall in the former category in contrast to only few in the later.

This competition between the two tendencies in Mn systems to either maximise the magnetic moment[44, 50, 67–73] or the metallic bond strength[43, 64, 74–76] has lead to a rule of thumb regarding the Mn-Mn distance in the system and its magnetic nature.

The conventional wisdom in the Mn based magnetic systems is the following rule of thumb:

"If the Mn-Mn distance in a system is less than 2.7 Å the system exhibits the phenomena of itinerant magnetism and if Mn-Mn distance is greater than 2.7 Å it exhibits the phenomena of local magnetism."

This can be intuitively understood by the fact that the lesser the Mn-Mn distance in real space corresponds to more bandwidth in the inverse space, thus leading to itinerant nature of magnetism. For more Mn-Mn distance in real space the bandwidth is narrow in the inverse space leading to localisation of magnetic electrons in the real space.

The value of Mn-Mn distance in $CaMn_2Al_{10}$ is evident from Figure 3.1 and is always greater than 2.7 Å. Thus the conventional wisdom predicts that $CaMn_2Al_{10}$ should exhibit localised form of magnetism. We will discuss this in detail in the next subsection 3.1.3.

3.1.3 The curious case of $CaMn_2Al_{10}$

We will begin the discussions in this section with a brief introduction and background to the $CaMn_2Al_{10}$ system. We will then discuss the applicability of the conventional rule of thumb relating to Mn-Mn distance to $CaMn_2Al_{10}$ and then discuss the reasons and interests drawing us towards this system to be studied through the formalism of SCR theory of itinerant electron magnetism.

The crystal structure of $CaMn_2Al_{10}$ is shown in Figure 3.1. It has been reported that single crystal samples of $CaMn_2Al_{10}$ were grown as square rods as big as $1 \times 1 \times 10\, mm^3$ with the crystallographic axes coinciding c-axis with the rod axis[64]. X-ray studies reported on these samples of $CaMn_2Al_{10}$ has ruled out any appreciable site disorders leading us to believe that the experimental data we will be using to compare theoretical results are very reliable.

A closer inspection of the crystal structure reveals that the inter planar and intra planar Mn-Mn distance in $CaMn_2Al_{10}$ is 5.17 Å and 4.53Å respectively. Both of these values are greater than the critical value of 2.7Å predicted by the rule of thumb. This leads to the conclusion that according to the conventional wisdom $CaMn_2Al_{10}$ should exhibit localised form of magnetism with high magnetic moment per Mn atom.

However the experimental data for different physical properties paint a different picture than the one informed by the conventional wisdom. The data for magnetisation as a function of applied field shows that there is no saturation for high applied fields. But the glaring example is that of the inverse of paramagnetic susceptibility as a function of temperature and the value of the Curie-Weiss moment (μ_{CW}) obtained from that data shown in Figure 3.2. The value of μ_{CW} obtained from the fit is $0.83\mu_b$/Mn atom which is much lesser than expected and cannot be originating from a localised form of magnetism.

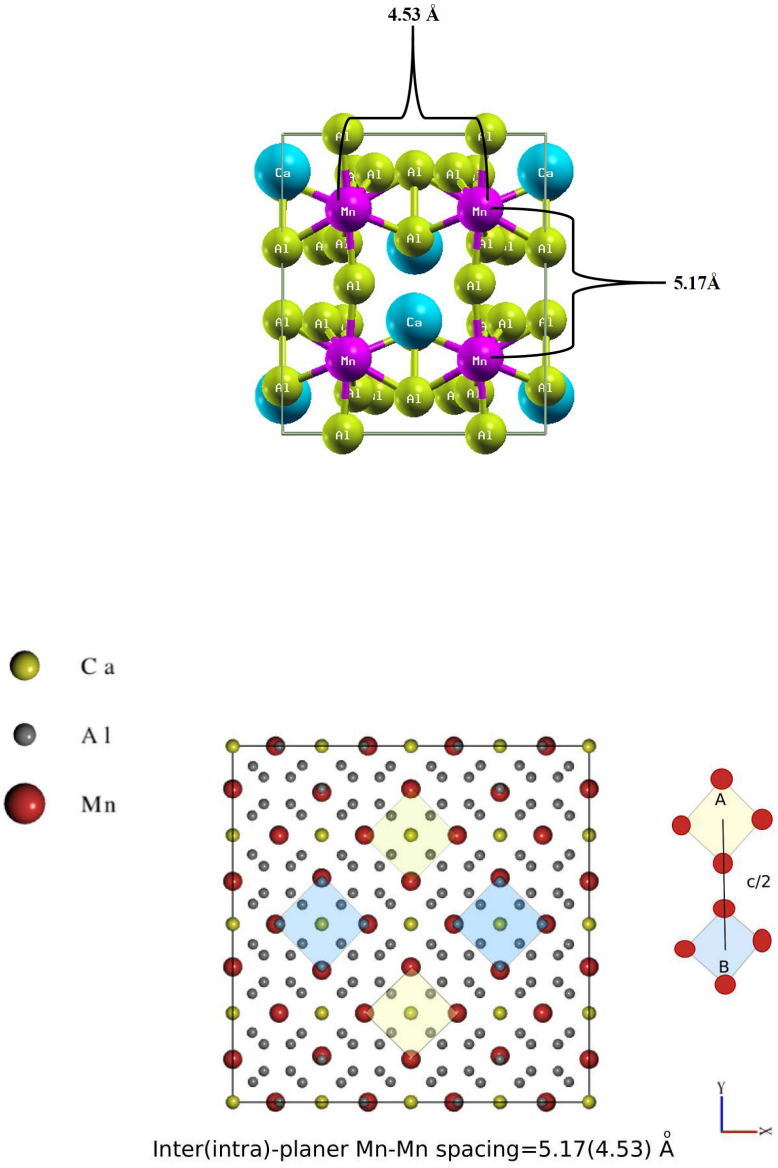

Figure 3.1: Crystal structure of $CaMn_2Al_{10}$ in 3d projection and 2d projection (top to bottom). Notice that the inter and intra planar Mn-Mn distance is greater than the cut-off value of 2.7 Å.

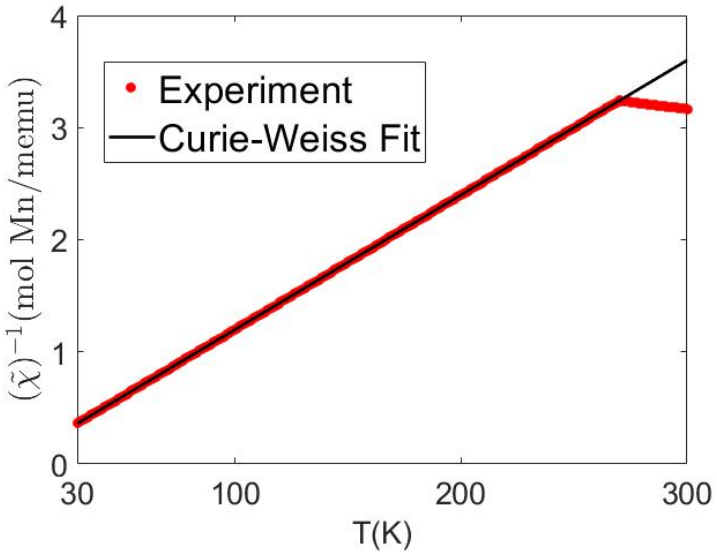

Figure 3.2: Inverse of Static susceptibility plotted as a function of temperature and the Curie-Weiss fit to the data.

The above discussions point to the fact that the magnetism in $CaMn_2Al_{10}$ is indeed novel and needs more theoretical understanding to be fully unpacked. As a first step in this direction we attempt to reproduce the static susceptibility data of this system and extract theoretical parameters which would be helpful for further explorations in this system.

3.2 Equations of the SCR theory

In this section we will quickly recall the equations of the Self-Consistent Renormalisation (SCR) theory that we will have to solve self consistently to obtain the value of static susceptibility at various temperatures. We will also explain the various terms in these equations in short. For a detailed discussion on the SCR theory the reader is suggested to consult chapter 2.

The basic recipe of the SCR theory is that the Stoner expression for static susceptibility being a mean field expression does not include the effects of electronic correlations. Thus an extra temperature dependent term should be added to the

Stoner expression modifying it as:

$$\chi(T) = \frac{\chi_0}{1 - \frac{1}{2}U\chi_0 + \lambda(T)}, \tag{3.1}$$

where $\chi(T)$ is the static susceptibility, χ_0 is the Pauli susceptibility (which is nearly independent of temperature in the temperature range of our interest), U is the Hubbard interaction parameter and $\lambda(T)$ is the newly added extra term.

It now remains to determine the value of $\lambda(T)$ and the complete guide for this is given in chapter 2. In short this requires some particular three equations to be solved self consistently.

The three equations of the SCR theory derived in subsection 2.1.2 (Equation 2.20, Equation 2.25 and Equation 2.26), that has to be solved self consistently are:

$$\lambda(T) = \frac{1}{2\pi}\int_{-\infty}^{+\infty} d\omega \coth\left(\frac{1}{2}\beta\omega\right) g(\omega) \tag{3.2}$$

$$\delta = \chi_0/\alpha\chi = 2/U\chi = (1 - \alpha + \lambda)/\alpha. \tag{3.3}$$

$$\begin{aligned} g(\omega) = -\xi(4\pi)^{-1} Im \int \mathrm{d}q\{\alpha f_0 \left(\partial^2 f_0/\partial B^2\right)(\delta + 1 - f_0)^{-1} + \\ (\partial f_0/\partial B)^2(\delta + 1 - f_0)^{-2}\}. \end{aligned} \tag{3.4}$$

here,

$$\left.\begin{aligned} f_0 = f_0(q, \omega + \mathrm{is}) = \chi_0^{+-}(q, \omega + \mathrm{is})/(\chi_0/2) \\ \xi = (k_\mathrm{F}^3/2\pi^2\varepsilon_\mathrm{F}\chi_0)\,, \quad \alpha = U\chi_0/2 \end{aligned}\right\} \tag{3.5}$$

where ζ equals to 1 for an electron gas model at $T = 0$ K and k_F (ϵ_F) is the Fermi

wave-vector (Fermi-energy).

We should also mention here that the temperature in the equations of SCR theory is in the scaled units of (T/T_F) where T_F is the Fermi temperature of the system and the wave vector is in the scaled units of (q/q_F) with q_F being the Fermi wave vector.

Solving the above set of three equations self consistently with the procedure outlined in the algorithm in chapter 2, we can obtain the theoretically calculated plots of static susceptibility from SCR theory. We will discuss the theoretical plots and compare it with the experimental data in the next section i.e. section 3.3.

3.3 Comparison of SCR Theory results with experiments

In this section we will present the theoretically calculated results through the formalism of SCR theory and compare them with experimental data. We will first survey and calculate the necessary pre-requisites for such an analysis in subsection 3.3.1. Once this is complete we will then discuss the agreement between theoretical calculations and experimental data in subsection 3.3.2 and conclude this section summarising all the results obtained and their importance.

3.3.1 Pre-requisites for comparing theoretical results with experimental data

The three equations of SCR theory Equation 3.1, Equation 3.3 and Equation 3.4 are to be solved self consistently to obtain the static susceptibility. But as mentioned in section 3.2 these equations are in reduced units of Fermi energy and needs to be brought to conventional units to be compared with actual experimental data. For this we need the value of the Fermi temperature or Fermi energy to estimate the Fermi temperature of the system of interest. Also the equations contain the Pauli susceptibility (χ_0) implying its value should also be known to

be able to compare the theoretical results with the experimental ones.

The value of the Pauli susceptibility (χ_0) for the system of interest, $CaMn_2Al_{10}$ is reported already in the literature to be[64]:

$$\chi_0 = 3.2 \times 10^{-5}\, emu\, mol^{-1}\, Mn. \tag{3.6}$$

However neither the value of Fermi energy or Fermi temperature has been reported in the literature.

The value of the Fermi temperature can be extracted from the specific heat capacity data as a function of temperature. Given that the specific heat data has already been reported for the system $CaMn_2Al_{10}$ in the literature, we have estimated the value of Fermi temperature from this data. Specific heat capacity in a solid state system has contributions from two sources:

1. **Phononic contribution**: The phononic contribution to specific heat scales as a function of temperature is given as:

$$C_V^{pho} = 9\, N\, K_B \left[\frac{T}{T_D}\right]^3 \int_0^{T_D/T} \frac{x^4 e^x}{(e^x - 1)^2} dx, \tag{3.7}$$

   where, T_D is the Debye temperature, K_B is the Boltzman constant.

2. **Electronic contribution:** The electronic contribution to specific heat (C_V^{elec}) is linearly proportional to temperature (T) i.e.,

$$C_V^{elec} = \gamma_{som}\, T, \tag{3.8}$$

   where γ_{som} is the Sommerfeld coefficient. The expression for the Sommerfeld coefficient is:

$$\gamma_{som} = \frac{\pi^2}{2} \frac{K_B}{T_F} \tag{3.9}$$

To calculate the Fermi temperature of $CaMn_2Al_{10}$, we follow the procedure mentioned below. The plot of specific heat of $CaMn_2Al_{10}$ as a function of temper-

ature is given in Figure 3.3. From the raw specific heat data we have to subtract the phononic contribution to obtain the electronic contribution to specific heat. This can be done with the help of Equation 3.7, as the Debye temperature (that fits the data well) for $CaMn_2Al_{10}$ has already been reported to be 450 K.

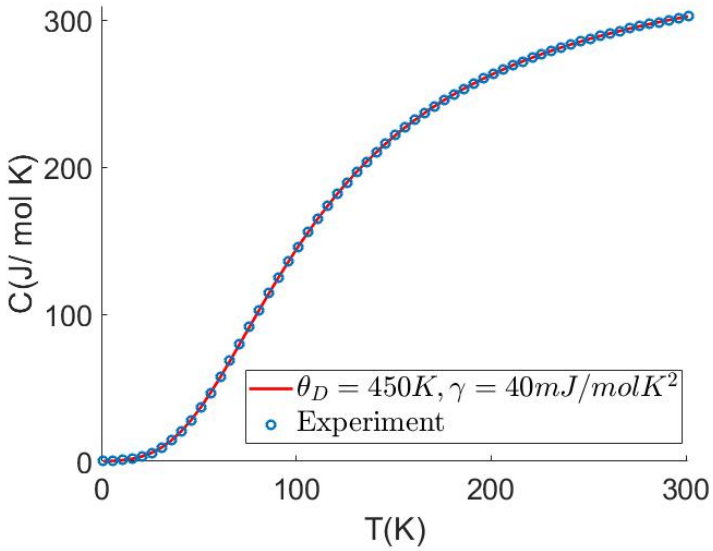

Figure 3.3: Specific heat of $CaMn_2Al_{10}$ as a function of temperature (T). The value of Debye temperature θ_D that fits the data well is 450 K and the value of Sommerfeld coefficient of the electronic component of specific heat is $40mJ/molK^2$. The plot is reconstructed from the data reported in [64].

Once the electronic contribution is obtained the Sommerfeld coefficient can be obtained by estimating the slope of the plot of electronic contribution to specific heat as a function of temperature. After obtaining the value of Sommerfeld coefficient it is straight forward to calculate the Fermi temperature (T_F) by substituting its value in Equation 3.9. The value of the Sommerfeld coefficient obtained for $CaMn_2Al_{10}$ is $40mJ/molK^2$. The value of the Fermi temperature calculated this way turns out to be, $T_F = 1025$ K.

Finally we have both the physical quantities that are required for comparing theoretical results with actual experimental data. The value of the Pauli susceptibility is $\chi_0 = 3.2 \times 10^{-5}\, emu\, mol^{-1}\, Mn.$ and the value of Fermi temperature is, $T_F = 1025$ K. We will now compare these results in the next subsection, subsection 3.3.2.

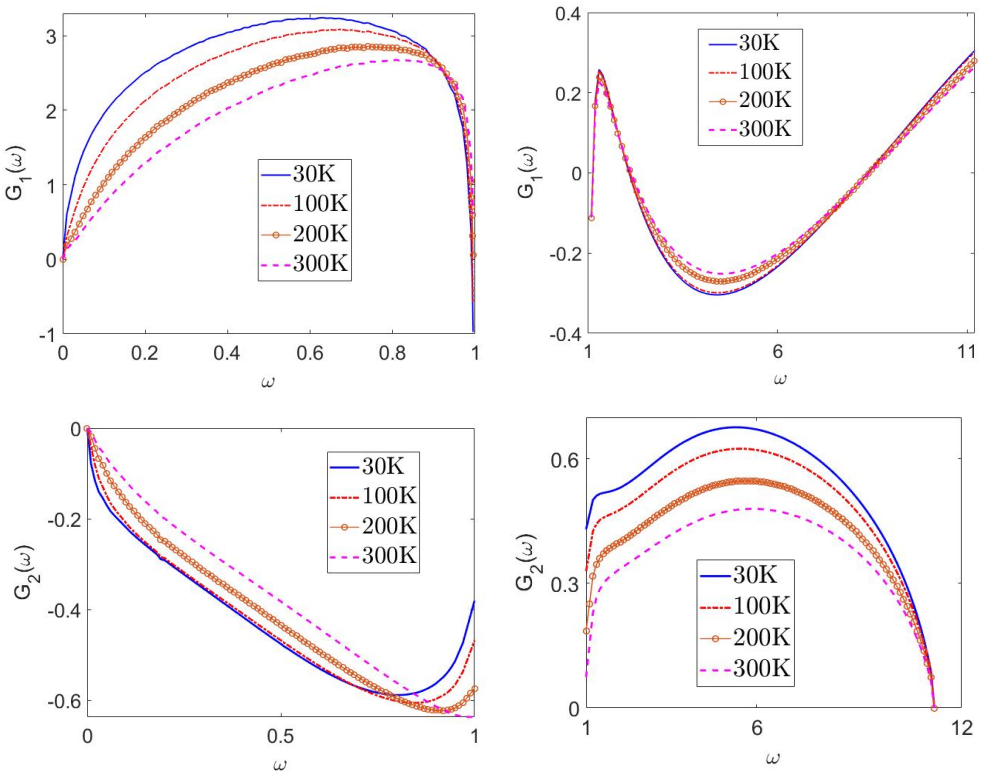

Figure 3.4: Spin fluctuation function ($g(\omega) = \alpha G_1(\omega) + G_2(\omega)$) as a function of frequency. Notice the ω axis of the plots in the same row are continuation of each other but are scaled differently.

3.3.2 Comparison between theoretical calculations and experimental data

After discussing in detail the formalism of SCR theory in chapter 2 and obtaining the values of physical quantities that will be required to compare theoretical results with that of experimental ones, we are all set to compare the results of static susceptibility of $CaMn_2Al_{10}$ obtained from SCR theory to that of actual experimental results.

We have obtained the correct value of the static susceptibility self consistently by iterating on δ until finding the correct value of $g(\omega) = \alpha G_1(\omega) + G_2(\omega)$ which gives the value of $\lambda(T)$ through Equation 3.4, whose value is the same as obtained from the expression Equation 3.3, involving only λ, δ and α. This correct value of $G_1(\omega)$ and $G_2(\omega)$ for some temperature values is shown in Figure 3.4.

With the correctly calculated value of $g(\omega)$ and subsequently the correct value of $\lambda(T)$ and $\delta(T)$ for a particular temperature, T, we can further repeat the process for the desired temperature range. We will the get a theoretically predicted plot of static susceptibility from the SCR theory for a given interaction parameter α and cut-off wave vector q_c. With the values of χ_0 and T_F that we have in hand already this theoretical plot can be directly compared with the experimental data. The values of α and q_c can then be tuned to get an accurate plot from SCR theory that matches with the experimental data very well.

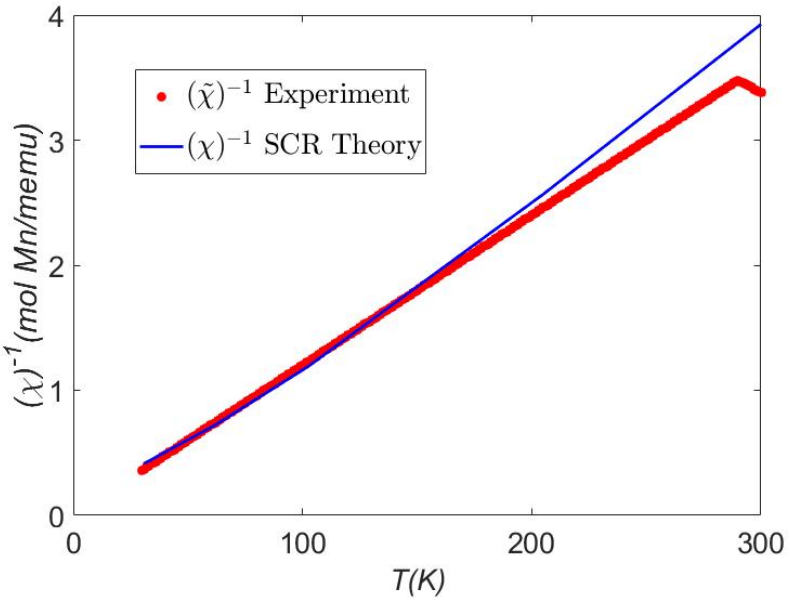

Figure 3.5: Plot of inverse susceptibility as a function of temperature obtained from SCR theory calculations (blue line) compared with experimental data (red dots). The agreement is excellent between 30 K and 150 K. The experimental plot is reconstructed from the data reported in [64].

Such a plot obtained by us is shown in Figure 3.5. As evident from Figure 3.5, the agreement between theory and experiment is very good. In fact, the agreement is excellent between 30 K and 150 K, and the theoretical value starts deviating from the experimental data beyond 150 K. The only fitting parameter used in the SCR theory fit is the Hubbard interaction parameter U which is a microscopic physical parameter.

This is remarkable because agreement up to 150 K translates to temperatures nearly 50 times the T_C of the system.

The results of SCR theory are reliable up to 10 times the T_C of the system, after which finite temperature effects that are not accounted for in the SCR theory, begin to contribute to the susceptibility. With this we can conclude that $CaMn_2Al_{10}$ has passed the litmus test of SCR theory and the magnetism in $CaMn_2Al_{10}$ is indeed a case of itinerant magnetism.

From the optimum value of α that gives the excellent agreement between the theoretical and experimental results we can calculate the value of the Hubbard interaction parameter, U as α is given by the expression,

$$\alpha = \frac{U\chi_0}{2} \tag{3.10}$$

The calculated value of U this way turns out to be, $U = 0.3136$ eV. This is consistent with the fact that $CaMn_2Al_{10}$ is a weakly correlated system as strong correlation would have lead to localisation of electrons and that is not the case here. The value of the Hubbard interaction parameter U calculated by us would be helpful for future studies like optical conductivity in this system.

After proving that the magnetism in $CaMn_2Al_{10}$ is itinerant magnetism, We will now probe the origin of the itinerant magnetism in $CaMn_2Al_{10}$. For this our calculated value of Hubbard interaction parameter U will also be helpful. We will further discuss the origin of itinerant magnetism in $CaMn_2Al_{10}$ in the next section, section 3.4.

3.4 Origin of itinerant magnetism in $CaMn_2Al_{10}$

After proving the type of magnetism in $CaMn_2Al_{10}$ is indeed itinerant magnetism, we will probe its origin in this section. We will employ the Density functional theory (DFT) and DFT+U methods for the same. Before proceeding to the results some general comments on the DFT and DFT+U methods that we have used should be made.

We will explain briefly the DFT and DFT+U methods in subsection 3.4.1. We will then discuss the DFT and DFT+U results and demystify the origins of itinerant magnetism in $CaMn_2Al_{10}$ in subsection 3.4.2.

3.4.1 Comments on DFT and DFT+U calculations

Our DFT and DFT+U results were obtained through QUANTUM ESPRESSO simulation package[77] and the computations were performed in the Vikram 100 HPC facility in the Physical Research laboratory, Ahmadabad, India.

The first principle (DFT) calculations were performed using the projector augmented wave method implemented within the QUANTUM ESPRESSO simulation package. The DFT+U method is a simplified rotationally invariant formalism by Dudarev et al[78] and is found convenient to use for correlated systems like $CaMn_2Al_{10}$.

Generalized Gradient approximation has been used in the calculations performed with the Perdew–Burke–Ernzerhof with exchange-correlation functional[79]. The structural optimisation has been carried out with gamma-centered Monkhrost-Pack of $12 \times 12 \times 12$ k-point mesh having an energy cut-off of 60 Ry. All the atoms and cell parameters have been relaxed by minimizing the inter-atomic force up till 5 meV $Å^{-1}$. The Ca (4s), Mn (3d) and Al (3s–3p) are being treated as the corresponding valence states. The on-site Coulomb interaction parameter U and

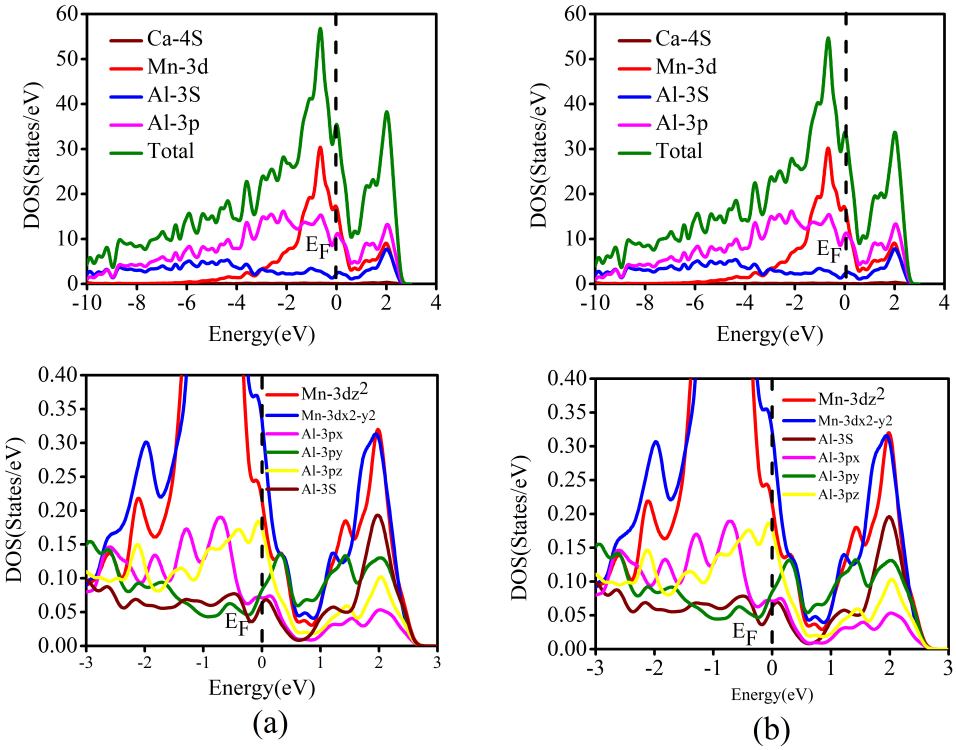

Figure 3.6: Total DoS and partial DoS for $CaMn_2Al_{10}$ with orbital contribution obtained from (a) DFT studies and (b) DFT+U studies

the exchange parameter J (setting $J = 0$) are combined into a single parameter $U_{eff} = U - J$. The value of J has been set to zero because of the lack of local moments in the system.

3.4.2 Evidence for hybridisation between Mn and Al orbitals: DFT and DFT+U studies

In this section we will discuss the results of the DFT and DFT+U calculations that we performed on $CaMn_2Al_{10}$ and discuss the origin of itinerant magnetism in this system. The results from DFT and DFT+U calculations is shown in Figure 3.6.

We have calculated the total Density of States (DoS) and the partial DoS with weights of each orbital's individual contribution to the DoS with both DFT and

DFT+U methods.

We find that the magnetic moment of Mn atoms (0.83 μ_B per Mn atom) are anti-parallel to both Ca (0.01 μ_B per Ca atom) and Al (0.01 μ_B per Al atom) atoms, which confirms the ferromagnetic nature of this Compound. The larger electronic density peak in the Mn DoS that is near the Fermi energy level shows that the major contribution in magnetization is of Mn atoms.

The orbital contributions of each orbital in the compound $CaMn_2Al_{10}$ can be obtained by calculating the partial density of the states (PDOS). We have therefore calculated the PDOS for both DFT and DFT+U calculations. The total DoS and the orbital resolved partial DoS is given for the DFT calculations in fig.3.6(a) and for DFT+U calculations in fig.3.6(b). We find that in both of these calculations the following signatures, of hybridisation between the Mn-3d and Al-3p orbitals is observed:

- The presence of a pronounced pseudogap at the Fermi level indicates that the hybridisation is between the Mn d and Al p orbitals [80]. In both the fig.3.6(a) and 3.6(b) a pseudogap is observed which suggests there is hybridisation between Mn 3d and Al 3p orbitals[80].
- In fig.3.6(a) and 3.6(b) there is a significant overlap of the Mn PDOS and Al PDOS between $0-1$ eV range of energy indicating hybridisation. It is more clearer in the orbital resolved PDOS, where we notice overlap of Mn $3d_{z^2}$ and Mn $3d_{x^2-y^2}$ with Al $3p_y$ in energy range of 0 to 1 eV. Similarly there is an overlap of Mn $3d_{z^2}$ and Mn $3d_{x^2-y^2}$ with Al $3p_z$ close to the Fermi energy. There is also an overlap of Al $3p_x$ and Al $3p_z$ in the energy range of -1 to 0 eV.

In the partial DOS of DFT+U calculation, we observe that at the Fermi level Mn-$3d_{x^2-y^2}$ orbital contribution (0.38 States/eV) is greater than DFT (0.33

States/eV) calculation. After implementing the Hubbard parameter (U), Mn 3 d states originally that were lying close to the Fermi level are now shifted to higher binding energy due to the onsite Coulomb-interaction present among Mn 3 d electrons. This will close the bands that are at the Fermi level in DFT+U calculations. This causes the width of the pronounced pseudo gap at the Fermi level of the spin-up bands to be slightly increased.

3.5 Summary

The recently synthesised Mn based magnetic system $CaMn_2Al_{10}$ is an interesting system for its peculiar behavior. Notably it goes against the conventional wisdom relating to the Mn-Mn distance. In this chapter we have investigated the itinerant nature of magnetism in $CaMn_2Al_{10}$ through the lens of SCR theory and verified it is indeed a case of itinerant magnetism. By fitting the theoretically calculated value of static susceptibility to the experimental data, we have estimated the Hubbard interaction parameter U to be $U = 0.3136$ eV. With this value of U we have performed DFT and DFT+U studies to determine the origin of itinerant magnetism in $CaMn_2Al_{10}$. We have found that it is the hybridisation between Mn 3d and Al 3p orbitals which leads to the delocalisation of Mn electrons and is the reason for itinerant magnetism in this system.

Part II

Topology, Su-Schrieffer-Heeger model and its generalisations

"Dharmathin vazhvu adhanai Sudhu Kavum, Dharmam marupadi vellum"

Mahakavi Bharathiyar

4

Topological tight binding model over non-trivial lattices: The Su-Schrieffer-Heeger model with any bulk

In this chapter, we introduce a tight binding model to generalise the Su-Schrieffer-Heeger model over some non-trivial lattices. We term this new model as the SSH model with Any Bulk or in short the SAB model. In this model we introduce two newer degrees of freedom at each site. These newer degrees of freedom allows us to study SSH like models (that is with dimer structure) over lattices with branching and twists. After introducing the rules of the SAB model we discuss interesting physical properties of a certain class of lattices with different number of bands in the SAB model.

4.1 Introduction: The Su-Schrieffer-Heeger model

The Su-Schrieffer-Heeger (SSH) model is a model first formulated to explain the formation of domain walls in the chains of poly-acetylene[2]. It considers staggered hopping amplitudes between the dimers forming the chain. This model has been a standard pedagogic toy model to explain the topological properties in condensed matter systems due to its conceptual simplicity but at the same time its rich topological structure capturing all the central aspects like bulk boundary correspondence, interplay of symmetries and topology, topological invariants, non-trivial edge states etc.[4, 27].

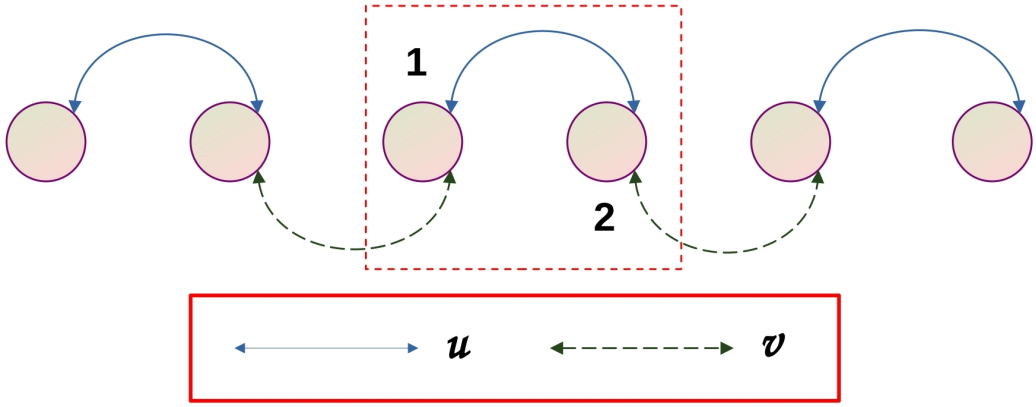

Figure 4.1: Graphical representation of the hopping amplitudes in a conventional Su-Schrieffer-Heeger chain.

The Hamiltonian for the SSH chain with N unit cells is as follows:

$$H = \sum_{X=1}^{N} [u\,(c^{\dagger}_{X,1}\,c_{X,2}) + v\,(c^{\dagger}_{X+1,2}\,c_{X,1}) + H.C.] \tag{4.1}$$

This Hamiltonian as we will see subsequently, exhibits various topological phases with change in the value (more specifically the ratio of the) of the hopping parameters (u and v)[27].

4.2 Topological invariants of the SSH model

As mentioned before the SSH model provides an excellent framework to study and understand various quantities associated with a topological system which characterise the topological phase of the system and are referred to as the topological invariants[27]. As the name suggests these quantities remain invariant across a particular topological phase and a change in their value is indicative of a topological phase transition. Defining and characterising these invariants has been the cornerstone of topology in condensed matter systems[81]. In this section we will define and elaborate on three such topological invariants of the SSH model namely:

1. Winding number.
2. Zak phase.
3. Zero energy edge states.

These invariants are particularly important because their behavior helps us in understanding various principles central to topological condensed matter like the bulk boundary correspondence[5]. These three invariants are also defined only based on the boundary condition we will be choosing. The first two invariants (winding number and Zak phase) are bulk invariants and require an infinite bulk without boundaries. This is equivalent to having periodic boundary conditions (P.B.C.) in the system. The last invariant (number of zero energy edge states) as its name suggests needs a boundary to be defined. This is equivalent to having open boundary conditions (O.B.C.) in the system. We will now dwell in detail on the nature and properties of these invariants.

4.2.1 Winding number

As mentioned the winding number is a bulk invariant implying it is defined only when the bulk is infinite. If we consider an infinite bulk then the Hamiltonian for

the infinite SSH chain is given as:

$$H = \sum_{X=-\infty}^{+\infty} [u\,(c^{\dagger}_{X,1}\,c_{X,2}) + v\,(c^{\dagger}_{X+1,2}\,c_{X,1}) + H.C.]. \tag{4.2}$$

Since the summation is from $-\infty$ to $+\infty$, one can do a Fourier transformation of Equation 4.2 to obtain:

$$H(k) = \sum_{k}[(u + ve^{ik})\,(c^{\dagger}_{1}(k)\,c_{2}(k)) + (u + ve^{-ik})\,(c^{\dagger}_{2}(k)\,c_{1}(k)) + H.C.]. \tag{4.3}$$

Equation 4.3 can be expressed more compactly in a matrix form as,

$$H(k) = \begin{bmatrix} 0 & u + ve^{ik} \\ u + ve^{-ik} & 0 \end{bmatrix} \tag{4.4}$$

Since Equation 4.4 is a two dimensional matrix and the set of all Pauli matrices with the identity matrix of two dimensions forms a complete basis for all two dimensional Hamiltonian matrices, we can express the Hamiltonian $H(k)$ as:

$$H(k) = \sum_{0,1,2,3} d_n(k).\sigma_n \tag{4.5}$$

where σ_o is the two dimensional identity matrix and σ_1, σ_2, σ_3 are the Pauli matrices and,

$$d_0(k) = 0,\ d_1(k) = u + v\,cos(k),\ d_2(k) = v\,sin(k)\ and\ d_3(k) = 0. \tag{4.6}$$

Notice here that the values of $d_0(k)$ and $d_3(k)$ are zero. The presence of chiral symmetry and time reversal symmetry in the SSH Hamiltonian implies the respective terms to be zero. The only non-zero contribution comes from the terms $d_1(k)$ and $d_2(k)$ both of them being functions of the conjugate momentum, k. The locus of the points as k is varied from 0 to 2π in the plane formed by the axes $d_1(k)$

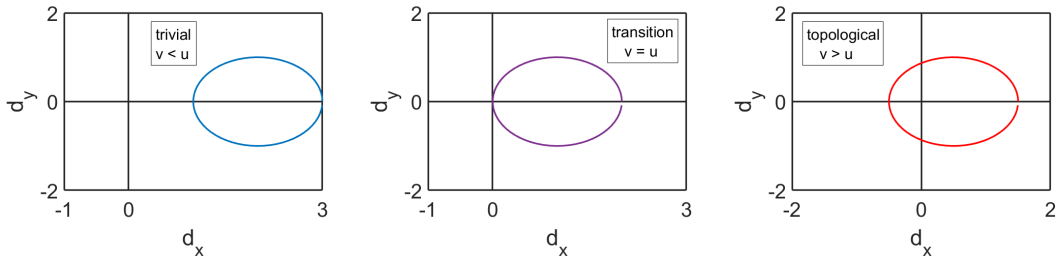

Figure 4.2: The components $d_1(k)$ and $d_2(k)$ of the SSH Hamiltonian plotted in the $d_x - d_y$ plane for (left to right) trivial phase, phase transition point and topological phase with winding numbers along the origin of $d_x - d_y$ plane as zero, not defined and one respectively.

and $d_2(k)$, is going to be a closed loop. If we plot this for the values $d_1(k)$ and $d_2(k)$ in Equation 4.6, the closed loop is a circle. The number of times this circle goes around any point in the $(d_1(k), d_2(k))$ plane is called the winding number of the loop with respect to that point. The winding of this circle with respect to the origin of the $(d_1(k), d_2(k))$ plane is called the winding number of the SSH Hamiltonian $(\mathcal{W})$[4, 27]. This has been pictorially depicted in Figure 4.2. This circle moves and grows in the plane depending on the values of the hopping parameters u and v. This causes the winding number also to change and it takes three values which are,

1. $\mathcal{W} = 0$, when the ratio of the intercell to intracell hopping parameters is less than one, that is $(v/u) < 1$. In this case the circle doesn't enclose the origin of the plane and the origin lies outside the circle. This corresponds to the "trivial" phase.

2. $\mathcal{W}$ is not defined, when the ratio of the intercell to intracell hopping parameters is equal to one, that is $(v/u) = 1$. In this case the circle touches the origin of the plane and the origin lies on the circle. This corresponds to the "topological phase transition" point.

3. $\mathcal{W} = 1$, when the ratio of the intercell to intracell hopping parameters is greater than one, that is $(v/u) > 1$. In this case the circle encloses the origin of the plane and the origin lies inside the circle.This corresponds to the "topological" phase.

We can thus calculate the value of the winding number of the system for a par-

ticular configuration of the system parameters which in this case is the hopping amplitudes. The value of the winding number is then indicative whether the system is in the trivial or the topological phase for that configuration of system parameters.

4.2.2 Zak phase

Zak phase like the winding number is another bulk invariant which indicates the topological phase of the system. Since it is also a bulk invariant it also requires the bulk to be infinite and can be obtained for the Hamiltonian in Equation 4.2 which after Fourier transformation gives Equation 4.4. Unlike the winding number which is directly calculated from the winding of the Hamiltonian in the $(d_1(k), d_2(k))$ plane, this is obtained by calculating the geometric phase or the Pancharatnam-Berry phase of the eigenstates of the Hamiltonian[25, 26]. Zak derived this for the SSH Hamiltonian and had shown that the Zak phase like the winding number takes three different values which characterise the topological phase of the system[28]. The expression for the Zak phase (ϕ^i) of the i^{th} eigenstate is given as,

$$\phi^i = \frac{1}{\pi}\int_{-\pi}^{\pi} \frac{\langle u_k^i|\, \partial_k\, |u_k^i\rangle}{\langle u_k^i|u_k^i\rangle} dk \tag{4.7}$$

where u_k^i is the periodic part of the Bloch wavefunction corresponding to the i^{th} eigenstate. From Equation 4.7 it is clear that to calculate the Zak phase, one requires the eigenvalues and eigenstates of the system. The eigenvalues and eigenstates for the SSH model are as follows (we first introduce some shorthand notations to keep the expressions in this section compact),

$$\begin{aligned} \xi^+(k) &= -\sqrt{u^2+v^2+2\,u\,v\,cos(k)}, \\ \xi^-(k) &= -\sqrt{u^2+v^2-2\,u\,v\,cos(k)}, \\ \kappa(k) &= (u+v\,e^{-ik})^{-1}, \end{aligned} \tag{4.8}$$

,

$$\begin{bmatrix} E_a \\ \hline E_b \end{bmatrix} = \begin{bmatrix} -\xi^+(k) \\ \hline \xi^+(k) \end{bmatrix}, \tag{4.9}$$

$$|\psi_a\rangle = \begin{bmatrix} -\xi^+(k)\,\kappa(k) \\ \hline 1 \end{bmatrix}, \tag{4.10}$$

$$|\psi_b\rangle = \begin{bmatrix} \xi^+(k)\,\kappa(k) \\ \hline 1 \end{bmatrix}. \tag{4.11}$$

where $|\psi_x\rangle$ denotes the eigenstate corresponding to the eigenvalue x. Plotting the eigenvalues as a function of the conjugate momentum (k) gives us the band dispersion. The band dispersion for the SSH model is given in Figure 4.3. We can infer from Figure 4.3 that there is a finite band gap for the cases $u > v$ and $u < v$ and they look completely identical if the values of u and v are swapped. For the case of $u = v$, the band gap closes with the two band gap touching each other at the boundaries of the first Brillouin zone.

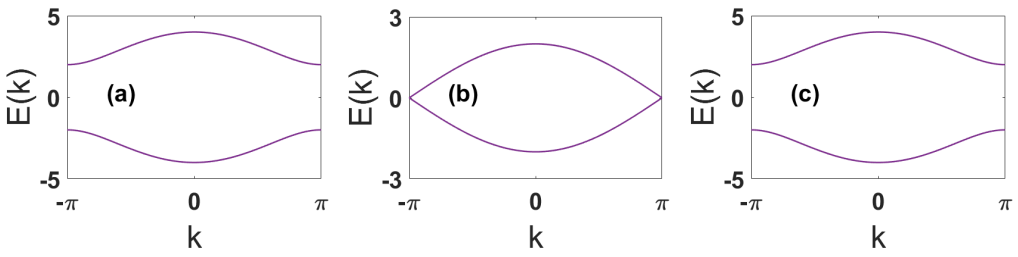

Figure 4.3: Band dispersion for the cases (a) $u > v\,(u = 3, v = 1)$,(b) $u = v\,(u = 1, v = 1)$, (c) $u < v\,(u = 1, v = 3)$.

After obtaining $|u_k^i\rangle$ from the expression of the eigenstate $|\psi_k^i\rangle$ given in Equation 4.10 and Equation 4.11, one can perform the integration in Equation 4.7 to obtain the values of the Zak phase (ϕ^i) as,

$$\phi^i = \begin{cases} 0 & \text{for}, u > v, \\ \text{not defined} & \text{for}, u = v, \\ 1 & \text{for}, u < v. \end{cases} \tag{4.12}$$

Here a zero value of Zak phase indicates that the system is in the trivial phase and a value of one indicates that the system is in the topological phase. When the value of intercell and intracell hopping becomes equal, the Zak phase is not defined indicating that it is the topological phase transition point.

Similar to the winding number, the Zak phase invariant can be calculated for any configuration of system parameters and its value indicates the phase of the system for that configuration.

4.2.3 Zero energy edge states

The zero energy edge states are an important topological invariant particularly in the case of the SSH model. Unlike the previous invariants, winding number and Zak phase, this is not a bulk invariant and needs boundary in the system to be defined[2]. Hence this requires a finite system and can be realised only with open boundary conditions (O.B.C.). The Hamiltonian for a finite SSH chain with N unit cells is given in Figure 4.1. If we consider a SSH chain having 20 unit cells, the Hamiltonian for this chain is as follows,

$$H = \sum_{X=1}^{20} [u\,(c^{\dagger}_{X,1}\,c_{X,2}) + v\,(c^{\dagger}_{X+1,2}\,c_{X,1}) + H.C.] \tag{4.13}$$

This Hamiltonian in the matrix form is given as,

$$H = \begin{bmatrix} \mathbf{U} & \mathbf{V} & \cdots & \cdots & \cdots & & \\ \mathbf{V}^\dagger & \mathbf{U} & \cdots & \cdots & \cdots & & 0 \\ \vdots & & \ddots & & & & \vdots \\ \vdots & & 3 \text{ blocks} & & & & \vdots \\ \vdots & & & & \ddots & & \vdots \\ & & \cdots & \cdots & \cdots & \mathbf{U} & \mathbf{V} \\ & 0 & \cdots & \cdots & \cdots & \mathbf{V}^\dagger & \mathbf{U} \end{bmatrix} \tag{4.14}$$

where $\mathbf{U}$ and $\mathbf{V}$ are given as:

$$\mathbf{U} = \begin{bmatrix} 0 & u \\ u & 0 \end{bmatrix} \text{ and } \mathbf{V} = \begin{bmatrix} 0 & 0 \\ v & 0 \end{bmatrix} \tag{4.15}$$

We can diagonalise the Hamiltonian in Equation 4.14 numerically to obtain the eigenvalues and energy spectrum of the finite SSH chain. The energy eigenvalues of the finite SSH chain with 20 unit cells are shown in Figure 4.4.

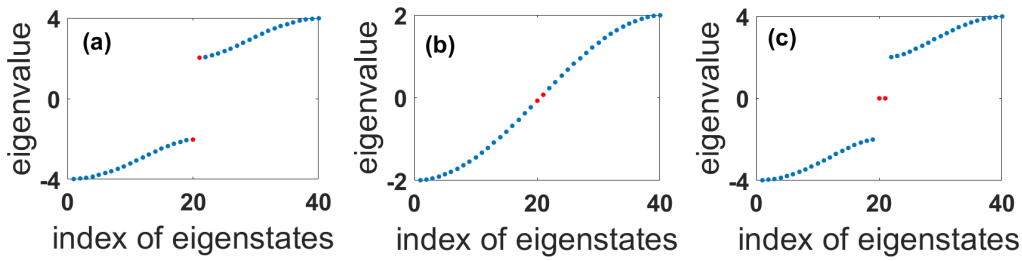

Figure 4.4: Energy eigenvalues for the open chain of a C-SSH model with 20 unit cells, sorted from low to high plotted with respect to total number of states indexed from 1 to 20 for (a) $u > v$, (b) $u = v$ and (c) $u < v$

We can infer the following from Figure 4.4:

1. In the case where the intracell hopping amplitude (u) is greater than the intercell hopping amplitude (v) (as shown in Figure 4.4(a)) there is a band gap in the system with no in gap states.

2. In the case where the intracell hopping amplitude (u) is equal to the intercell hopping amplitude (v) (as shown in Figure 4.4(b)) the band gap closes in the system.

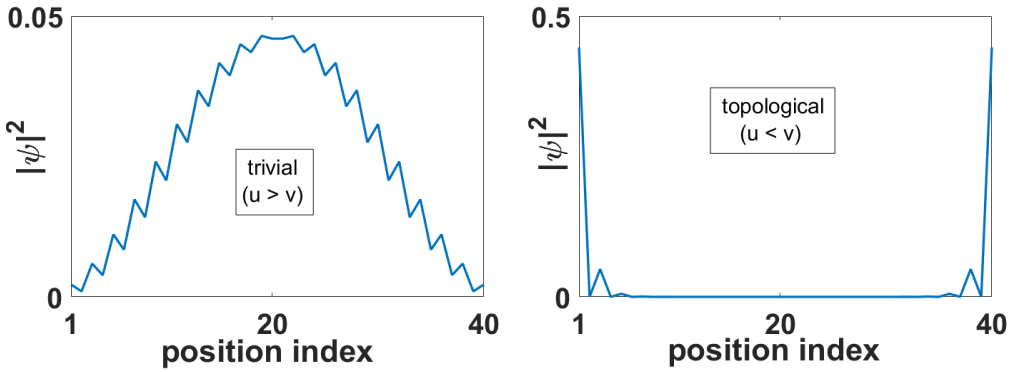

Figure 4.5: The squared absolute value of the wave functions corresponding to the red dots in Figure 4.4 for the trivial and topological phases.

3. In the case where the intracell hopping amplitude (u) is less than the intercell hopping amplitude (v) (as shown in Figure 4.4(c)) the band gap reappears but with two zero energy in gap states. These zero energy states are localised in the two edges and are referred to as the "zero energy edge states".

4. The squared absolute value of the wave functions corresponding to the red dots in Figure 4.4 for the trivial and topological phases is given in Figure 4.5. From Figure 4.5 it is clear that the wave functions are extended in the trivial phase and localised at the edges in the topological phase (the wave functions corresponding to both the red dots are identical).

In this fashion we can calculate the number of zero energy edge states by diagonalising the Hamiltonian and obtaining the eigenvalues for the desired configuration of system parameters. There are no zero energy edge states in the trivial phase and there are two of them in the topological phase as evident from the above discussion.

4.2.4 Bulk Boundary correspondence in the SSH model

Bulk boundary correspondence is a principle at the heart of topological condensed matter physics. Simply put, it states that the information of topological boundary states is available in the bulk invariants[27]. From the discussions in the previous subsections, we can easily observe that this is true for the SSH model. We see that:

1. In the parameter space where the intercell hopping amplitude is less than the intracell hopping amplitude ($v < u$), the bulk invariants, winding number ($\mathcal{W}$) and the Zak phase (ϕ^i) corresponding to both the eigenstates are zero. This corresponds to the trivial phase when there are no zero energy edge states.

2. However when ($v > u$), the bulk invariants, winding number ($\mathcal{W}$) and the Zak phase (ϕ^i) corresponding to both the eigenstates has a value of one. this corresponds to the topological phase when there are two zero energy edge states.

3. The bulk invariants are not defined when $u = v$, and the band gap closes in the finite chain for this set of parameters making the concept of in gap states ill defined.

The above points clearly allows us to write the following relations (we denote the number of zero energy edge states as $\mathcal{N}$):

$$\mathcal{N} = 2\mathcal{W} \qquad \text{and} \qquad \mathcal{N} = \sum_i \phi^i. \tag{4.16}$$

The above relations clearly demonstrate the existence of bulk boundary correspondence in the SSH model.

4.3 Lattice geometry and flat bands

Flat bands in condensed matter systems have recently generated a lot of interest due to the possibility of several exotic physical properties they can host. The kinetic energy of an electron in a flat band is quenched which gives rise to strong electronic correlations in the presence of interactions. This has given rise to intensive searches for platforms that can host flat bands. There are many methods to generate systems with flat bands. One method is to increase the distance between the adjacent sites making the overlap of orbitals in adjacent sites extremely small and effectively making the hopping amplitude to hop between adjacent sites zero. However another elegant approach is to make the lattice geometry such

that for any value of the hopping parameters the electrons departing particular sites destructively interfere leading to a localisation of electron in that site. The celebrated Lieb lattice falls in to this category[82]. In this section we will discuss certain properties which govern the geometry of the lattice such as branching and twists which influence the band structure of the electrons in the lattice and can give rise to flat bands.

4.3.1 Branching

In mathematical terms, a lattice is homogeneous if the number of edges coming out of each vertex is the same and is equal to $2N$ where the lattice dimension is N except at the edges. If there are points in the bulk which have more number of edges than $2N$, these points are called branching points and the lattice is said to have branched at these points. If we adapt and apply this definition to the one dimensional crystal lattice in systems of our interest, we can identify the sites in the crystal lattice as vertices and the tunneling channels coming out of each site as edges coming out of a vertex, branching points are those vertices that have more than two tunneling channels coming out of that site[83].

In mathematics the number of edges coming out of a vertex is defined as the order of ramification of that vertex[84]. It is a measure of branching at that particular vertex. In one dimension an order of ramification of two implies no branching and any higher value implies branching at that vertex. This is graphically shown in Figure 4.6. Here since we identify each site as a vertex and the number tunneling channels coming out of each site as the number of edges coming out of a vertex, we can define the order of ramification analogous to the mathematical definition for each site. This allows us to quantify the branching at each site. If the order of ramification is the same for all sites in a lattice (greater than 2) then the lattice exhibits homogeneous branching and if it is different for different sites then it exhibits inhomogeneous branching.

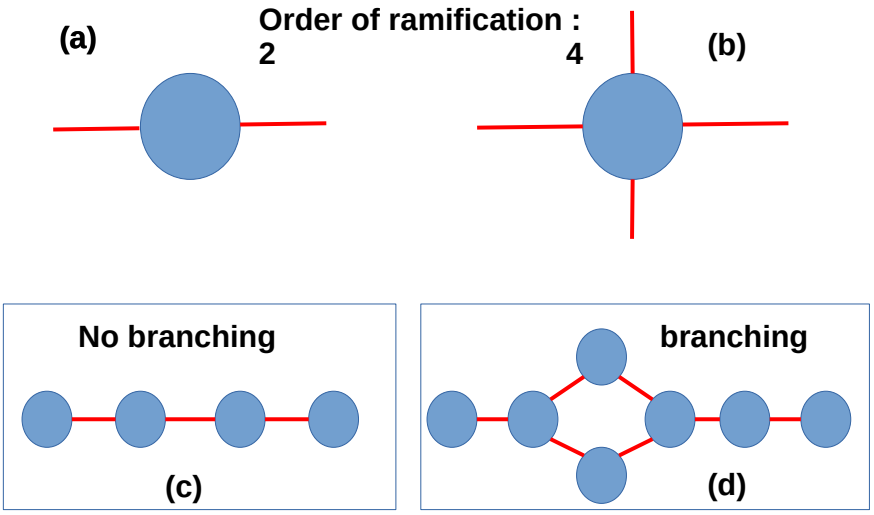

Figure 4.6: Graphical explanation of order of ramification and its connection to branching. (a) order of ramification the vertex is two, (b) order of ramification the vertex is four, (c) one dimensional lattice without branching and (d) one dimensional lattice with branching.

For the SSH model the order of ramification for all the sites in the lattice (excluding the edges) is two implying that the lattice is homogeneous and there are no branching points. However the number of branching points, their location and the homogeneity of the lattice which are essentially governed by the geometry of the lattice and play a profound role on the electronic structure of electrons in that lattice.

4.3.2 Twists

In mathematics twist(s) in a manifold results in the loss of orientability of that manifold making the manifold non-orientable. We will adapt this definition to apply to the lattice associated with condensed matter systems of our interests. Similar to the case of branching twists in a lattice can play an important role in the electronic structure of the electrons in a lattice. These can be twists in the actual manifold forming the lattice like in the case of the integer quantum hall effect on a Mobius strip or twisting not in the manifold of the lattice but with respect to some degree of freedom associated with every lattice site.

We will be concerned about the later case of twists which are defined with respect to additional degree of freedom in our further discussions. We will have to clearly explain the rules of the topological tight binding model that we have formulated before we can define the term twist in our context. Therefore we will define "twist" after defining the rules of the model in section 4.4. It is worthy to mention here that there has only been one reported work relating to topological insulators and non-orientable manifolds[85].

4.3.3 Flat bands

Flat bands are states in the electronic structure which have no dispersion with respect to the conjugate momentum k. The effective mass of electrons in these bands diverge giving rise to complete localisation of electrons. This leads to quenching of kinetic energy of electrons in these bands giving rise to strong electronic correlations between electrons in presence of interactions. This can give rise to several important phases of matter like superconductivity, Wigner crystallisation, magnetism etc.[86–98]

There have been several generalisations of the C-SSH model like the generalised SSH model[99–101], super SSH model[102–104], Cruetz ladder[105], with long range hopping[106–108], with a non-Hermitian Hamiltonian[109] etc. There have also been many studies of C-SSH model including effects of Coulomb repulsion[110, 111], electron-phonon interaction[112] and C-SSH model in the ultra strong coupling regime with counter-rotating coupling terms playing a pivotal role[113]. But none of them have considered the effects of the geometry of the bulk on the physical properties rigorously. We attempt to explore more in this direction.

4.4 Su-Schrieffer-Heeger model with Any Bulk (SAB)

In this section we will discuss in detail about the topological tight binding model that has been formulated by us. In this model we associate two new degrees of freedom with each site. The reason for introducing these newer degrees of freedom and only two of them is as follows:

- Our main objective in formulating this new topological tight binding model is to study SSH like systems which have a twist in the hopping amplitudes. To introduce twists we need to have a notion of orientability in our system. As explained in section 4.3, we will only consider a "twist" as change in some degree of freedom that occurs by traversing the lattice. This is realised by introducing the first degree of freedom which can have two values. We call these values as left and right for simplicity (left and right are indices to denote two values and has nothing related to the physical directions). We will explain the realisation of twists with this newer degree of freedom after explaining the rules of this model.
- As mentioned above our objective is to realise twists in SSH like systems. To generate consistently hopping patterns that are SSH like when the bulk is not a line but an extended object, we require the second degree of freedom. Based on this new degree of freedom we can consistently define a SSH like hopping pattern with intercell and intracell hopping amplitudes.

We call this newly formulated tight binding model as the SSH model with Any Bulk (SAB model). It is because this tight binding model exhibits SSH like hopping pattern but with the bulk being any one dimensional object and is not restricted to a line. Thus the name SSH model with any bulk abbreviated as SAB model. The rules of the SAB model are as follows (for clearer understanding, the rules are explained with the help of Figure 4.7):

- In the SAB model, there are two new degrees of freedom associated with each site. The first degree of freedom can have two values, which we denote

as right and left. This is just a notation for denoting a degree of freedom that can take two values and has nothing to do with right and left directions in real physical space. Each site in the lattice has overall two, but only one left and only one right value for this degree of freedom associated with it.

- The second degree of freedom has three components $(+, -, 0)$. Each value of the first degree of freedom contains any one and only one component from this second degree of freedom. Thus each site in the lattice has two values of the first degree of freedom and each value of the first degree of freedom has one component from the second degree of freedom. This evident from all the four sites in Figure 4.7 where each site has one left and one right value. Both left and right values for the first degree of freedom have the value of the second degree of freedom (+) for the sites labeled as 1 and 2, whereas the value is (-) for the sites labeled 3 and 4.

- Hopping amplitudes are non zero only when hopping is from left to left or right to right value between two sites unless there is a twist. If there is a twist hopping amplitudes are non zero only if the hopping is from left to right or from right to left value. This is clear from Figure 4.7, where there is no twist between sites 1 and 2 and there is a twist between sites 1 and 4.

- Intracell hopping happens only if the two components between the two values have the same components other than 0. If the component is 0, then is no hopping to and from that value (left/right) in that site. In Figure 4.7. this is the reason for the hopping amplitude between 1 and 2 to be intracell.

- Intercell hopping happens only if the two components between the two values have different components other than 0. If the component is 0, there is no hopping to and from that value (left/right) in that site. In Figure 4.7. this is the reason for the hopping amplitude between 2 and 3 to be intercell.

- Only same cell (denoted by u) and nearest cell hopping (denoted by v) is considered.

- Hopping amplitudes between two sites is the same for both directions (i.e. the Hamiltonian is Hermitian).

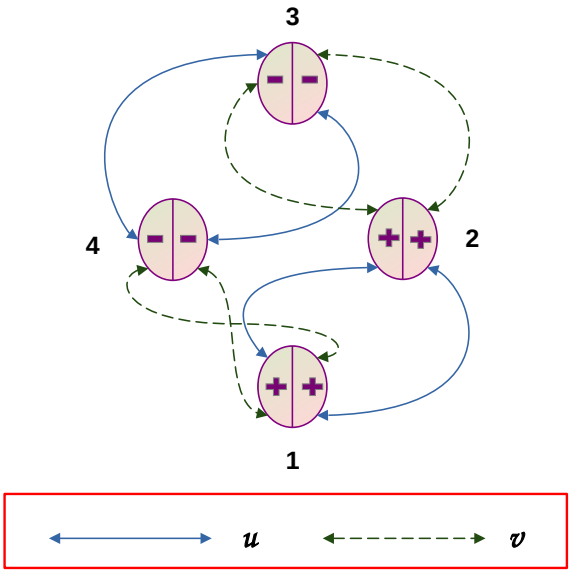

Figure 4.7: An illustration to understand the rules governing the hopping amplitudes in the SAB model.

We can see from the above rules that when there is a "twist" as defined by us earlier in a particular lattice, while traversing that lattice after starting from either value of the first degree of freedom (left/right), we end up in the other value before traversing the lattice completely. Branching in this model can be quantified in the same way as it was introduced for any general lattice in section 4.3 using the value of order of ramification for each site.

We will now discuss several cases arising from different geometries of the bulk and different configurations within those geometries through the framework of the SAB model. Before going in to specific cases, we should also mention that these two newer degrees of freedom control the pattern of the hopping amplitudes because the rules defining the hopping pattern are influenced by their values. However they do not directly appear in the Hamiltonian. This makes them different from the conventional degrees of freedom that we regularly encounter. However this does not make them non-physical. For example these degrees of freedom can physically correspond to some quantum numbers like the pseudo spin quantum number in the case of one-dimensional array of quantum dots.

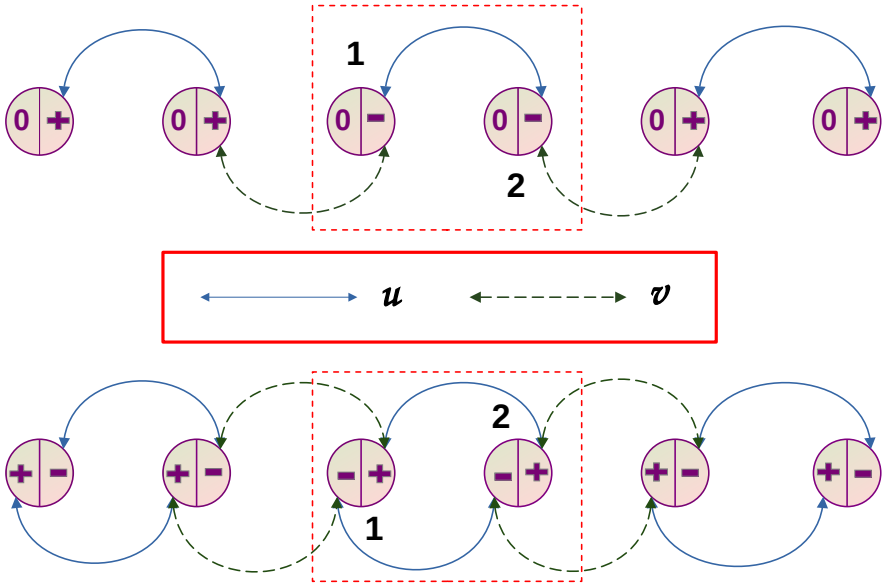

Figure 4.8: Conventional SSH model as a particular case in SAB model.

4.5 Two band SAB models

In this section we will present the results for the case of the bulk being a line or a "linear bulk". Linear bulk is a bulk in which there is no single path to reach back to the same starting point without traversing the entirety of the lattice (Figure 4.8). A minimalistic SSH type model requires at least two sites per unit cell and a minimalistic linear bulk requires at least one unit cell. The above condition makes the minimalistic linear bulk to require at least two sites per unit cell making it a two band model. All possible configurations in the two band models fall in to two categories as shown in Figure 4.8.

All the two band SAB models are described the same Hamiltonian:

$$H = \sum_{X=-\infty}^{+\infty} [u\,(c^{\dagger}_{X,1}\,c_{X,2}) + v\,(c^{\dagger}_{X+1,2}\,c_{X,1}) + H.C.]. \tag{4.17}$$

Since the summation is from $-\infty$ to $+\infty$, one can do a Fourier transformation of Equation 4.17 to obtain:

$$H(k) = \sum_k [(u + ve^{ik})\,(c_1^\dagger(k)\,c_2(k)) + (u + ve^{-ik})\,(c_2^\dagger(k)\,c_1(k)) + H.C.]. \quad (4.18)$$

Equation 4.18 can be expressed more compactly in a matrix form as,

$$H(k) = \begin{bmatrix} 0 & u + ve^{ik} \\ u + ve^{-ik} & 0 \end{bmatrix} \quad (4.19)$$

The band dispersion and the eigenvalue spectrum of the two band models which are obtained using periodic boundary conditions and open boundary conditions are shown in Figure 4.9 and Figure 4.10 respectively.

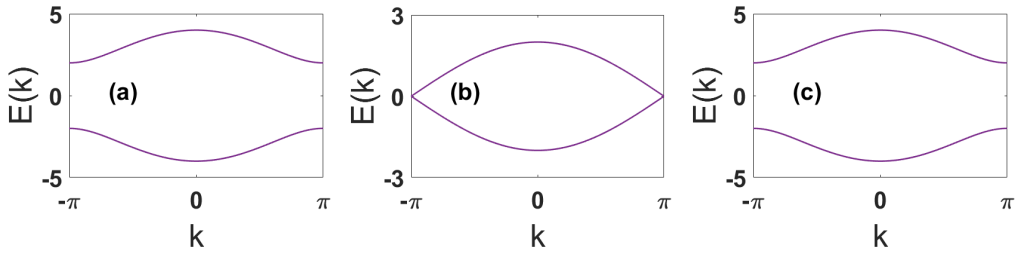

Figure 4.9: Band dispersion for the cases (a) $u > v(u = 3, v = 1)$,(b) $u = v(u = 1, v = 1)$, (c) $u < v(u = 1, v = 3)$.

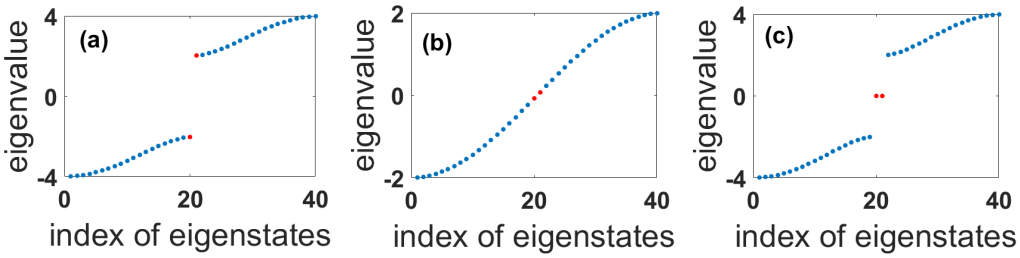

Figure 4.10: Energy eigenvalues for the open chain of a C-SSH model with 20 unit cells, sorted from low to high plotted with respect to total number of states indexed from 1 to 20 for (a) $u > v$,(b) $u = v$ and (c) $u < v$

Comparing Figure 4.9 and Figure 4.10 with Figure 4.3 and Figure 4.4, we note that they are exactly the same. We can thus conclude that the two band SAB models are nothing but the conventional SSH models (denoted as C-SSH model). The Hamiltonian and the discussion regarding various topological invariants of the

C-SSH model discussed in section 4.2 are applicable here and we skip repeating them here for brevity.

4.6 SAB model with circular bulk

We will discuss the case of circular bulk in this section. In the previous section we defined the linear bulk as a bulk such that there is not a single path to reach back to the same starting point without traversing the entirety of the lattice. On the contrary in the case of circular bulk there is at least a single path to reach back to the same starting point without traversing the entirety of the lattice.

A minimalistic SSH type model requires at least two sites per unit cell and a minimalistic circular bulk requires at least two unit cells to have at least a single path to come back without traversing the entirety of the lattice. The above condition makes the minimalistic circular bulk to require at least four sites per unit cell making it a four band model.

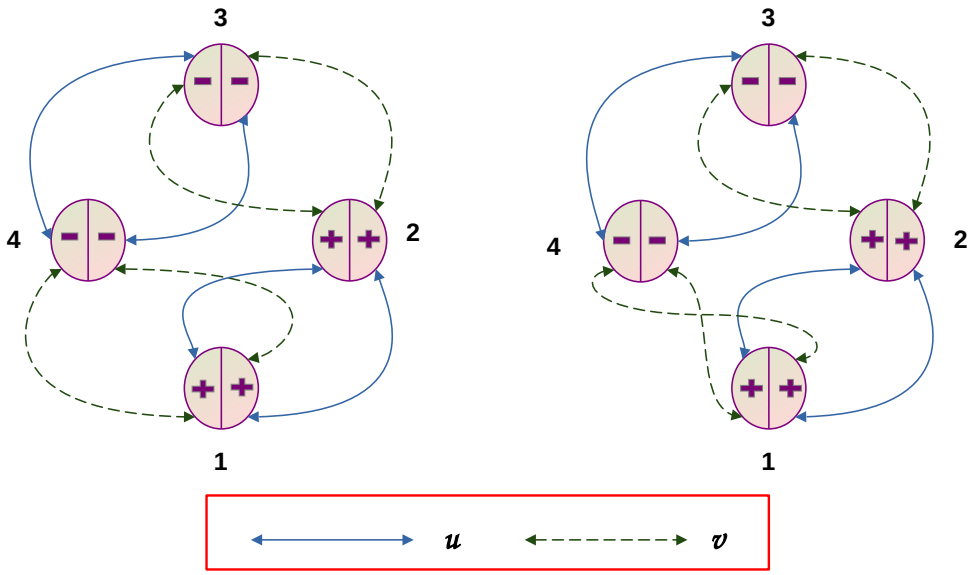

Figure 4.11: Unit cell of SAB model (with P.B.C.) for two orientable configurations (with and without twist).

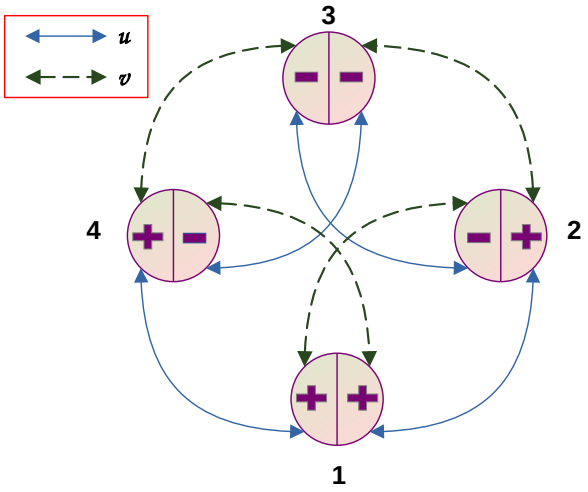

Figure 4.12: Unit cell of SAB model (with P.B.C.) for the non-orientable configuration.

Before proceeding further we should resume here our discussion on orientability and twists as promised in section 4.3. As we had explained in section 4.3, twist in our terminology is that condition when a degree of freedom changes its value as we traverse the lattice and before completely traversing the lattice.

In mathematics twist(s) in a manifold lead to loss of orientability of the manifold. This orientability is defined in mathematical terms as the ability to define a consistent system of co-ordinates in that manifold. If this is possible, then the manifold is called an orientable manifold. If it is not possible to define a consistent system of co-ordinates in the manifold then it is called a non-orientable manifold. If a manifold has twists it becomes a non-orientable manifold.

However we will introduce a new definition of orientability inspired from the mathematical definition but contextualised for the SSH type models we will be dealing with. In our definition, orientability is the ability to consistently identify neighboring sites belonging to the same dimer or to adjacent dimer when periodic boundary condition is applied to the unit cell. If we can identify the dimers consistently as belonging to either same dimers or adjacent dimers, then the model is orientable. If we cannot consistently identify the dimers as belonging to either same dimers or adjacent dimers, then the model is non-orientable (This can be

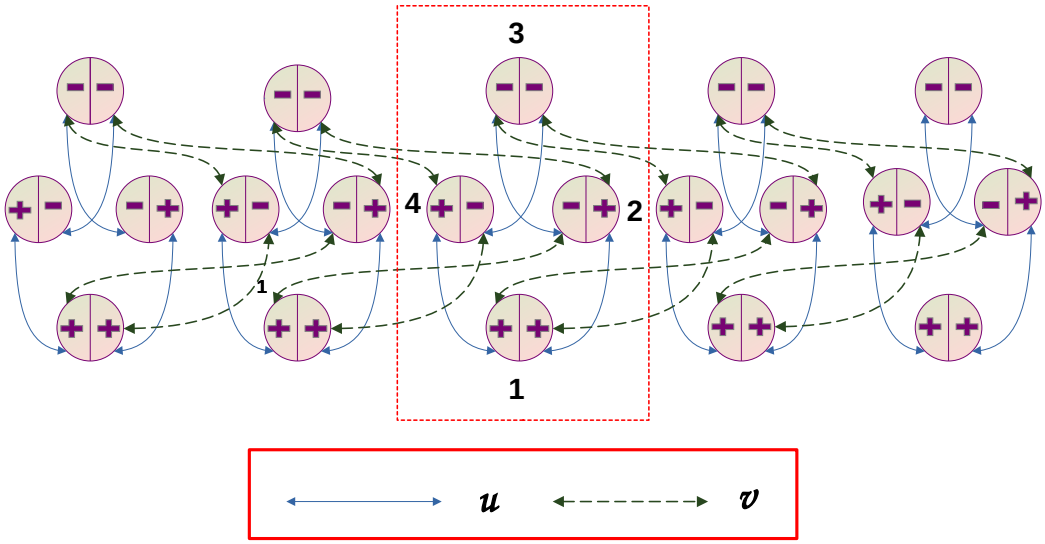

Figure 4.13: An open chain of SAB model with a circular non-orientable bulk with 5 unit cells.

understood as the electron at the i^{th} site in unit cell n has non zero hopping amplitude to either $i \pm 1^{th}$ site at either n^{th} unit cell (intracell hopping) or $n \pm 1^{th}$ unit cell (intercell hopping), but not both). This can be understood by looking at Figure 4.11 which are orientable configurations and Figure 4.12 which is a non-orientable configuration. Hence the twist in degrees of freedom may not always lead to the model being non-orientable. Similarly there can be non-orientable configurations without twists in the degrees of freedom. It is a combination of the geometry of the bulk and the twists in degrees of freedom that gives rise to non-orientable models.

All possible configurations in the four band models fall in to three categories and one example from each category is shown in Figure 4.11 and Figure 4.12. The first figure (from left) in Figure 4.11 and the figure in Figure 4.12 do not have any twist, whereas the second figure (from left) in Figure 4.11 has a twist between the sites indexed 1 and 4. These three sets can be further grouped in to two categories, (1) orientable and (2) non-orientable configurations. Examples of the orientable configurations are presented in Figure 4.11 while example of the non-orientable configuration is presented in Figure 4.12. According to the

definition of orientability defined in the context of the SSH model (in section 4.6), orientability is the ability to consistently identify neighboring sites belonging to the same dimer or to adjacent dimer when periodic boundary condition is applied to the unit cell. Applying this definition, to the lattices depicted in Fig. 4.9, we see that we can consistently define the hopping patterns to either inter cell or intra cell when periodic boundary condition is applied. For this reason we call them orientable configuration. Similarly, in the lattice depicted in Fig. 4.10, we cannot consistently define the hopping patterns to either inter cell or intra cell when periodic boundary condition is applied and the configuration is termed non-orientable. This makes the three groups as:

1. Orientable configuration without a twist as in Figure 4.11 first figure (from left).
2. Orientable configuration with a twist between sites labeled as 1 and 4, as in Figure 4.11 second figure (from left).
3. Non-orientable configuration without a twist as in Figure 4.12.

An open chain of the non-orientable configuration with 5 unit cells is shown in Figure 4.13.

We will now present the results obtained for the case of four band models. As discussed before there are two sets of configurations in the four band models namely the orientable and non-orientable configurations. The properties of all the orientable four band models are same for all orientable configurations and the properties of all the non-orientable four band models are same for all non-orientable configurations. We will discuss them one by one in the subsequent subsections.

4.6.1 Orientable four band models

We will present the bulk and edge invariants along all the supporting calculations and results related to the four band orientable models. We will begin with the

Hamiltonian of the four band orientable model for an infinite chain which is given as:

$$H = \sum_{X=-\infty}^{\infty} \left[u \left(c_{X,1}^{\dagger} c_{X,2} + c_{X,3}^{\dagger} c_{X,4} \right) + v \left(c_{X+1,4}^{\dagger} c_{X,1} + c_{X+1,2}^{\dagger} c_{X,3} \right) + H.C. \right] \quad (4.20)$$

Since the summation is from $-\infty$ to $+\infty$, one can do a Fourier transformation of Equation 4.20 and obtain the Hamiltonian as a function of conjugate momentum, k which is given below in matrix form for brevity,

$$H(k) = \begin{bmatrix} 0 & u & 0 & ve^{ik} \\ u & 0 & ve^{-ik} & 0 \\ 0 & ve^{ik} & 0 & u \\ ve^{-ik} & 0 & u & 0 \end{bmatrix} \quad (4.21)$$

The eigenvalues (denoted as $E_{a_1}, E_{b_1}, E_{c_1}, E_{d_1}$) and the eigenstates denoted as, $(|\psi_{a_1}\rangle, |\psi_{b_1}\rangle, |\psi_{c_1}\rangle, |\psi_{d_1}\rangle)$ of Equation 4.21 are given below,

$$\begin{bmatrix} E_{a_1} \\ \hdashline E_{b_1} \\ \hdashline E_{c_1} \\ \hdashline E_{d_1} \end{bmatrix} = \begin{bmatrix} -\xi^{-}(k) \\ \hdashline \xi^{-}(k) \\ \hdashline -\xi^{+}(k) \\ \hdashline \xi^{+}(k) \end{bmatrix}, \quad (4.22)$$

$$|\psi_{a_1}\rangle = \begin{bmatrix} \xi^{-}(k)\,\kappa(k) \\ \hdashline -1 \\ \hdashline -\xi^{-}(k)\,\kappa(k) \\ \hdashline 1 \end{bmatrix}, \quad (4.23)$$

$$|\psi_{b_1}\rangle = \begin{bmatrix} -\xi^{-}(k)\,\kappa(k) \\ \hline -1 \\ \hline \xi^{-}(k)\,\kappa(k) \\ \hline 1 \end{bmatrix} \tag{4.24}$$

$$|\psi_{c_1}\rangle = \begin{bmatrix} -\xi^{+}(k)\,\kappa(k) \\ \hline 1 \\ \hline -\xi^{+}(k)\,\kappa(k) \\ \hline 1 \end{bmatrix}, \tag{4.25}$$

$$|\psi_{d_1}\rangle = \begin{bmatrix} \xi^{+}(k)\,\kappa(k) \\ \hline 1 \\ \hline \xi^{+}(k)\,\kappa(k) \\ \hline 1 \end{bmatrix}. \tag{4.26}$$

By plotting the eigenvalues in Equation 4.22 as a function of conjugate momentum (k), we obtain the band dispersion. The band dispersion for various cases is shown in Figure 4.14.

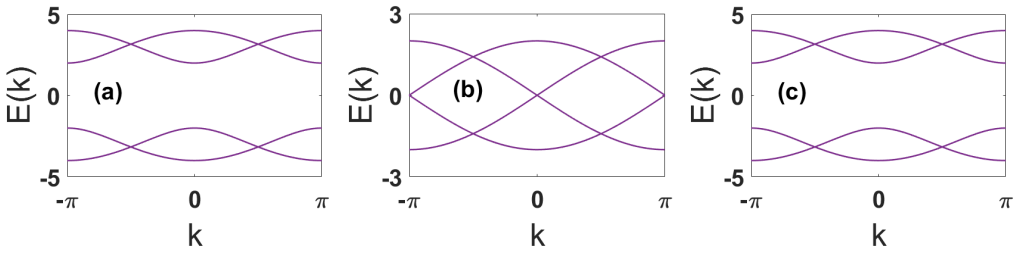

Figure 4.14: Band dispersion for the orientable bulk with cases (a) $u > v(u = 3, v = 1)$,(b) $u = v(u = 1, v = 1)$, (c) $u < v(u = 1, v = 3)$.

Next, we calculate the Zak for each eigenstate of the orientable four band models using the expression for the eigenstates given in Equation 4.22 and the definition of Zak phase given in Equation 4.7. The calculated Zak phase is as follows:

$$\phi^i = \begin{cases} 0 & \text{for}, u > v \\ 1 & \text{for}, u < v \end{cases} \tag{4.27}$$

where $i = 1, 2, 3, 4$ correspond to the four eigenstates. From Equation 4.27 it is clear that the Zak phase invariant for the orientable four band models is similar to that of the C-SSH model only addition being the presence of two extra bands.

We have also calculated the eigenvalues of the open chain Hamiltonian of the four band orientable models with twenty unit cells. The Hamiltonian is:

$$H = \sum_{X=1}^{20} [u\,(c^\dagger_{X,1}\,c_{X,2} + c^\dagger_{X,3}\,c_{X,4}) + v\,(c^\dagger_{X+1,4}\,c_{X,1} + c^\dagger_{X+1,2}\,c_{X,3}) + H.C.] \tag{4.28}$$

By calculating the eigenvalues we can obtain the energy spectrum of the finite chain.

From the above discussion it becomes evident that the orientable four band cases are not very interesting as they bring no new physical properties and are just replicas of the C-SSH model but with higher number of bands.

4.6.2 Non-orientable four band models

We will now discuss the bulk and edge invariants and all the other supporting calculations for the non-orientable four band models. These models unlike the orientable models exhibit novel physical properties which will be discussed in detail here. We will begin by presenting the following expression for the infinite chain

Hamiltonian of the Four band non-orientable model,

$$H = \sum_{X=-\infty}^{\infty} [u\,(c^{\dagger}_{X,1}\,c_{X,2} + c^{\dagger}_{X,2}\,c_{X,3} + c^{\dagger}_{X,3}\,c_{X,4} + c^{\dagger}_{X,4}\,c_{X,1}) \\ +v\,(c^{\dagger}_{X+1,2}\,c_{X,1} + c^{\dagger}_{X+1,4}\,c_{X,1} + c^{\dagger}_{X+1,4}\,c_{X,3} + c^{\dagger}_{X+1,2}\,c_{X,3}) + H.C.] \tag{4.29}$$

Since the chain is infinite and the summation runs from $-\infty$ to $+\infty$, we can do a Fourier transformation of Equation 4.29 and obtain the Hamiltonian as a function of conjugate momentum, k. The Hamiltonian as a function of k is given below and is shown in matrix form for compactness,

$$H(k) = \begin{bmatrix} 0 & u + ve^{ik} & 0 & u + ve^{ik} \\ u + ve^{-ik} & 0 & u + ve^{-ik} & 0 \\ 0 & u + ve^{ik} & 0 & u + ve^{ik} \\ u + ve^{-ik} & 0 & u + ve^{-ik} & 0 \end{bmatrix} \tag{4.30}$$

The eigenvalues (denoted as $E_{a_2}, E_{b_2}, E_{c_2}, E_{d_2}$) of Equation 4.30 and the corresponding eigenstates (denoted as $|\psi_{a_2}\rangle, |\psi_{b_2}\rangle, |\psi_{c_2}\rangle, |\psi_{d_2}\rangle$) are as follows,

$$\begin{bmatrix} E_{a_2} \\ \hline E_{b_2} \\ \hline E_{c_2} \\ \hline E_{d_2} \end{bmatrix} = \begin{bmatrix} 0 \\ \hline 0 \\ \hline -2\,\xi^{+}(k) \\ \hline 2\,\xi^{+}(k) \end{bmatrix}, \tag{4.31}$$

$$|\psi_{a2}\rangle = \begin{bmatrix} 0 \\ \hline -1 \\ \hline 0 \\ \hline 1 \end{bmatrix}, \qquad |\psi_{b_2}\rangle = \begin{bmatrix} -1 \\ \hline 0 \\ \hline 1 \\ \hline 0 \end{bmatrix}, \tag{4.32}$$

$$|\psi_{c_2}\rangle = \begin{bmatrix} -\xi^{+}(k)\,\kappa(k) \\ \hdashline 1 \\ \hdashline -\xi^{+}(k)\,\kappa(k) \\ \hdashline 1 \end{bmatrix}, \tag{4.33}$$

$$|\psi_{d_1}\rangle = \begin{bmatrix} \xi^{+}(k)\,\kappa(k) \\ \hdashline 1 \\ \hdashline \xi^{+}(k)\,\kappa(k) \\ \hdashline 1 \end{bmatrix}. \tag{4.34}$$

Plotting the eigenvalues of the Hamiltonian $H(k)$ as a function of the conjugate momentum, k, we can obtain the band dispersion for this model. The band dispersion for the four band non-orientable model is shown in Figure 4.15. From

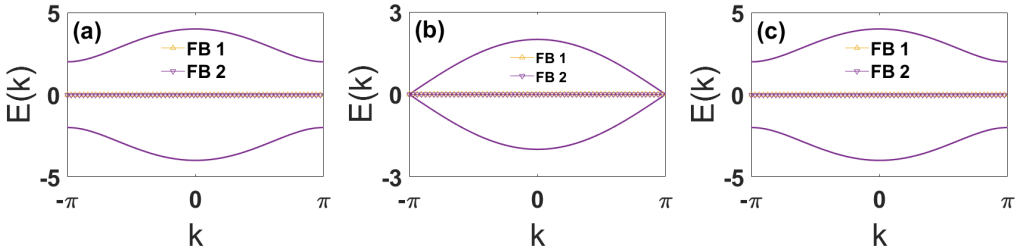

Figure 4.15: Band dispersion for the non-orientable bulk with cases (a) $u > v\,(u = 3, v = 1)$,(b) $u = v\,(u = 1, v = 1)$, (c) $u < v\,(u = 1, v = 3)$.

the eigenstates corresponding to the eigenvalues in Equation 4.31 given above, the value of Zak phase corresponding to each eigenstate can be calculated. The value of Zak phase thus obtained is as follows:

$$\phi^{disp} = \begin{cases} 0 & \text{for}, u > v \\ 1 & \text{for}, u < v \end{cases} \tag{4.35}$$

$$\phi^{flat} = 1,\ \forall\,\{u, v\} \in \mathbf{R} \tag{4.36}$$

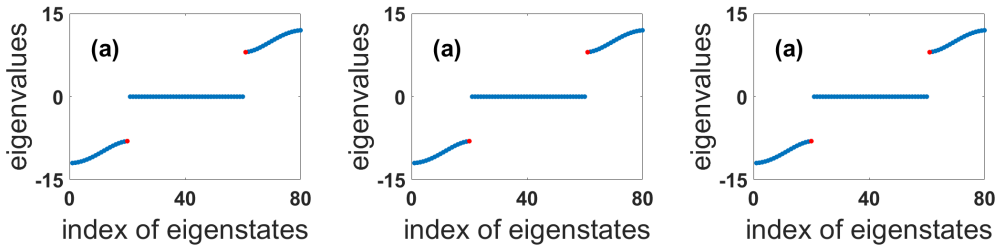

Figure 4.16: Energy eigenvalues for the open chain of a four band non-orientable SAB model with 20 unit cells, sorted from low to high plotted with respect to total number of states indexed from 1 to 80 for (a) $u > v$,(b) $u = v$, (c) $u < v$

where ϕ^{disp} and ϕ^{flat} are the Zak phase for the dispersive bands and flat bands respectively. From Equation 4.35 and Equation 4.36 it can be inferred that there are both similarities and differences the value that Zak phase takes in the four band non-orientable models and the C-SSH models. However, these features are common across all the non-orientable models irrespective of the number of bands and hence will be discussed together in the next section.

We will now present the results for the case of a finite chain of four band non-orientable model. Firstly the Hamiltonian for this model with 20 unit cells is as follows:

$$H = \sum_{X=1}^{20} [u\,(c^{\dagger}_{X,1}\,c_{X,2} + c^{\dagger}_{X,2}\,c_{X,3} + c^{\dagger}_{X,3}\,c_{X,4} + c^{\dagger}_{X,4}\,c_{X,1}) \\ +v\,(c^{\dagger}_{X+1,2}\,c_{X,1} + c^{\dagger}_{X+1,4}\,c_{X,1} + c^{\dagger}_{X+1,4}\,c_{X,3} + c^{\dagger}_{X+1,2}\,c_{X,3}) + H.C.] \tag{4.37}$$

By calculating the eigenvalues of the above Hamiltonian we can plot the energy spectrum of the finite chain and investigate the changes in the energy spectrum with change in various system parameters. The plots of energy spectrum for the open chain with various values of intercell and intracell hopping amplitudes is shown in Figure 4.16. From Figure 4.16, it is clear that there are a total of $2N+2$ zero energy modes and they are of two types. $2N$ zero energy modes are present for all values of system parameters and 2 of them appear only when the intercell hopping amplitude is greater than the intracell hopping amplitude.

Inverse participation ratio (IPR) is a quantity that acts as a measure of lo-

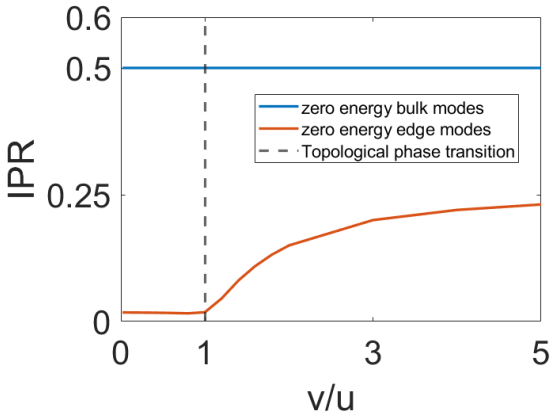

Figure 4.17: Inverse participation ratio (IPR) for the four band non-orientable model plotted with respect to the change in the ratio between inter cell and intra cell hopping denoted by v and u respectively.

calisation in any system. Its value gives an estimate of the number of sites the particular eigenstate being considered is localised. If the eigenstate is localised at only one site its IPR value is one. As the number of sites in which the eigenstate is localised keeps increasing the IPR value becomes lesser and lesser. If the eigenstate over all sites in a lattice with N sites then the IPR for that eigenstate is $1/N$ and in the limit of $N \to \infty$ the IPR value tends to zero. The formal definition of IPR is given by the expression,

$$IPR = \frac{\sum_{i=1}^{L} |\psi_i|^4}{(\sum_{i=1}^{L} |\psi_i|^2)^2}. \tag{4.38}$$

The plot of IPR value as a function of the ratio of intercell to intracell hopping amplitudes (v/u) is given in Figure 4.17. We observe in Figure 4.17 that the IPR value corresponding to the first type zero energy modes are a constant for all value of ratio of hopping parameters. For the second type of zero energy modes the IPR value is nearly equal to zero for $(v/u) < 1$. As (v/u) crosses the value of one, the IPR value starts increasing suddenly and keeps increasing monotonously indicating the delocalisation to localisation transition of these modes at $(v/u) = 1$.

The IPR plot is a very good method to show localisation transitions in a system. However, one cannot conclude whether the localisation is happening at the edges or in the bulk based on these plots. To determine this we need to explicitly

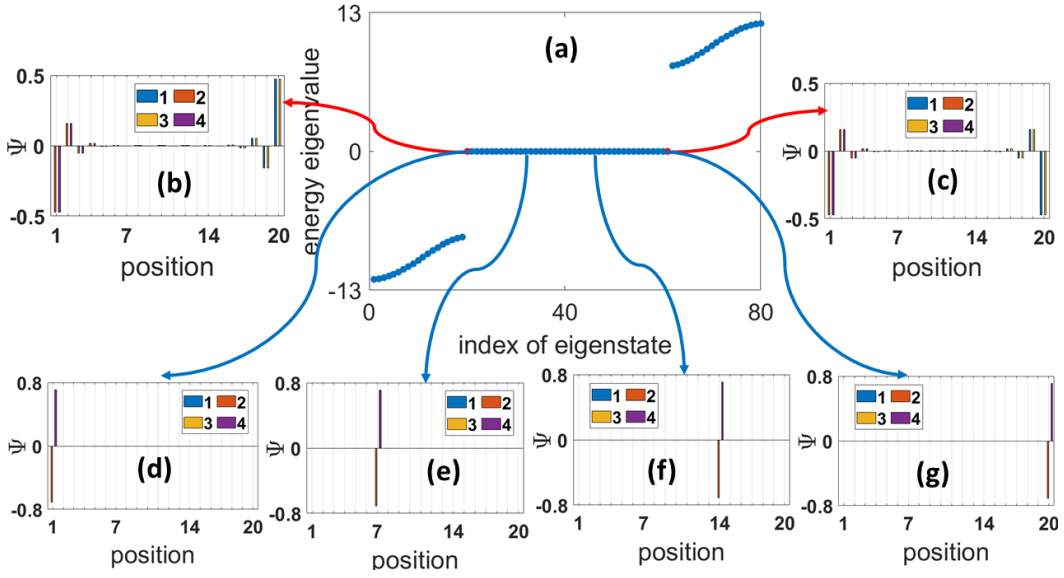

Figure 4.18: (a) Energy eigenvalues for the open chain of the non-orientable four band case with 20 unit cells (b)-(c) zero energy edge states (d)-(g) some of the zero energy states localised in the bulk.

plot the wavefunction value i.e. the eigenstate value at each site. This is shown in Figure 4.18. We can see from Figure 4.18 that the wavefunction corresponding to the $2N$ zero energy states that remain for all ratios of hopping parameters are localised in the bulk and the wavefunction corresponding to the two zero energy states that appear when $(v/u) > 1$ are localised at the edges.

These results obtained for the four band non-orientable models are similar to the C-SSH model in terms of zero energy edge states but also exhibit new features like zero energy modes localised in the bulk. In fact these signatures are universal in all the non-orientable models and we will summarise these unique features in the next section to avoid repetition.

4.7 SAB model with a non-orientable bulk

In this section we will discuss a six band SAB model whose bulk is an one dimensional non-orientable manifold. As discussed in the previous sections we need

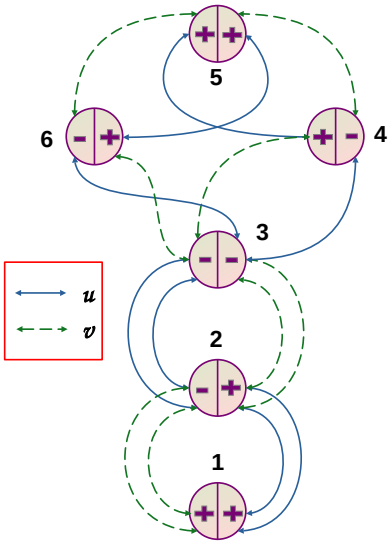

Figure 4.19: Unit cell of SAB model (with P.B.C.) for the six band non-orientable bulk (notice the twist).

at least two sites for a linear bulk and four sites for a circular bulk. An one dimensional non-orientable manifold can be obtained by fusing one end of a line segment to a circle and leaving the other free. With the same analogy we will use a combination of a linear bulk and circular bulk, making the number of sites required for a minimalastic SAB model with a non-orientable bulk as six. This makes the minimalastic SAB model with non-orientable bulk as a six band model. Figure 4.19 presents a graphical image of the SAB model with a non-orientable bulk in a periodic boundary condition set-up. Figure 4.19 shows a graphical image of the SAB model with a non-orientable bulk in a open boundary condition with five unit cells. Notice in both Figure 4.19 and Figure 4.20, the twist is in between the sites labeled as 3 and 6 in the unit cell.

We will begin by presenting the Hamiltonian for the infinite chain of the six band SAB model with a non-orientable bulk. This is given as:

$$H = \sum_{X=-\infty}^{\infty} [2u(c^{\dagger}_{X,1}c_{X,2} + c^{\dagger}_{X,2}c_{X,3}) + u(c^{\dagger}_{X,3}c_{X,4} + c^{\dagger}_{X,4}c_{X,5} \tag{4.39}$$
$$+c^{\dagger}_{X,5}c_{X,6} + c^{\dagger}_{X,6}c_{X,3}) + 2v(c^{\dagger}_{X+1,2}c_{X,1} + c^{\dagger}_{X+1,2}c_{X,3}) + v(c^{\dagger}_{X+1,4}c_{X,3} + c^{\dagger}_{X+1,6}c_{X,3}$$
$$+c^{\dagger}_{X+1,4}c_{X,5} + c^{\dagger}_{X+1,6}c_{X,5})] + H.C.$$

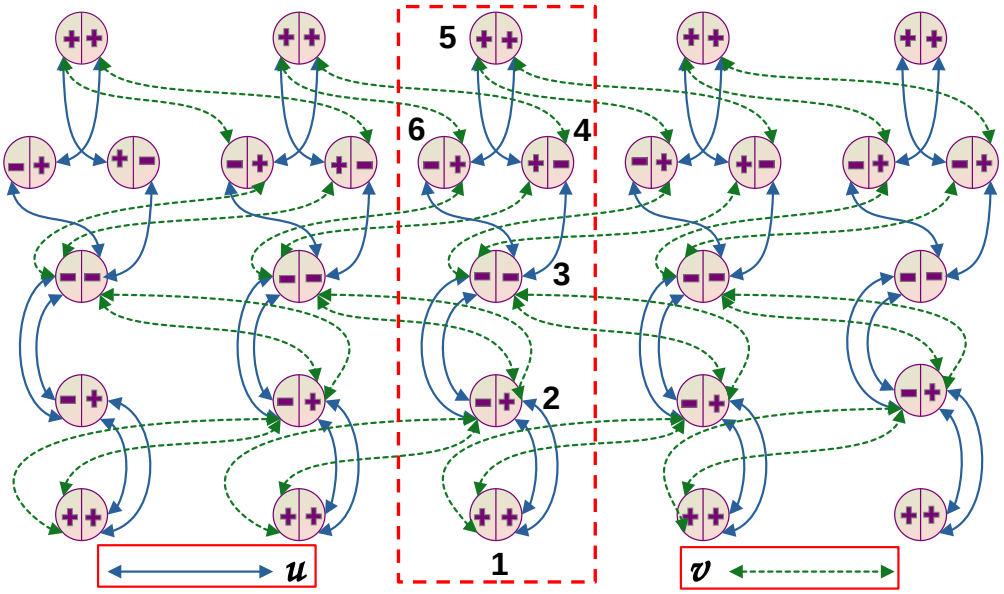

Figure 4.20: Open chain of six band non-orientable bulk SAB model with five unit cells

The Hamiltonian in Equation 4.39 after Fourier transformation can be expressed in the matrix form as:

$$H(k) = \begin{bmatrix} 0 & 2a & 0 & 0 & 0 & 0 \\ 2a^* & 0 & 2a^* & 0 & 0 & 0 \\ 0 & 2a & 0 & a & 0 & a \\ 0 & 0 & a^* & 0 & a^* & 0 \\ 0 & 0 & 0 & a & 0 & a \\ 0 & 0 & a^* & 0 & a^* & 0 \end{bmatrix} \tag{4.40}$$

where $a = u + ve^{ik}$ and $a^* = u + ve^{-ik}$.

The eigenvalues and eigenvectors of the $H(k)$ in Equation 4.40 can be calculated

and their expression are as follows.

$$\begin{bmatrix} E_{a_3} \\ \hline E_{b_3} \\ \hline E_{c_3} \\ \hline E_{d_3} \\ \hline E_{e_3} \\ \hline E_{f_3} \end{bmatrix} = \begin{bmatrix} 0 \\ \hline 0 \\ \hline -\sqrt{2\,(3-\sqrt{3})}\,\xi^{+}(k) \\ \hline \sqrt{2\,(3-\sqrt{3})}\,\xi^{+}(k) \\ \hline -\sqrt{2\,(3+\sqrt{3})}\,\xi^{+}(k) \\ \hline \sqrt{2\,(3+\sqrt{3})}\,\xi^{+}(k) \end{bmatrix}, \tag{4.41}$$

$$|\psi_{a_3}\rangle = \begin{bmatrix} 0 \\ \hline 0 \\ \hline 0 \\ \hline -1 \\ \hline 0 \\ \hline 1 \end{bmatrix}, \qquad |\psi_{b_3}\rangle = \begin{bmatrix} 1 \\ \hline 0 \\ \hline -1 \\ \hline 0 \\ \hline 1 \\ \hline 0 \end{bmatrix}, \tag{4.42}$$

$$|\psi_{c_3}\rangle = \begin{bmatrix} \frac{\sqrt{2(3-\sqrt{3})}\,\xi^{+}(k)\,\kappa(k)}{3} \\ \hline 1-\sqrt{3} \\ \hline \frac{\sqrt{2}\,(\sqrt{3}-2)\,\xi^{+}(k)\,\kappa(k)}{\sqrt{3-\sqrt{3}}} \\ \hline 1 \\ \hline -\frac{\sqrt{2}\,\xi^{+}(k)\,\kappa(k)}{(\sqrt{3-\sqrt{3}})} \\ \hline 1 \end{bmatrix}, \tag{4.43}$$

$$|\psi_{d_3}\rangle = \begin{bmatrix} -\frac{\sqrt{2(3-\sqrt{3})}\,\xi^+(k)\,\kappa(k)}{3} \\ \hline 1-\sqrt{3} \\ \hline \frac{\sqrt{2}(\sqrt{3}-2)\,\xi^+(k)\,\kappa(k)}{\sqrt{3-\sqrt{3}}} \\ \hline 1 \\ \hline \frac{(3+\sqrt{3})\sqrt{(3-\sqrt{3})}\,\xi^+(k)\,\kappa(k)}{3\sqrt{2}} \\ \hline 1 \end{bmatrix}, \tag{4.44}$$

$$|\psi_{e_3}\rangle = \begin{bmatrix} -\frac{\sqrt{2(3+\sqrt{3})}\,\xi^+(k)\,\kappa(k)}{3} \\ \hline 1+\sqrt{3} \\ \hline -\frac{\sqrt{2}(\sqrt{3}+2)\,\xi^+(k)\,\kappa(k)}{\sqrt{3+\sqrt{3}}} \\ \hline 1 \\ \hline -\frac{\sqrt{2}\,\kappa^*(k)}{(3+\sqrt{3})(\xi^+(k))^2} \\ \hline 1 \end{bmatrix}, \tag{4.45}$$

$$|\psi_{f_3}\rangle = \begin{bmatrix} \frac{\sqrt{2(3+\sqrt{3})}\,\xi^+(k)\,\kappa(k)}{3} \\ \hline 1+\sqrt{3} \\ \hline \frac{\sqrt{2}(\sqrt{3}+2)\,\xi^+(k)\,\kappa(k)}{\sqrt{3+\sqrt{3}}} \\ \hline 1 \\ \hline \frac{\sqrt{2}\,\kappa^*(k)}{(3+\sqrt{3})(\xi^+(k))^2} \\ \hline 1 \end{bmatrix}. \tag{4.46}$$

We can plot the eigenvalues in Equation 4.41 as a function of the conjugate

momentum, k. This is called the band dispersion and the band dispersion of the six band non-orientable manifold as the bulk is shown in Figure 4.21 for various configuration of the intercell and intracell hopping values.

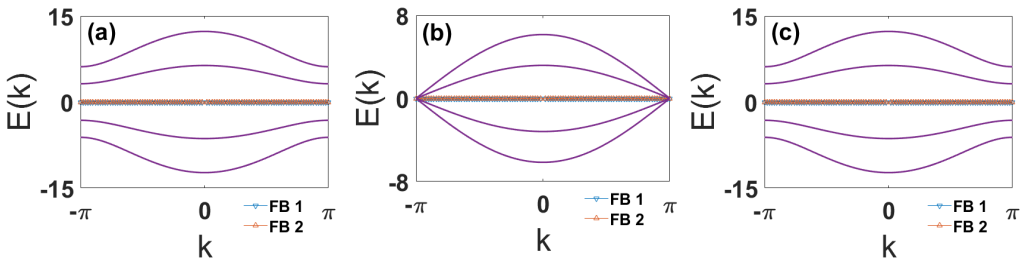

Figure 4.21: Band dispersion for the six band non-orientable SAB model with cases (b) $u > v(u = 3, v = 1)$,(c) $u = v(u = 1, v = 1)$, (d) $u < v(u = 1, v = 3)$.

From the expression of the eigenstates of the SAB model with non-orientable bulk given above we can calculate the Zak phase for these eigenstates from the expression of Zak phase given in Equation 4.7. The values of the Zak phase are listed below,

$$\phi^{disp} = \begin{cases} 0 & \text{for}, u > v \\ 1 & \text{for}, u < v \end{cases} \tag{4.47}$$

$$\phi^{flat} = 1, \forall \{u, v\} \in \mathbf{R} \tag{4.48}$$

where ϕ^{disp} and ϕ^{flat} are the Zak phase for the dispersive bands and flat bands respectively.

After discussing the results for an infinite bulk let us now move our focus to the case of a finite bulk. The Hamiltonian of the six band SAB model with a non-orientable manifold as bulk is given below:

$$H = \sum_{X=1}^{20} [2u(c^{\dagger}_{X,1}c_{X,2} + c^{\dagger}_{X,2}c_{X,3}) + u(c^{\dagger}_{X,3}c_{X,4} + c^{\dagger}_{X,4}c_{X,5} \tag{4.49}$$
$$+c^{\dagger}_{X,5}c_{X,6} + c^{\dagger}_{X,6}c_{X,3}) + 2v(c^{\dagger}_{X+1,2}c_{X,1} + c^{\dagger}_{X+1,2}c_{X,3}) + v(c^{\dagger}_{X+1,4}c_{X,3} + c^{\dagger}_{X+1,6}c_{X,3}$$
$$+c^{\dagger}_{X+1,4}c_{X,5} + c^{\dagger}_{X+1,6}c_{X,5})] + H.C.$$

By diagonalising the above Hamiltonian we can obtain the energy eigenvalues of the Hamiltonian. By plotting the values of these energy eigenvalues, we can obtain the energy spectrum. The energy spectrum for the six band SAB model with a non-orientable bulk is given in Figure 4.22 for different configurations of the intercell and intracell hopping amplitudes.

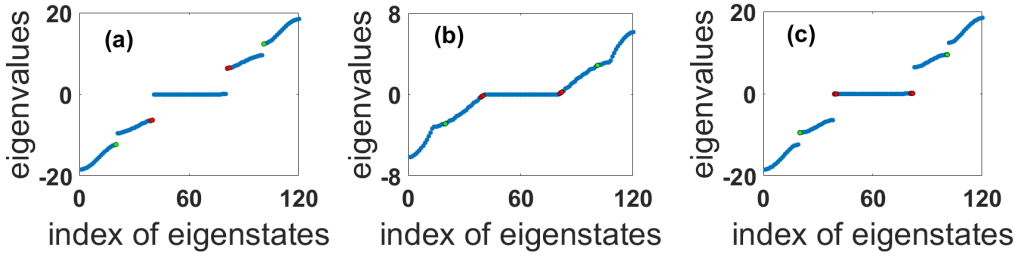

Figure 4.22: Energy eigenvalues for the open chain of a non-orientable bulk with 20 unit cells, sorted from low to high plotted with respect to total number of states indexed from 1 to 120 for (a) $u > v$,(b) $u = v$, (c) $u < v$

From Figure 4.22 it is clear that there are $2N$ zero energy modes that are always present in the system for all possible combinations of the intercell and intracell hopping amplitudes. There is an additional four zero energy modes that appear when the value of intercell hopping is greater than the value of intracell hopping. Thus there is a total of $2N+4$ zero energy modes possible in the system.

To understand these zero energy modes more clearly we plot the inverse partic-

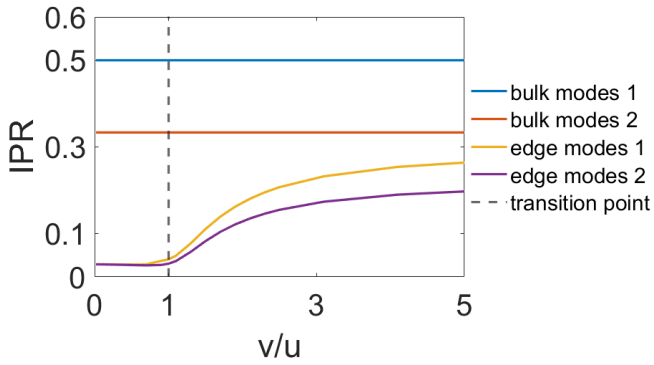

Figure 4.23: Inverse participation ratio (IPR) for the six band non-orientable model plotted with respect to the change in the ratio between inter cell and intra cell hopping denoted by v and u respectively.

ipation ratio (IPR) of these modes. The IPR plot is shown in Figure 4.23, where the IPR value is plotted as a function of the ratio of hopping amplitudes. We make the following observations based on the IPR plot in Figure 4.23:

- The value of the IPR for the $2N$ zero energy states present throughout for all possible combinations of intercell and intracell hopping amplitudes is constant.
- Among the $2N$ zero energy modes, N of them have the IPR value as 0.5 and the other N has the IPR value as 0.33.
- The value of IPR for the 4 zero energy edge states that appear when $(v/u) > 1$, the IPR value remain close to zero when the ratio $(v/u) < 1$. As we cross the $(u/v) = 1$ point (which we indicate as the topological phase transition point), the value of IPR starts increasing. It increases monotonously with increase in the value of (v/u) when $(v/u) > 1$.
- Among these 4 modes there are two sets of IPR values as IPR is plotted as a function of (v/u). Each set has two eigenstates in them having the same value of IPR. This shows that even in these zero energy states the localisation is over different number of sites.

The IPR plots have revealed that these zero energy states are localised states. To understand more about these zero energy modes and the exact position at which these localised states exist, we plot the value of the wave function at each site. This is shown in Figure 4.24.

4.8 Three band SAB model

In this section we will discuss a three band non-orientable SAB model which is very simple to visualise. This can be imagined to be obtained by fusing certain sites periodically in two different C-SSH chains as illustrated in Figure 4.25. The

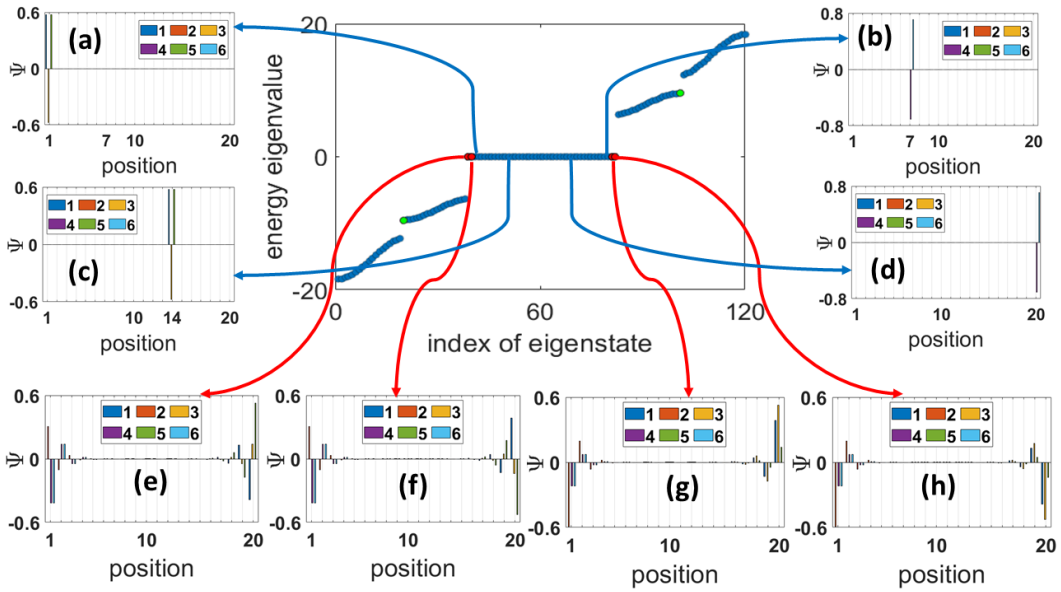

Figure 4.24: Energy eigenvalues for the open chain of the non-orientable six band case with 20 unit cells (center) (a)-(d) wave functions of some of the zero energy eigenstates localised in the bulk and (e)-(h) zero energy edge states.

Hamiltonian for the infinite chain of the three band SAB model is given as:

$$H = \sum_{X=-\infty}^{\infty} [u(c^{\dagger}_{X,1}c_{X,2} + c^{\dagger}_{X,1}c_{X,3}) + v(c^{\dagger}_{X+1,1}c_{X,2} + c^{\dagger}_{X+1,1}c_{X,3})] + H.C. \quad (4.50)$$

We can do the Fourier transformation of Equation 4.50 to obtain the Hamiltonian as a function of the conjugate momentum, k. The Hamiltonian as a function of k is shown below in the matrix form:

$$H(k) = \begin{bmatrix} 0 & u + ve^{ik} & u + ve^{ik} \\ u + ve^{-ik} & 0 & 0 \\ u + ve^{-ik} & 0 & 0 \end{bmatrix} \quad (4.51)$$

The eigenvalues and the eigenvectors of Equation 4.51 are obtained and are listed below,

$$\begin{bmatrix} E_{a_4} \\ \hline E_{b_4} \\ \hline E_{c_4} \end{bmatrix} = \begin{bmatrix} 0 \\ \hline -\xi^{+}(k) \\ \hline \xi^{+}(k) \end{bmatrix}, \quad (4.52)$$

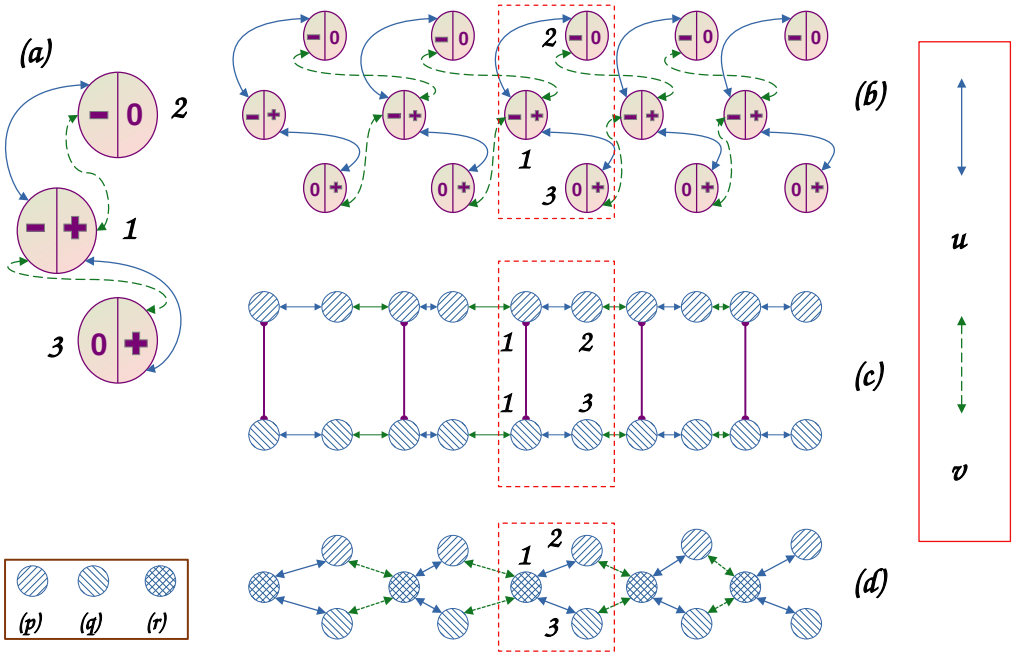

Figure 4.25: (a) Unit cell of the three band non-orientable bulk SAB model (with P.B.C.) (b) Open chain the three band non-orientable bulk SAB model with five unit cells (c) two independent C-SSH chains whose corresponding alternate sites have to be be fused periodically to obtain (d) three band non-orientable bulk SAB model (p)-(q) sites belonging to two different C-SSH chains and (r) represents fused sites

$$|\psi_{a_4}\rangle = \begin{bmatrix} 0 \\ \hline -1 \\ \hline 1 \end{bmatrix}, \tag{4.53}$$

$$|\psi_{b_4}\rangle = \begin{bmatrix} -\sqrt{2}\,\xi^{+}(k)\,\kappa(k) \\ \hline 1 \\ \hline 1 \end{bmatrix}, \tag{4.54}$$

$$|\psi_{c_4}\rangle = \begin{bmatrix} \sqrt{2}\,\xi^{+}(k)\,\kappa(k) \\ \hline 1 \\ \hline 1 \end{bmatrix}. \tag{4.55}$$

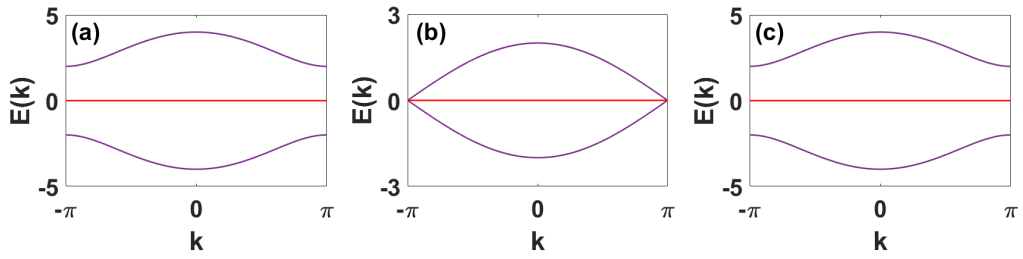

Figure 4.26: Band dispersion of the three band non-orientable bulk with the cases (a) $u > v(u = 3, v = 1)$,(b) $u = v(u = 1, v = 1)$, (c) $u < v(u = 1, v = 3)$.

We can plot the eigenvalues in Equation 4.51 as a function of the conjugate momentum, k. This is called the band dispersion and the band dispersion for various configurations of the intercell and intracell hopping amplitudes is shown in Figure 4.26.

From the above expression of the eigenstates we can calculate the value of Zak phase from the expression of Zak phase given in Equation 4.7. The value of Zak phase for the eigenstates of the three band SAB model are:

$$\phi^{disp} = \begin{cases} 0 & \text{for}, u > v \\ 1 & \text{for}, u < v \end{cases} \tag{4.56}$$

$$\phi^{flat} = 1, \forall \{u, v\} \in \mathbf{R} \tag{4.57}$$

where ϕ^{disp} and ϕ^{flat} are the Zak phase for the dispersive bands and flat band respectively.

If we consider a finite chain of three band SAB model with 20 unit cells, the corresponding Hamiltonian is given as:

$$H = \sum_{X=1}^{20} [u(c^{\dagger}_{X,1}c_{X,2} + c^{\dagger}_{X,1}c_{X,3}) + v(c^{\dagger}_{X+1,1}c_{X,2} + c^{\dagger}_{X+1,1}c_{X,3})] + H.C. \tag{4.58}$$

Calculating the eigenvalues of Equation 4.58, we can get the energy spectrum.

We also plot the IPR values as a function of the ratio of intercell and intracell

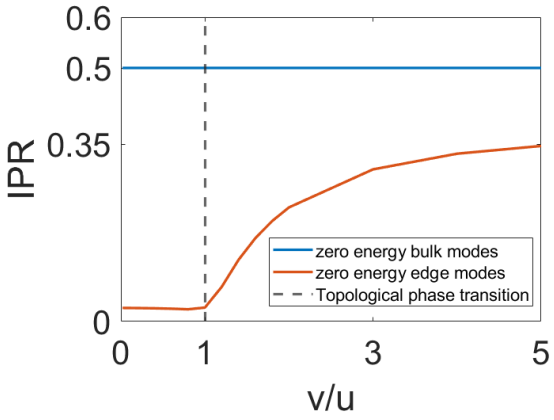

Figure 4.27: Inverse participation ratio (IPR) for the three band model plotted with respect to the change in the ratio between inter cell and intra cell hopping denoted by v and u respectively.

hopping amplitudes in Figure 4.27. To determine the spatial profile of localisation of the zero energy states we explicitly calculate and plot the value of the wave-function at each site in Figure 4.28. From Figure 4.28 it is clear that the zero energy states that appear for all parameter values are localised in the bulk and the zero energy states that appear when $(v/u) > 1$ are localised only at the edges.

4.9 Discussion

In this section we will discuss all the novel and exotic physical properties that are present in all the non-orientable SAB models that we have discussed so far. We will sequentially discuss for each topological or physical property both the similarities and the novelties of the non-orientable SAB model in comparison to the C-SSH model. We will begin first with the properties associated with an infinite bulk which will be followed by the ones associated with a finite bulk. We will end with a discussion the prospects for experimentally realising these models.

4.9.1 Band Dispersion

In all the cases of non-orientable SAB models, the band dispersion has the common feature that it has two kinds of bands, (1) dispersive band, and (2) flat band. The

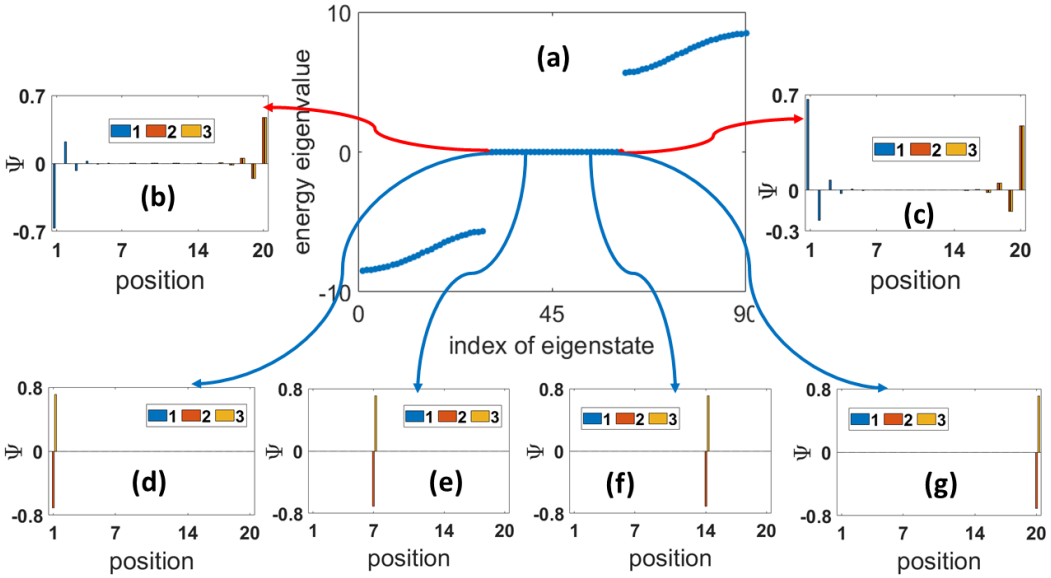

Figure 4.28: (a) Energy eigenvalues for the open chain of the non-orientable three band case with 20 unit cells (b)-(c) zero energy edge states (d)-(g) some of the zero energy states localised in the bulk

number of dispersive bands and the degeneracy of the flat band varies from model to model.

- In the four band non-orientable SAB models there are two dispersive bands which are symmetric with respect to the particle hole symmetry level and a doubly degenerate flat band exactly at the particle hole symmetry level (refer to Figure 4.15).
- In the six band SAB model with a non-orientable bulk there are four dispersive bands forming two pairs of bands symmetric with respect to the particle hole symmetry level and a doubly degenerate flat band exactly at the particle hole symmetry level (refer to Figure 4.21).
- In the three band non-orientable SAB models there are two dispersive bands which are symmetric with respect to the particle hole symmetry level and a non-degenerate flat band exactly at the particle hole symmetry level (refer to Figure 4.26).

Since the dispersion in the flat band is independent of the conjugate momentum, k the effective mass of the electron diverges making it localised in the flat band.

The dispersive bands in the non-orientable SAB models are similar to the C-SSH model whereas the flat bands are new additions.

4.9.2 Zak Phase

In all the cases of non-orientable SAB model there are both dispersive and flat bands. The Zak phase of these bands show the following signatures.

- The Zak phase value for all the flat bands has a value of one irrespective of the value of the ratio of hopping amplitudes.
- The Zak phase value of all the dispersive bands have a value of zero when the ratio of intercell and intracell hopping amplitude $(v/u) < 1$. It has a value of one when $(v/u) > 1$.

The behavior of the Zak phase value for the dispersive bands is similar to the C-SSH model whereas the constant value of the Zak phase for the flat band is a new feature in the non-orientable models.

4.9.3 Zero Energy States

In all the cases of non-orientable SAB model there are zero energy states localised at the bulk and localised at the edges. The number of such is specific to each model and we list that below for comparison:

- For the four band non-orientable SAB models there are $2N$ zero energy states localised in the bulk and 2 states localised in the edges.
- For the six band SAB model with a non-orientable bulk there are $2N$ zero energy states localised in the bulk and 4 states localised in the edges.
- For the three band non-orientable SAB models there are N zero energy states localised in the bulk and 2 states localised in the edges.

The zero energy modes localised in the bulk exists for all values of ratio of the intercell to intracell hopping amplitudes (v/u). However the zero energy modes localised in the edges appear only when $(v/u) > 1$. The zero energy edge states when $(v/u) > 1$ are similar to that of the C-SSH model but the zero energy states localised in the bulk are unique to the non-orientable SAB models.

4.9.4 Inverse Participation Ratio

We have also discussed the value of the inverse participation ratio (IPR) as a function of the ratio of intercell and intracell hopping amplitude (v/u) for all the non-orientable SAB models. The salient features of the IPR plots are:

- The IPR plots for the four band non-orientable models show that there are two sets of zero energy modes. The IPR value of the first set is a constant as a function of (v/u). This set corresponds to the zero energy modes localised in the bulk. The second set has an IPR value close to zero for $(v/u) < 1$. It starts increasing as we cross the point $(v/u) = 1$ and increases monotonously for $(v/u) > 1$. This set corresponds to the zero energy modes localised in the edges (refer to Figure 4.17).

- The IPR plots for the three band non-orientable SAB model is essentially the same as the four band non-orientable model except for the fact that the number of zero energy states with constant IPR value is half the number in the three band case (refer to Figure 4.27).

- The IPR plots for the six band SAB model with a non-orientable bulk show that there are four sets of zero energy modes. The IPR value of the first and second set is a constant as a function of (v/u). These sets corresponds to the zero energy modes localised in the bulk. However, the value of this constant is different indicating that the number of sites the electron is localised is different for the different sets of these zero energy states. The third and fourth set has an IPR value close to zero for $(v/u) < 1$. It starts increasing as we cross the point $(v/u) = 1$ and increases monotonously for $(v/u) > 1$. These sets corresponds to the zero energy modes localised in the edges. Again

the qualitative behavior of the IPR values of these sets of zero energy states maybe similar but the explicit value of IPR is different for the third and fourth set. This clarifies that the number of sites in which the electrons are localised at the edges are different (refer to Figure 4.23).

The behavior of the IPR values of the zero energy edge states are similar to that of the C-SSH model. However, since the zero energy states localised in the bulk are new to the non-orientable SAB models their IPR behavior is novel.

4.9.5 Bulk Boundary Correspondence

We have presented both the bulk invariants and the boundary invariants for the non-orientable SAB models. The value of the bulk invariants like the Zak phase and the boundary invariants like the number of zero energy edge states of the non-orientable SAB models show an one-to-one correspondence validating the applicability of the bulk boundary correspondence to these models.

4.9.6 Prospects for experimental realisation of SAB models

We believe that the SAB models discussed in this chapter can be realised by making certain tweaks and changes to some available versatile experimental platforms. These are:

- The first promising experimental platform is the emerging area of quantum dot lattices. It is worth while to mention here that C-SSH chains have been already realised in this platform along with several other variations of the C-SSH model[114]. The effects of the spin and the orbital momentum of the electron in the carbon nanotube quantum dot has also been studied[110]. In this note it is possible to identify the spin of the electron in the carbon nanotube quantum dot as the first degree of freedom which we have introduced and the orbital angular momentum of the electron in the carbon nanotube quantum dot as the second degree of freedom. If the value of these quantum numbers can be tuned to the values required by the model and the system

is tuned in such a way that the hopping occurs between these quantum dots based on the rules we have formulated the properties predicted by our study for different SAB models can be realised experimentally.

- The second promising experimental platform is that of photonic lattices. Like the case of quantum dot lattices, C-SSH chains have been realised in this platform too[98]. However, this is particularly well suited for the three band SAB model as the lattice of this model is the one dimensional diamond lattice. In this direction it is important to note that the one dimensional diamond lattice has already been realised in this platform it will be straight forward to realise the three band SAB model here. The only new addition to this platform would be to stagger the hopping amplitudes like the SSH model.

4.10 Conclusion

In this chapter we introduced a topological tight binding model which we termed as the Su-Schrieffer-Heeger model with any bulk (SAB model). After introducing the rules of the hopping in this model, we presented the results for the four band, six band and three band SAB models. In all the non-orientable SAB models along with the topological zero energy edge states, there are also zero energy states localised in the bulk. These states correspond to the flat bands in the band dispersion. This model is a demonstration of emergence of flat bands in SSH model like systems.

"He who can listen to the music in the midst of noise can achieve great things"

Vikram Sarabhai

5

Effects of Disorders on the SAB models

In this chapter, we study the effects of various kinds of static disorders on the SAB models. We will first briefly discuss two localisation effects in tight binding models arising from the geometry of the lattice and the disorder in the lattice. After this we will introduce the chiral symmetry of the SSH model. We will then discuss the effects of both chiral symmetry preserving and breaking disorders.

In physics it is important to verify theoretically obtained predictions in available or soon to be available experimental platforms. The most important bridge that connects these two paradigms of theoretical prediction and experimental verification is that experimental observations are not performed in ideal pristine setups over which theoretical calculations have been performed. Experimental observations are always performed a midst other unknown and unwanted noises and disturbances to the ideal setup envisioned theoretically.

In this context the study of disorders in tight binding models was important to make a more meaningful connection between the theoretical tight binding calculations and the experimental observations. However the role of disorder took a central stage with the onset of concepts like Anderson localisation wherein the effects of disorder was not an ancillary effect just to help theory connect with experiment but was the dominant effect[115].

We also understand based on the discussions in the previous chapter the role of lattice geometry in the emergence of flat bands in the system. If the lattice geometry is such that the hopping amplitudes for an electron to hop out of that site destructively interfere, the electron effectively gets localised in that site which leads to the emergence of these flat bands in the electronic dispersion[82].

From the above mentioned points it is clear that there are two localisation effects in tight binding models.The first is due to the disorder in the lattice and the second is due to the geometry of the lattice. This naturally rises the question that ***"what will be the net effect on the system if both these localisation effects are present simultaneously?. Will their simultaneous presence add up to or cancel each other?"***

From the discussions of the previous chapters, it is evident that the non-orientable SAB models have flat bands. This makes it an ideal system to study

the effects of disorder in a system with flat bands. Moreover from an experimental perspective also it is important to study the effects of disorder on the properties of non-orientable SAB models. Further disorders can be of many origins. Broadly the static disorder for SSH model can be classified in to chiral symmetry breaking and preserving disorders.

This chapter is organised as follows. In section 5.1 we will present an introduction to disorders in tight binding models. Following this in section 5.2 we will discuss the chiral symmetry and more particularly the sub-lattice symmetry in the context of SSH model. With this background we can define chiral symmetry preserving and breaking disorders. We will wind up this section with a quick recap of the geometry of the lattice and flat bands in section 5.3. We will explain our implementation of the static disorder both chiral symmetry preserving and breaking cases in section 5.4, followed with the discussion of results in section 5.5. We will summarise the chapter in section 5.6.

5.1 Disorder in tight binding models

The role of disorder in tight binding models became a subject of research in itself with the revolutionary work of Anderson describing the phenomenon of Anderson localisation[115]. Anderson arrived at the conclusion that beyond a critical disorder there will be no diffusion in a three dimensional tight binding system. That is there will be a metal to insulator transition (MIT) beyond a critical disorder strength. It was later proven that in one dimension this MIT occurs for even tiny amount of disorder. In this section we will motivate this MIT by some numerical calculations performed on an one dimensional tight binding model with onsite disorders.

Let us consider the following tight-binding Hamiltonian:

$$H = \sum_n c_n^\dagger c_n + c_{n+1}^\dagger c_n + c_{n-1}^\dagger c_n. \tag{5.1}$$

It is one band tight binding model and the wavefunctions are extended on the entire lattice i.e. over all n sites as illustrated in Figure 5.1.

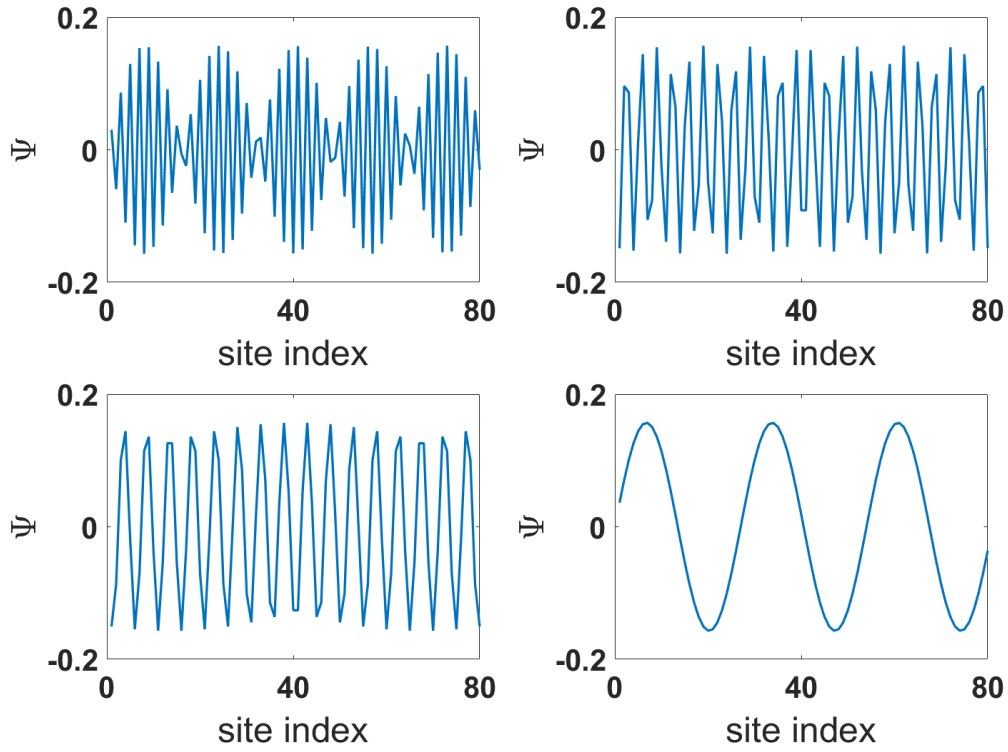

Figure 5.1: Some of the eigenstates of the 1D one band tight binding model described by the Hamiltonian in Equation 5.1 with 80 sites in the chain. The plots are sample from all the 80 eigenstates which are all extended.

If we add an onsite disorder at each site to the model in Equation 5.1, we get the following Hamiltonian:

$$H_{dis} = \sum_{n} d\gamma_n c_n^\dagger c_n + c_{n+1}^\dagger c_n + c_{n-1}^\dagger c_n. \tag{5.2}$$

where d is the disorder strength and γ_n is randomly chosen from the uniform distribution: $[-1, 1]$.

We can diagonalise the Hamiltonian with disorder (H_{dis}) and obtain its eigenvalues and eigenstates for a range of disorder strength d. To identify the metal to insulator transition one can look in to the value of inverse participation ratio defined in Equation 5.3.

$$IPR = \frac{\sum_{i=1}^{L} |\psi_i|^4}{(\sum_{i=1}^{L} |\psi_i|^2)^2}. \tag{5.3}$$

A value of IPR close to zero is indicative of the support of eigenstates nearly equal to the size of the lattice. An higher IPR indicates localisation of the eigenstates on fewer sites. The IPR plots of some of the eigenstates is given in Figure 5.2.

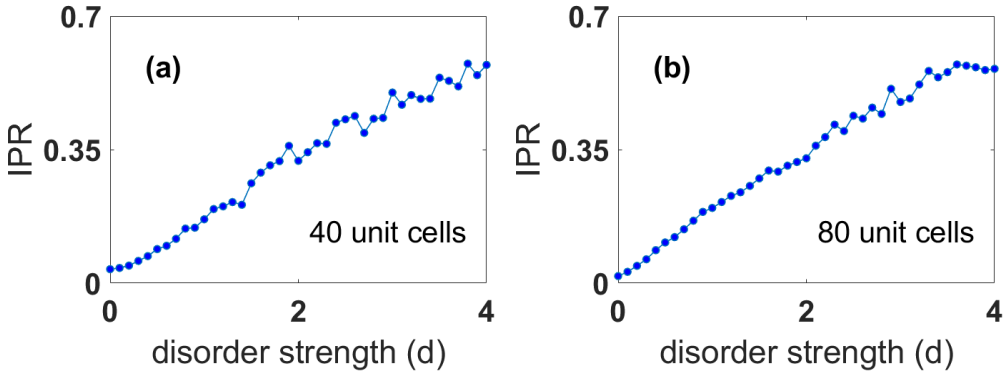

Figure 5.2: IPR values as a function of disorder strength for lattices with (a) 40 sites and (b) 80 sites.

From the plots in Figure 5.2, it is clear that the IPR value for the clean system is close to zero. However even with the onset of small onsite disorder the IPR value begins to increase. This indicates that even small amounts of disorders in an one dimensional system bring about MIT.

5.2 Symmetries and its relation to disorders

In this section we will discuss the symmetries of the SSH model and the classification of the disorders based on these symmetries. In the context of topological insulators three symmetries are discussed prominently, as in the case of the periodic table of topological invariants. These symmetries are:

1. **Chiral (sub-lattice) symmetry**: It is an anti-commuting unitary symmetry "$\mathcal{S}$" defined as $\mathcal{S}\mathcal{H}_k\mathcal{S} = \sigma_z\mathcal{H}_k\sigma_z$ and $\mathcal{S}^2 = 1$. One can readily verify $\{\mathcal{S}, \mathcal{H}_{SSH,k}\} = 0$, where $\mathcal{H}_k$ is the SSH Hamiltonian.

2. **Time reversal symmetry**: It is a commuting anti unitary symmetry "$\mathcal{T}$"

defined as $\mathcal{T}\mathcal{H}_k\mathcal{T} = \mathcal{H}^*_{-k}$ and $\mathcal{T}^2 = 1$. One can readily verify $[\mathcal{T}, \mathcal{H}_{SSH,k}] = 0$, where $\mathcal{H}_{SSH,k}$ is the SSH Hamiltonian.

3. **Particle hole symmetry**: It is an anti commuting anti unitary symmetry "$\mathcal{C}$" which can simply be defined as the product of the first two symmetries, $\mathcal{C} = \mathcal{S}\mathcal{T}$. It is straight forward to observe: $\mathcal{C}^2 = 1$ and $\{\mathcal{C}, \mathcal{H}_{SSH,k}\} = 0$, where $\mathcal{H}_{SSH,k}$ is the SSH Hamiltonian.

We will now discuss in detail about the chiral (sub-lattice) symmetry of the SSH model.

5.2.1 Chiral (sub-lattice) symmetry of the SSH model

Chiral symmetry is a very general symmetry and is found to be present in many prominent physical theories like the Dirac equation. It can be defined with an operator "$\mathcal{S}$" which anti commutes with the Hamiltonian, $\mathcal{H}$. The presence of this symmetry leads to a particle hole symmetric spectrum, where any eigenstate $|u_E\rangle$ with an energy E has a corresponding partner $|u_{-E}\rangle$ with an energy $-E$.

A particular class of chiral symmetries known as the sub-lattice symmetry is defined as follows. Given the chiral symmetry operator $\hat{\mathcal{S}}$, we can define the orthogonal sub-lattice projectors:

$$\hat{P}_A = \frac{1}{2}(\mathbb{I} + \mathcal{S}); \qquad \hat{P}_B = \frac{1}{2}(\mathbb{I} - \mathcal{S}), \tag{5.4}$$

where $\mathbb{I}$ denotes the identity operator over the Hilbert space of the system. From Equation 5.4 it is easy to verify:

$$\hat{P}_A + \hat{P}_B = 1; \qquad \hat{P}_A\hat{P}_B = 0. \tag{5.5}$$

The essence of sub-lattice symmetry is that the Hamiltonian does not induce transitions from any given site on a sub-lattice to any other site on the same sub-lattice,

$$\hat{P}_A H \hat{P}_A = \hat{P}_B H \hat{P}_B = 0; \qquad H = \hat{P}_A H \hat{P}_B + \hat{P}_B H \hat{P}_A. \tag{5.6}$$

It is to note that in light of the above definition any onsite term breaks the above symmetry. In this way we can define the chiral symmetry using the projectors $\hat{P}_A$ and $\hat{P}_B$.

If we now focus our discussion to the chiral symmetry of the SSH model. The two crucial observations from the inspection of the Hamiltonian of the C-SSH model given in Equation 5.7 is (1) the Hamiltonian is bipartite and (2) it contains no hopping terms between sites with the same sub-lattice index.

$$H_{SSH} = \sum_n u(|n, A\rangle \langle n, B|) + v(|n+1, A\rangle \langle n, B|) + H.C. \tag{5.7}$$

The projectors to the sub-lattices are as follows:

$$\hat{P}_A = \sum_{m=1}^{N} |m, A\rangle \langle n, A|; \qquad \hat{P}_B = \sum_{m=1}^{N} |m, B\rangle \langle n, B|. \tag{5.8}$$

With these projectors the chiral symmetry is represented through the sub-lattice operator:

$$\Sigma_z = \hat{P}_A - \hat{P}_B. \tag{5.9}$$

It is readily verifiable that this operator has all the requisite properties of the chiral symmetry operator, It is unitary, Hermitian and local. It is also to be noted that it multiplies all the components of a wavefunction on a sub-lattice B by a negative sign. This leads to the conclusion that the chiral symmetry of the SSH model is a consequence of the Hamiltonian being bipartite, i.e.

$$\hat{P}_A H \hat{P}_A = \hat{P}_B H \hat{P}_B = 0; \qquad \Rightarrow \qquad \Sigma_z H \Sigma_z = -H. \tag{5.10}$$

The above relation is true because of the fact that the Hamiltonian H contains only terms that are multiples of $|m, A\rangle \langle n, B|$ or $|m, B\rangle \langle n, A|$ but where m, n are integers and multiplication of H from left and right by Σ_z picks up only one neg-

ative sign.

Now if we consider the bulk momentum space Hamiltonian:

$$H(k) = \mathbf{d}(\mathbf{k}) \cdot \sigma \tag{5.11}$$

where, $H(k)$ is obtained by performing a Fourier transformation on H_{SSH}, and σ are the Pauli matrices. Due to the presence of the chiral symmetry we have the following relation:

$$\sigma_z H(k) \sigma_z = -H(k) \qquad \Rightarrow \qquad d_z(k) = 0. \tag{5.12}$$

The above equation implies $\mathbf{d}(\mathbf{k})$ is constrained to lie on the $d_x d_y$ plane.

5.2.2 Disorders preserving and breaking the sub-lattice symmetry

From the discussions in the previous subsection it is clear that the presence of any on-site term destroys chiral symmetry. These is evident from both Equation 5.10 and Equation 5.12. In Equation 5.10 presence of onsite terms would not produce exactly one amount of (-1) when multiplied by Σ_z from left and right and hence breaks the chiral symmetry. In Equation 5.12 addition of onsite terms in the Hamiltonian would make the diagonal terms in $H(k)$ non-zero and would break the chiral symmetry.

If disorder is introduced in the value of the hopping amplitudes, it does not change the terms in the Hamiltonian and does not break any symmetry. This is because the relation Equation 5.10 still holds for the disordered Hamiltonian, as evident from Equation 5.13:

$$\hat{P}_A H_{dis} \hat{P}_A = \hat{P}_B H_{dis} \hat{P}_B = 0; \qquad \Rightarrow \qquad \Sigma_z H_{dis} \Sigma_z = -H_{dis}. \tag{5.13}$$

Thus we can appreciate that there can be both symmetry breaking and preserving disorders in the C-SSH model. Since the SAB model shares the same symmetry class as the C-SSH model all the above discussions hold true for the SAB model too. We will discuss the implications of these disorders in the SAB model after a brief discussion of flat bands in the SAB models.

5.3 Flat bands in SAB model

The SAB models with different number of bands are an unique platform with SSH like staggered hopping and flat bands in electronic dispersion. As evident from the discussions in the previous chapter it is clear that the electrons are localised within the bulk due to the presence of these flat bands. This makes it an ideal platform to test the effects of simultaneous presence of flat bands and disorders.

It is also important to note that depending on the particular SAB model one considers, the degeneracy of the flat band at the particle hole symmetry level changes. This enables us not only to study the effects of disorders on flat bands but also it's relation to the degeneracy of the flat band.

This difference that will be arising in the effects of disorder due to the degeneracy of the flat band can be understood by taking two different examples in the SAB models:

1. The three band SAB model which has two dispersive bands and a non degenerate flat sandwiched between these two bands exactly at the particle hole symmetry level.
2. The six band SAB model with a non-orientable bulk which has four dispersive bands two above and two below the particle hole symmetry level and a doubly degenerate flat band sandwiched exactly at the particle hole symmetry level.

Our analysis of the effects of various kinds and types of disorders on the SAB model will be through the above two SAB models. In this way we can cover both

non-degenerate and doubly degenerate flat bands that we encounter in the SAB model.

To illustrate this point let us show the finite chain energy spectrum of the three band SAB model and the six band SAB model with a non-orientable bulk in Figure 5.3 with the chain containing 20 unit cells in each case.

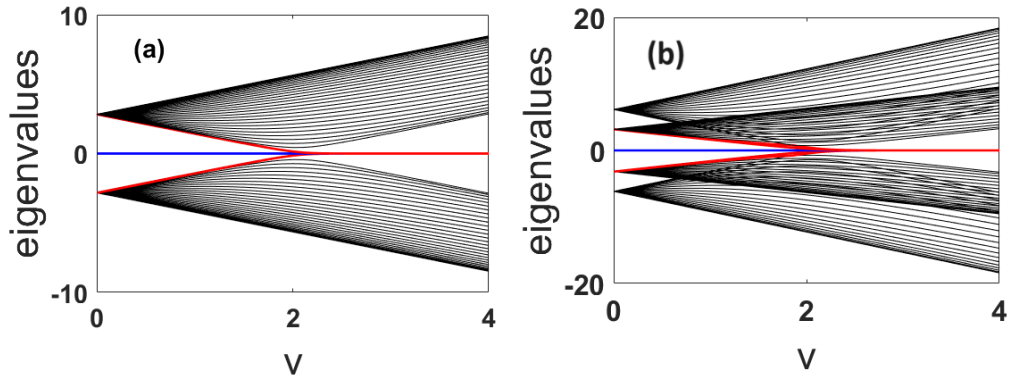

Figure 5.3: Energy spectrum as a function of the inter cell hopping parameter v with the intra cell hopping parameter u kept constant ($u = 2$) of the finite chain of (a) the three band SAB model, (b) six band SAB model with a non-orientable bulk. We consider 20 unit cells in the finite chain. Zero energy states localised in the bulk are denoted by blue lines and zero energy edge states are denoted by red lines.

From Figure 5.3 it is clear that both the three band SAB model and the six band SAB model with non-orientable bulk have in addition to the zero energy edge states that appear when $v > u$ and zero energy states localised in the bulk for all values of u and v. We will now check the robustness of these zero energy states to various kinds and types of static disorders.

5.4 Implementation of symmetry preserving and breaking disorders in various SAB models

In this section we will discuss our implementation of the disorder in the hopping amplitudes (chiral symmetry preserving) and implementation of the onsite disorder (chiral symmetry breaking) in the SAB models. We will discuss the various nuances in our implementation which makes our implementation of these disorders

very general.

5.4.1 Implementation of disorder in hopping amplitudes

The disorder in hopping amplitudes can be implemented in three ways. These are listed as follows:

1. Disorder only in intra cell hopping amplitude and no disorder in inter cell hopping.
2. Disorder only in inter cell hopping amplitude and no disorder in intra cell hopping.
3. Disorder in both inter cell and intra cell hopping amplitudes.

To make our study complete we study all the three types of disorder mentioned above. If we denote the hopping amplitudes of the clean system at unit cell n and sub-lattice site a within that unit cell as $u_{n.a}$ and $v_{n,a}$, then the hopping amplitudes $\tilde{u}_{n,a}$ and $\tilde{v}_{n,a}$ of the disordered system is given as follows:

$$u_{n,a} \to \tilde{u}_{n,a} = u_{n,a} + d\gamma^1_{n,a}, \tag{5.14}$$

$$v_{n,a} \to \tilde{v}_{n,a} = v_{n,a} + d\gamma^2_{n,a}. \tag{5.15}$$

where we denote d as the disorder strength and the quantities $\gamma^1_{n,a}$ and $\gamma^2_{n,a}$ are randomly chosen from the uniform distribution: $[-1, 1]$.

We want to make our implementation of the disorder in hopping amplitudes as general as possible. In this direction we had set the following benchmarks:

- The disorder is implemented in such a way that it acts differently on different unit cells.

- The disorder is also implemented in such a way that it acts differently on different hopping amplitudes of the same type (connecting different sub lattice sites) in the same unit cell.
- When the disorder is implemented on both types of hopping amplitudes, along with the above two conditions the disorder acts independently on both the hopping amplitudes.
- The disorder acts in such a way that the Hamiltonian always remains Hermitian.
- The results are obtained after averaging over one hundred simulations. This is quite reasonable as we checked that the results remain converged for averaging over around 50 simulations.

In this way our implementation of disorders in hopping amplitudes of the SAB model is fool proof and gives the most general treatment possible for such a study.

5.4.2 Implementation of onsite disorder

We will discuss here our implementation of onsite disorder in the SAB model. Let use denote the clean SAB model that we will be interested as H_c and the part that brings the onsite disorder as H_{dis}. Then the total Hamiltonian H is given as:

$$H = H_c + H_{dis} \tag{5.16}$$

where

$$H_{dis} = d\,\gamma_{n,a} \sum_{n} \sum_{a} c^{\dagger}_{n,a} c_{n,a} \tag{5.17}$$

here d is the disorder strength and $\gamma_{n,a}$ is randomly chosen from the uniform distribution: $[-1, 1]$.

Similar to the implementation of disorder in hopping amplitudes, to make our implementation of the onsite disorder as general as possible we set the following benchmarks:

- Disorder implemented independently across all unit cells.
- Disorder also implemented independently across all sites in an unit cell.
- The Hamiltonian remains Hermitian as the onsite disorder is implemented only on the diagonal terms.
- The results are obtained after averaging over one hundred simulations. This is quite reasonable as we checked that the results remain converged for averaging over around 50 simulations.

In this way we have bench marked that our implementation of onsite disorders in the SAB model is the most general treatment possible for such a study.

5.5 Results for SAB model with disorders

In this section we will discuss the results obtained for the studies with various static disorders in the SAB model. We will begin with discussing the results for the case of chiral symmetry preserving disorders (disorders in hopping amplitudes) in subsection 5.5.1 followed by chiral symmetry breaking disorder (onsite disorder) in subsection 5.5.2.

5.5.1 Results for disorders in hopping amplitudes

Based on the algorithm to implement the effects of static disorder in hopping amplitudes discussed in the previous section, we have performed numerical calculations and have obtained the results for all the three types of disorders in hopping amplitudes. These are disorder in both intra cell hopping amplitude (u) and inter cell hopping amplitudes (v), or only in u or only in v.

The results for all the three types of static disorders in hopping amplitudes for the case of three band SAB model is presented in the plots in Figure 5.4. It is worth to mention here that in the three band SAB model the flat band at the

particle hole symmetry level is non degenerate.

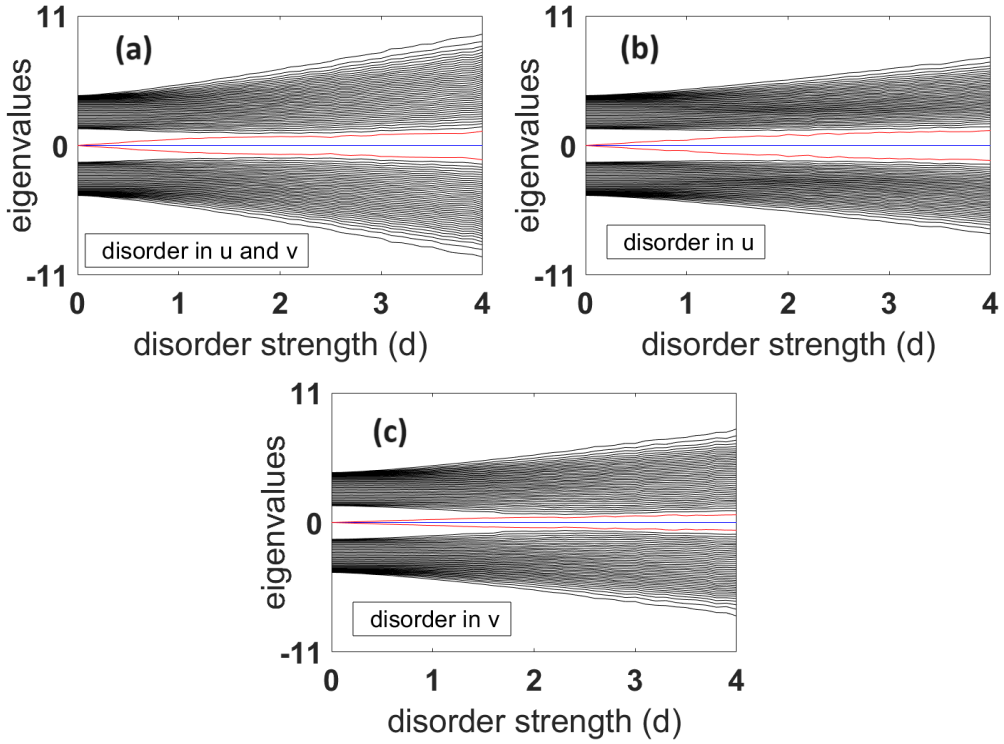

Figure 5.4: Energy spectrum of a finite three band non-orientable three band SAB model with 40 unit cells with increasing amount of disorder (zero energy states localised in the bulk are marked by blue lines and zero energy edge states are marked by red lines): Energy spectrum as a function of (a) disorder in u and v simultaneously, (b) disorder only in u and (c) disorder only in v. The results are averaged over 100 simulations. In (a),(b) and (c) the value of hopping parameters are set as u = 1 and v = 2.

Based on the plots in Figure 5.4 we can make the following inferences:

- In the case of disorder only in the intra cell hopping amplitude of the three band SAB model, the zero energy states localised in the bulk are robust to the disorder and remain as zero energy states for large amount of disorder. The zero energy edge states acquire finite energy but still remain as in-gap states (refer to Figure 5.4(b)).
- In the case of disorder only in the inter cell hopping amplitude of the three band SAB model, the zero energy states localised in the bulk are robust to the disorder and remain as zero energy states for large amount of disorder. The zero energy edge states acquire finite energy but still remain as in-gap states. However in this case compared to the case of disorder in intra cell

hopping amplitude the band gap is smaller with increase in disorder (refer to Figure 5.4(c)).

- In the case of disorder both in the intra cell and inter cell hopping amplitudes of the three band SAB model, the zero energy states localised in the bulk are robust to the disorder and remain as zero energy states for large amount of disorder. The zero energy edge states acquire finite energy but still remain as in-gap states. The behavior of the band gap in this case with increase in disorder is in between the cases of disorder only in the intra cell or inter cell hopping amplitudes as expected (refer to Figure 5.4(a)).

"We can thus conclude that the zero energy states localised in the bulk in the case of three band SAB model enjoy protection from the disorders in the hopping amplitudes and are robust to these disorders."

After discussing the results for the three band case let us now look in to the results for the case of six band model with a non-orientable bulk. These results are presented in Figure 5.5. In this case it is important to note that the flat band at the particle hole symmetry level is doubly degenerate.

Based on the plots in Figure 5.5 we can arrive at the following inferences.

- In the case of disorder only in the intra cell hopping amplitude of the the six band SAB model with a non-orientable bulk, the zero energy states localised in the bulk (corresponding to the flat bands in the band dispersion) begin to disperse with increase in disorder.
  As the disorder strength (d) is increased, the band gap keeps decreasing and beyond a critical disorder strength, the once zero energy states that were localised in the bulk connect the bands of finite positive and negative energy values (corresponding to the dispersive bands in band dispersion) and the band gap vanishes. The behaviour of the zero energy edge states is same as

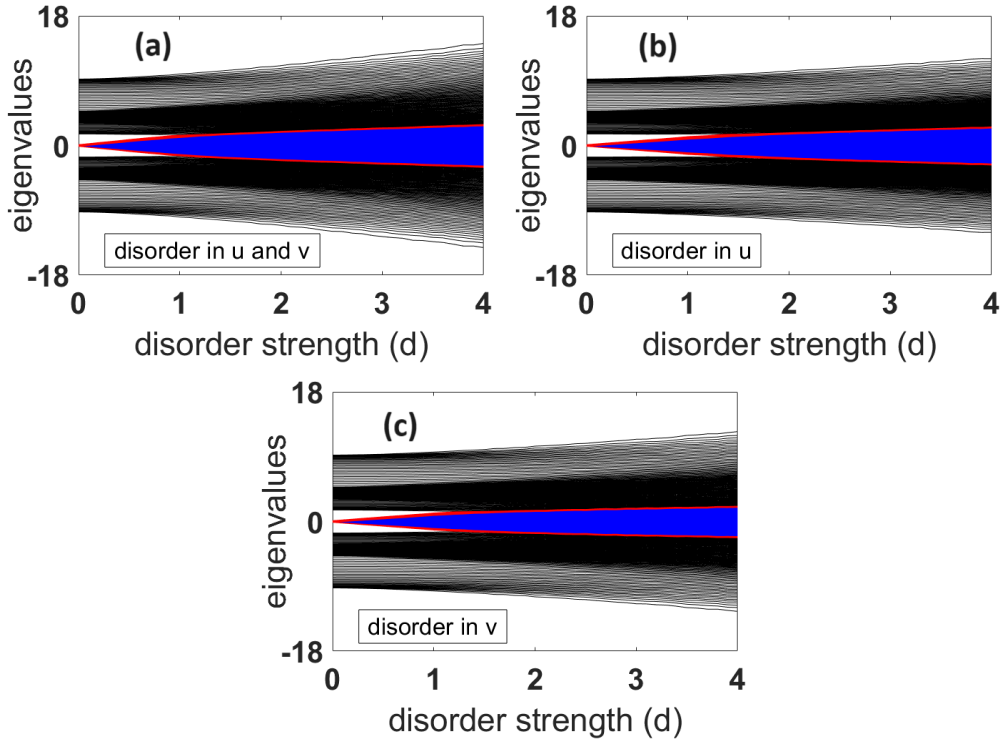

Figure 5.5: Energy spectrum of a finite non-orientable six band SAB model with 40 unit cells with increasing amount of disorder (zero energy states localised in the bulk are marked by blue lines and zero energy edge states are marked by red lines): Energy spectrum as a function of (a) disorder in u and v simultaneously, (b) disorder only in u and (c) disorder only in v. The results are averaged over 100 simulations. In (a),(b) and (c) the value of hopping parameters are set as u = 1 and v = 2.

that of the zero energy states localised in the bulk and act like an envelope to these states (refer to Figure 5.5(b)).

- In the case of disorder only in the inter cell hopping amplitude of the the six band SAB model with a non-orientable bulk, the behavior of the zero energy states localised in the bulk (corresponding to the flat bands in the band dispersion) and the zero energy edge states is same as the case of the disorder in intra cell hopping amplitude (refer to Figure 5.5(c)).

- In the case of disorder in both the inter cell and intra cell hopping amplitudes of the the six band SAB model with a non-orientable bulk, the behaviour of the zero energy states localised in the bulk (corresponding to the flat bands in the band dispersion) and the zero energy edge states is same as the case of the disorder in intra cell hopping amplitude (refer to Figure 5.5(a)).

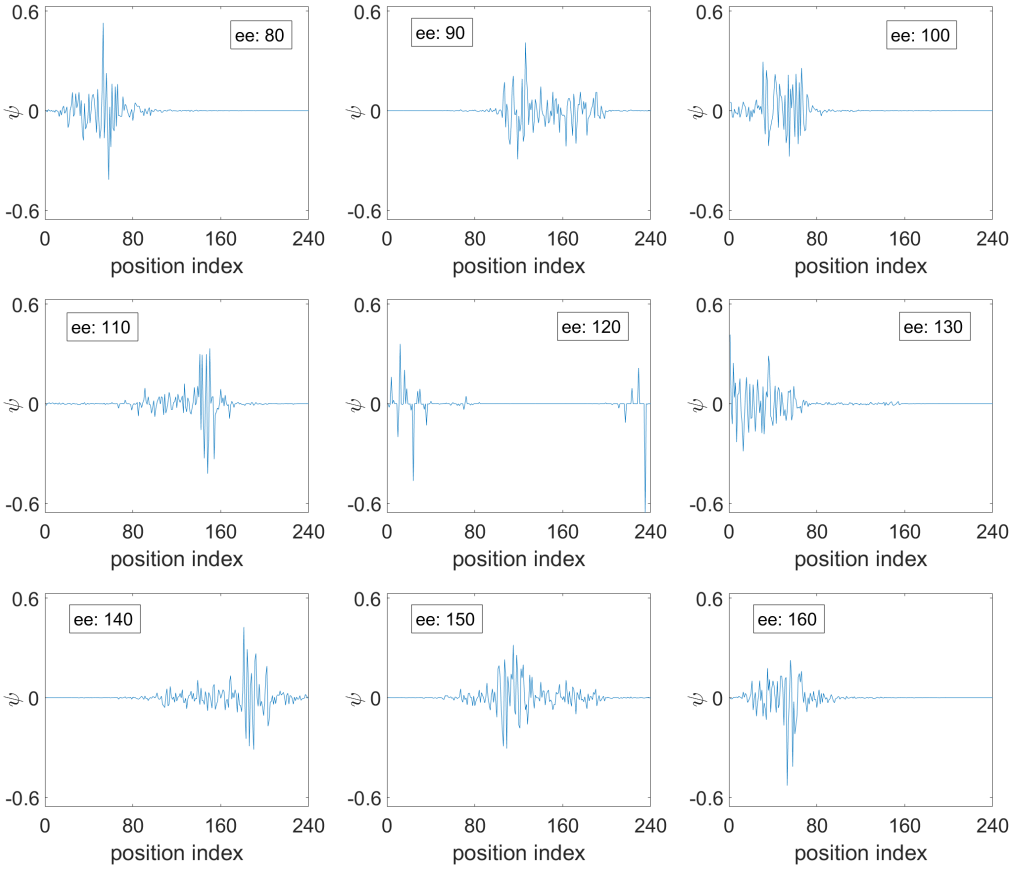

Figure 5.6: Plots of wave functions corresponding to the energy eigenvalues in the region marked in blue in Figure 5.5. This region corresponds to energy eigenvalue indexed from 81 to 160 of the total 240 energy eigenvalues (sorted in ascending order). The plots have been labeled with the corresponding index of the energy eigenvalue.

"Based on the above observations we can conclude that unlike the three band SAB model where the zero energy modes localised in the bulk enjoyed protection from disorder when subjected to various types of disorders in hopping amplitudes, the zero energy states of the six band SAB model with non-orientable bulk enjoy no protection from any type of disorder in hopping amplitudes."

For all kinds of disorder in hopping amplitudes applied to the six band SAB model with a non-orientable bulk, the zero energy states of the clean system begin to disperse and attain a finite band width with increase in disorder strength. For a critical disorder strength the band width of this new band formed by the zero energy states of the clean system is such that it closes the band gap between the

other bands with finite positive and negative energies.

"This is indicative of localisation to delocalisation transition with increase in disorder strength which is surprising and very rare to find."

To ascertain this localisation to delocalisation transition we have calculated the wave functions of the eigen energies corresponding to the middle band (that closed the gap) with the highest disorder strength applied. The plots of wave functions corresponding to the eigen energies which close the gap and are indicated by blue color in Figure 5.5 are given in Figure 5.6. These representative plots span the entire range of eigen energies in the blue region. It is clear from these plots that the wave functions are indeed extended. We will elaborate more on this after discussing the results for the case of onsite disorder in subsection 5.5.2.

5.5.2 Results for onsite disorder

After discussing the results for effects of disorders in hopping amplitudes of various SAB models, let us turn our focus to the case of onsite disorder. Based on the algorithm discussed by us in section 5.4 to implement the onsite disorder in a general and foolproof form, we have performed numerical calculations for the three band SAB model and six band SAB model with a non-orientable bulk. The results are presented in the plots in Figure 5.7.

Based on the plots of energy spectrum as a function of disorder strength given in Figure 5.7, we can make the following observations:

- In the case of onsite disorder on the three band SAB model, the zero energy states localised in the bulk (corresponding to the flat bands in the band dispersion) begin to disperse with increase in disorder. As the disorder strength (d) is increased, the band gap keeps decreasing and beyond a critical disorder strength, the once zero energy states that were localised in the bulk connect

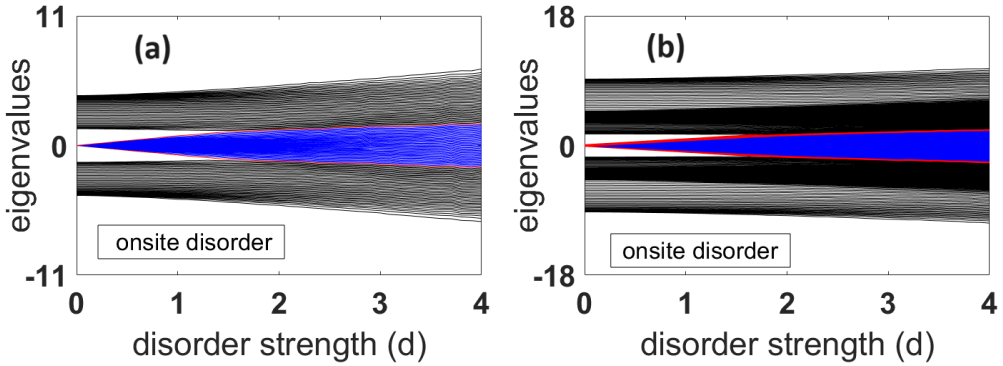

Figure 5.7: Energy spectrum of a finite (a) three band SAB model and (b) six band SAB model with a non-orientable manifold having 40 unit cells with increasing amount of onsite disorder with disorder strength (d) (zero energy states localised in the bulk are marked by blue lines and zero energy edge states are marked by red lines). The results are averaged over 100 simulations. The value of hopping parameters are set as u = 1 and v = 2.

the bands of finite positive and negative energy values (corresponding to the dispersive bands in band dispersion) and the band gap vanishes.(refer to Figure 5.7(a))

The behavior of the zero energy edge states is same as that of the zero energy states localised in the bulk and act like an envelope to these states.

- The behavior of the zero energy states of the six band SAB model with non-orientable bulk in presence of onsite disorder is similar to the case of onsite disorder in the three band SAB model. The zero energy states form a band of finite bandwidth and close the band gap for a critical disorder strength(refer to Figure 5.7(b)).

From the above observations it is clear that the zero energy states of both the three band SAB model and the six band SAB model with non-orientable bulk disperse with increase in disorder strength and attain a finite band width. For disorder strengths beyond a critical disorder strength the new band formed by the zero energy states close the band gap between the other bands with finite positive and negative energies. This is indicative of a localisation to delocalisation transition in the system.

Similar to the chiral symmetry preserving disorder, in this case also to ascertain the localisation to delocalisation transition we have calculated the wave functions

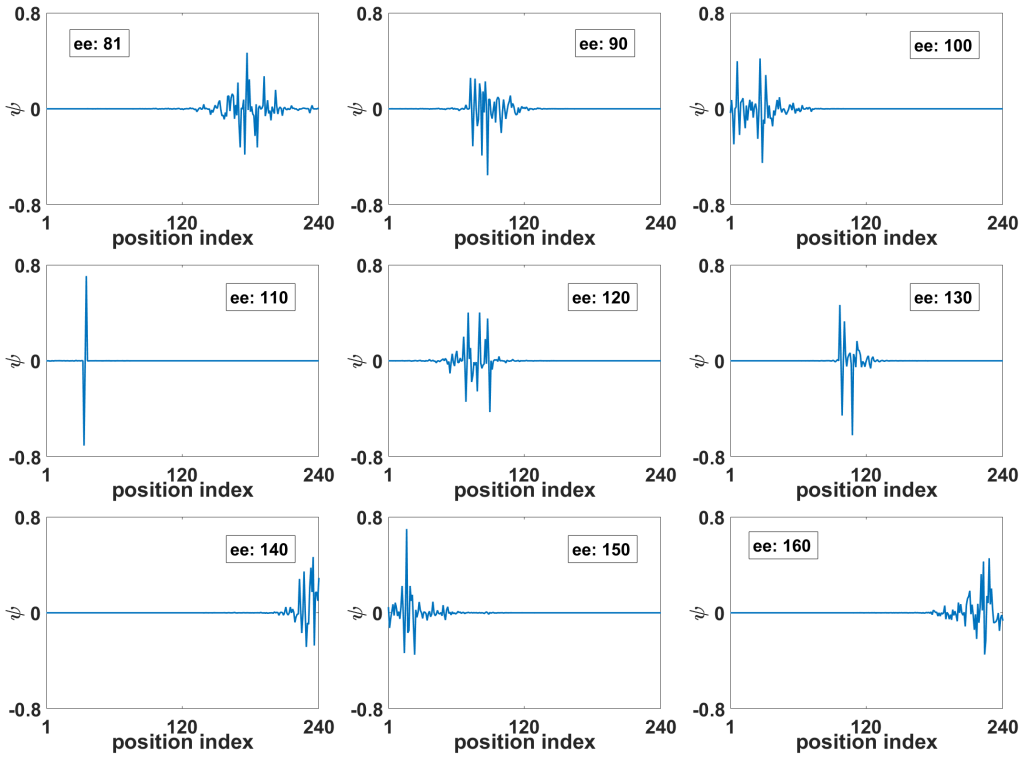

Figure 5.8: Plots of wave functions corresponding to the energy eigenvalues in the region marked in blue in Figure 5.7(b). This region corresponds to energy eigenvalue indexed from 81 to 160 of the total 240 energy eigenvalues (sorted in ascending order). The plots have been labeled with the corresponding index of the energy eigenvalue.

of the eigen energies corresponding to the middle band (that closed the gap) with the highest disorder strength applied. The plots of wave functions corresponding to the eigen energies which close the gap and are indicated by blue color in Figure 5.7(b) are given in Figure 5.8. These representative plots span the entire range of eigen energies in the blue region. It is clear from these plots that the wave functions are indeed extended.

5.6 Discussion and Summary

We have studied the effects of various static disorders on different SAB models in this chapter. We have particularly chosen two SAB models for this study, (1) the three band SAB model and (2) the six band SAB model with a non-orientable bulk. This choice of SAB models have stemmed from the objective of studying SAB models with non-degenerate and degenerate flat bands. Particularly since the zero energy states localised in the bulk have a geometrical rather than topological origin, it would be interesting to understand their robustness to various types of static disorders.

The results of our study indicate that there are two types of response of the zero energy states in the SAB model:

1. **The zero energy states enjoy complete protection to large amount of disorders:** This behavior has been observed only for the case of disorder in hopping amplitudes for the three band SAB model or in general when the flat band in the SAB model is non-degenerate.

   "This class of response is desirable from an experimental perspective as experimental set ups are seldom pristine and fully controlled. The robustness of the zero energy states to large disorders gives flexibility to the experimental set ups to realise these properties of the SAB model."

2. **The zero energy states disperse with disorder, form a band with finite band with and close the band gap:** This behavior has been observed for all types and kinds of disorders for the six band model with non-orientable bulk and with onsite disorder on the three band SAB model.

   "This response may not be encouraging at a first glance as the robustness of the zero energy states have been lost. However, on a deeper observation we realise that the dispersion and band formation of the zero energy modes leads to a localisation to delocalisation or in other words to insulator to metal transition. Such a transition from a physical perspective that to with increase in disorder strength is very rare while the opposite (metal to insulator transition) has become a standard phenomena with the most famous example being the Anderson localisation.

   Thus the effect of disorder in this class of response has not been limited to provide flexibility to the experiments to realise physical properties of the clean system but has brought about new physical transitions that cannot be defined only within the clean system.

In conclusion, we have studied the effects of various kinds and types of static disorders on SAB models with non-degenerate and degenerate flat bands. **Depending on the flat band degeneracy and the kind of disorder applied the zero energy states in the system are either robust to these disorders or undergo a insulator to metal transition based on beyond a critical disorder strength.**

"A method is more important than a discovery, since the right method will lead to new and even more important discoveries.".

Lev Landau

6

Summary

This chapter summarises the work done and the main results obtained in this thesis.

The objective of the thesis was to study the effects of interaction and topology in two paradigmatic condensed matter systems of itinerant magnetism and the Su-Schrieffer-Heeger model like (with dimerisation) systems. We had studied the interaction in the itinerant magnetism through the Hubbard model. Even though there have been many attempts in modeling itinerant magnetism like the Stoner model and the Random Phase Approximation (RPA) model, the Self-Consistent Renormalisation theory remains to be the most accurate approach to study itinerant magnetism.

After reviewing the formalism of the SCR theory, we have discussed the algorithm for developing computer codes to solve the equations of the SCR theory. Based on these algorithms we have developed versatile codes which not only reproduces the results available in the original SCR theory article[1], but can calculate susceptibility for other set of interaction parameters too. These numerical codes equip us to study real systems with some experimental signatures of itinerant magnetism but require more theoretical investigations.

In this direction we notice that $CaMn_2Al_{10}$ is an interesting material with several signatures of itinerant magnetism but predicted to be a local magnet based on the conventional wisdom relating to Mn-Mn distance[64]. The conventional wisdom in Mn based magnetic system states that if the Mn-Mn distance in the system is more than 2.7 Å, then the system will exhibit local magnetism. The Mn-Mn distance in $CaMn_2Al_{10}$ is more than the cut-off value of 2.7 Å to be a local magnet, but still it has signatures of itinerant magnetism. This prompted us to investigate $CaMn_2Al_{10}$ through the lens of the SCR theory.

We have calculated the static susceptibility of $CaMn_2Al_{10}$ from SCR theory calculations and found that it is in very good agreement with the experimental data. This enables us to decisively conclude that magnetism in $CaMn_2Al_{10}$ is indeed of itinerant nature. By fitting the theoretical calculation to the experimental data, we have obtained the value of the Hubbard interaction parameter U, that is

U = 0.3136 eV. This allows us to categorise $CaMn_2Al_{10}$ to be weakly correlated system. To understand the origin of itinerant magnetism, with this value of U, we have performed DFT+U calculations, and found evidence for hybridisation between Mn 3 d and Al 3 p orbitals, which is the reason for the origin of itinerant magnetism in $CaMn_2Al_{10}$.

After studying the effects of interaction in itinerant magnetism, we move on to study SSH like models which have non-trivial topology. The SSH model is a celebrated model to understand effects of non-trivial topology, owing not only to its conceptual simplicity but the same time its ability to capture all major principles in topological condensed matter physics like topological invariants and Bulk-Boundary correspondence[2].

Our interest is to study SSH like models (models with dimerisation) with twists and branching in the bulk. Such a study is not possible within the framework of the conventional SSH model. For this purpose we introduce a model called the Su-Schrieffer-Heeger model with Any Bulk (SAB). In the SAB model there are two more degrees of freedom at each site. The rules of the SAB model are defined in such a way that the values of the parameters in these degrees decide the presence or absence of twists and branching. They also will decide the hopping from any particular site to its neighbouring site be intercell or intracell. Based on the rules that we have formulated, we studied several SAB models with different number of bands like the three band SAB model, the four band SAB model and the six band SAB model.

The class of SAB models with certain configuration of hopping amplitudes called the non-orientable configuration show many novel and exotic physical properties. The most important property of the non-orientable SAB models is the emergence of either doubly degenerate or non-degenerate flat bands exactly at the particle hole symmetry level. Such flat bands are highly desired from the context of strongly correlated systems and superconductivity. These flat bands lead to

localisation of the electrons in the bulk of the lattice.

To verify the topological properties of the non-orientable SAB models we have calculated the Zak phase topological invariant for both the dispersive and flat bands in the system. We find that the Zak phase is quantised for the dispersive bands confirming that the dispersive bands are topological. The value of Zak phase for the flat bands is a constant for all configurations of hopping amplitudes. We also calculated the zero energy edge states and found that they emerge only for the configuration of parameters in the Hamiltonian for which the value of the Zak phase is non-zero. This proves the validity of Bulk-Boundary correspondence in the SAB models.

We have also calculated localisation measures like Inverse Participation Ratio (IPR) to study the localisation properties of the SAB model. The IPR plots show that the zero energy edge states undergo a delocalisation to localisation transition for the zero energy edge states at the topological phase transition point. However, the IPR values of zero energy states localised in the bulk is a constant for all configurations of system parameters. We have also calculated the eigenvalues and eigenstates with both periodic boundary conditions and open boundary conditions making our study complete.

Since the zero energy states localised in the bulk arise from the geometry of the lattice it will be of immense interest to study their robustness to disorder. For this reason we study three band and six band SAB model with both chiral symmetry preserving and breaking disorders. The reason behind choosing three band and six band SAB model is to have one case each from SAB models with non-degenerate (three) and doubly degenerate (six) flat band. We find that if the flat band is non-degenerate and the disorder is chiral symmetry preserving, then the zero energy states are robust to large amounts of disorder. However, in all other cases the zero energy states disperse and acquire a finite band width. For some critical disorder strength, the band width is such that it closes the band gap in the system. This

in indicative of an insulator to metal transition which is very rare and novel to find.

We believe based on the above studies, we have achieved our objective to study the effects of interaction and non-trivial topology in the paradigmatic models of itinerant magnetism and the SAB model. We expect our studies to have varied potential applications[116–119]. In the future, we would like to investigate the interplay of interaction and non-trivial topology when simultaneously present in the same system like the SAB model.

A

Equivalence of susceptibility of RPA model in zero frequency and long wavelength limit and Stoner model

A.1 Equivalence of susceptibility of RPA model in zero frequency and long wavelength limit and the susceptibility from Stoner model

In this appendix we will show from Equation 1.63 that in the limit: $q \to 0$ and $\omega = 0$ goes to the Stoner susceptibility expression. We have from Equation 1.61:

$$\Gamma_\sigma(\boldsymbol{q}, \omega) = \sum_k \frac{f_{k\sigma} - f_{k+q\sigma}}{\varepsilon(k+q) - \varepsilon(k) - \hbar\omega}. \tag{A.1}$$

In the long wavelength $q \to 0$ and zero frequency limit $\omega = 0$, we can perform a Taylor expansion to get:

$$f_{k+q\sigma} \simeq f_{k\sigma} + q\frac{\partial f_{k\sigma}}{\partial k} \tag{A.2}$$

and

$$\varepsilon(k+q) \simeq \varepsilon(k) + q\frac{\partial \varepsilon(k)}{\partial k} \tag{A.3}$$

substituting the above relations in Equation 1.61 we get:

$$\Gamma_\sigma(\boldsymbol{q}, 0) \simeq -\sum_k \frac{\partial f_{k\sigma}/\partial k}{\partial \varepsilon(k)/\partial k} = -\rho_\sigma(\varepsilon_F) \tag{A.4}$$

Substituting this relation in the equation for susceptibility in the RPA model, we get:

$$\chi_{zz}(\boldsymbol{q}, 0) \simeq \frac{1}{4}\frac{\rho_\downarrow(\varepsilon_F) + \rho_\uparrow(\varepsilon_F) + 2U_{eff}\rho_\downarrow(\varepsilon_F)\rho_\uparrow(\varepsilon_F)}{1 - U_{eff}^2\rho_\downarrow(\varepsilon_F)\rho_\uparrow(\varepsilon_F)} \tag{A.5}$$

Near the point of Ferromagnetic instability we have:

$$\rho_\downarrow(\varepsilon_F) \sim \rho_\uparrow(\varepsilon_F) \tag{A.6}$$

Substituting the above expression in Equation A.5, we get:

$$\chi_{zz}(\boldsymbol{q},0) \simeq \frac{1}{4}\frac{2\rho(\varepsilon_F)(1+U_{eff}\rho(\varepsilon_F))}{1-U_{eff}^2\rho(\varepsilon_F)^2} = \frac{\frac{\rho(\varepsilon_F)}{2}}{1-U_{eff}\rho(\varepsilon_F)} \tag{A.7}$$

$$= \frac{\chi_0}{1-U_{eff}\rho(\varepsilon_F)} = \chi_{stoner} \tag{A.8}$$

which is the same expression as that of Stoner model given in Equation 1.19.

B

Comments for preparing the numerical codes for SCR theory

B.1 Comments for preparing the numerical codes for SCR theory

In this appendix, we give some remarks regarding the computational aspects which should be kept in mind, while framing the algorithm for $G(\omega)$ numerical calculations. It is important to note here that, we are not presenting the complete algorithm but limit ourselves to making certain comments which will be useful for the reader interested in designing the algorithm for calculating static susceptibility. $G(\omega)$ is a sum of $\alpha\, G_1(\omega)$ and $G_2(\omega)$. Thus, to $G(\omega)$ we need to get both $G_1(\omega)$ and $G_2(\omega)$. We will now discuss separately the concepts which are involved in the numerical integration of both $G_1(\omega)$ and $G_2(\omega)$ step by step.

Numerical integration of $G_1(\omega)$

In all of the computations, the numerical integration of $G_1(\omega)$ is the most involved. The first thing that one should note is that for obtaining the value of $G_1(\omega)$, we will have to numerically integrate an integrand, which is a function of q, $f_0'(q,\omega)$, $f_0''(q,\omega)$, $\frac{\partial^2 f_0'(q,\omega)}{\partial^2 B}|_{B=0}$ and $\frac{\partial^2 f_0''(q,\omega)}{\partial^2 B}|_{B=0}$. Since $\frac{\partial^2 f_0''(q,\omega)}{\partial^2 B}|_{B=0}$ have in them various theta and delta functions, one should evaluate the integration with the parts involving the theta functions and the delta functions separately and should then take the sum at the end. The evaluation part involving the delta functions is straight forward except for something that we call the "Singularity Corrections". Before getting in to the complete details, let us recall the definitions of some special points q_0,q_1,q_2,q_3,

$$\left.\begin{matrix} q_1 \\ q_2 \end{matrix}\right\} = 1 \mp (1-\omega)^{1/2}$$

$$\left.\begin{matrix} q_0 \\ q_3 \end{matrix}\right\} = 1 \mp (1+\omega)^{1/2}$$

The aforementioned points are special as they are the roots of the functions that are inside the theta and delta functions. Since the integration of a delta function

will give the functional value of the integrand at the point where the delta function peaks provided it is present inside the region of integration and its value is zero otherwise. For understanding this, if we consider $q_c = 2$, the integration is performed for $q = 0$ to $q = q_c = 2$. If we consider the domain $\omega > 1$, then only the point $|q_0|$ lies inside the region of integration and for $1 < \omega < 8$ also the only contribution comes from this term. For $\omega > 8$, there is no peak inside the region of integration thus the contribution is zero. If we consider the domain $\omega < 1$, then there are three peaks that correspond to $|q_0|$, q_1 and q_2 which are inside the region of integration. Notice if we put the values of $|q_0|$, q_1 or q_2 directly in f_0' or $\frac{\partial^2 f_0'(q,\omega)}{\partial^2 B}|_{B=0}$ the expression diverges. To avoid this, we add a small value inside the logarithm and obtain a meaningful value. This is exactly what we call the "Singularity Corrections". The contributions from each of peak should be calculated separately. After this while integrating the parts involving the theta functions, like the above case for $\omega > 1$, the only non zero contribution comes from the theta function that involves $|q_0|$ for $1 < \omega < 8$ and we see that there are no non zero contributions for $\omega > 8$. It is important to notice that $\frac{\partial^2 f_0'(q,\omega)}{\partial^2 B}|_{B=0}$ diverges quadratically, for $|q_0|$ and one should now use some logical conditions to remove those points where the integrand diverges. For $\omega < 1$, the non zero contributions from the theta functions that involves $|q_0|$, q_1 and q_2. It is important to note that the function $\frac{\partial^2 f_0'(q,\omega)}{\partial^2 B}|_{B=0}$ quadratically diverging for $|q_0|$, q_1 and q_2 and is very similar to the $\omega > 1$ case. Like before, we will have to remove here also the points where the functional value of the integrand is infinite. It is also to be kept in mind that since the integrand is drastically peaking near these points, one should take more points near these regions for the integration to get a satisfactory accuracy after performing numerical integration.

Numerical integration of $G_2(\omega)$

The numerical integration of $G_2(\omega)$ is very straightforward when compared to that of $G_1(\omega)$, as it involves only theta functions and does not need any processing like "Singularity corrections". Like before for $\omega > 1$ only the theta function involving $|q_0|$ contributes unless $\omega = 8$ and there is no other contribution there-

after. For $\omega < 1$, there are contributions coming from $|q_0|$, q_1 and q_2 and can be calculated straightforwardly either by designing a routine for the theta function or directly using pre-defined theta functions which are readily available.

Publications

1. Devanarayanan, Bharathiganesh, Akariti Sharma, Pratik D. Patel, Navinder Singh, "The case of itinerant magnetism in CaMn2Al10: self-consistent renormalisation (SCR) theory study". In: *J. Phys.: Condens. Matter 34 465802.*(2022), DOI: https://doi.org/10.1088/1361-648X/ac92b6.

2. Devanarayanan, Bharathiganesh, "Topological tight binding models on some non-trivial lattices: union of geometry, flat bands and topology". In: *J. Phys.: Condens. Matter 36 455501.*(2024), DOI: https://doi.org/10.1088/1361-648X/ad5c32.

3. Pratik D. Patel, Akariti Sharma, Devanarayanan, Bharathiganesh, Navinder Singh, Paramita Dutta, "Tunable phase transitions in half-Heusler TbPtBi compound". In: *J. Phys.: Condens. Matter 35 035501.*(2022), DOI: https://doi.org/10.1088/1361-648X/aca0d6.

References

[1] Tôru Moriya and Arisato Kawabata. "Effect of Spin Fluctuations on Itinerant Electron Ferromagnetism". In: *Journal of the Physical Society of Japan* 34.3 (1973), pp. 639–651. DOI: 10.1143/JPSJ.34.639. eprint: https://doi.org/10.1143/JPSJ.34.639. URL: https://doi.org/10.1143/JPSJ.34.639.

[2] W. P. Su, J. R. Schrieffer, and A. J. Heeger. "Solitons in Polyacetylene". In: *Phys. Rev. Lett.* 42 (25 June 1979), pp. 1698–1701. DOI: 10.1103/PhysRevLett.42.1698. URL: https://link.aps.org/doi/10.1103/PhysRevLett.42.1698.

[3] D. J. Thouless. "Quantization of particle transport". In: *Phys. Rev. B* 27 (10 May 1983), pp. 6083–6087. DOI: 10.1103/PhysRevB.27.6083. URL: https://link.aps.org/doi/10.1103/PhysRevB.27.6083.

[4] C.L. Kane. "Chapter 1 - Topological Band Theory and the 2 Invariant". In: *Topological Insulators*. Ed. by Marcel Franz and Laurens Molenkamp. Vol. 6. Contemporary Concepts of Condensed Matter Science. Elsevier, 2013, pp. 3–34. DOI: https://doi.org/10.1016/B978-0-444-63314-9.00001-9. URL: https://www.sciencedirect.com/science/article/pii/B9780444633149000019.

[5] D. J. Thouless et al. "Quantized Hall Conductance in a Two-Dimensional Periodic Potential". In: *Phys. Rev. Lett.* 49 (6 Aug. 1982), pp. 405–408. DOI: 10.1103/PhysRevLett.49.405. URL: https://link.aps.org/doi/10.1103/PhysRevLett.49.405.

[6] A.Yu. Kitaev. "Fault-tolerant quantum computation by anyons". In: *Annals of Physics* 303.1 (2003), pp. 2–30. ISSN: 0003-4916. DOI: https://doi.org/10.1016/S0003-4916(02)00018-0. URL: https://www.sciencedirect.com/science/article/pii/S0003491602000180.

[7] Hubbard J. "Electron correlations in narrow energy bands". In: *Proc. R. Soc. Lond.* A276238–257 (1963). DOI: http://doi.org/10.1098/rspa.1963.0204.

[8] J. C. Slater and G. F. Koster. "Simplified LCAO Method for the Periodic Potential Problem". In: *Phys. Rev.* 94 (6 June 1954), pp. 1498–1524. DOI: 10.1103/PhysRev.94.1498. URL: https://link.aps.org/doi/10.1103/PhysRev.94.1498.

[9] Navinder Singh. "The story of magnetism: from Heisenberg, Slater, and Stoner to Van Vleck, and the issues of exchange and correlation". In: *arxiv* (2018). DOI: https://doi.org/10.48550/arXiv.1807.11291.

[10] Ajeet Kumar, Raman Sharma, and Navinder Singh. "Quantum oscillations in Stoner susceptibility: A theory". In: *Journal of Magnetism and Magnetic Materials* 487 (2019), p. 165302. ISSN: 0304-8853. DOI: https://doi.org/10.1016/j.jmmm.2019.165302. URL: https://www.sciencedirect.com/science/article/pii/S0304885318341428.

[11] Pierre Weiss. "L'hypothèse du champ moléculaire et la propriété ferromagnétique". In: *J. Phys. Theor. Appl.* 6.1 (1907), pp. 661–690.

[12] Charles Kittel. *Introduction to solid state physics*. John Wiley Sons, 2024.

[13] Bharathiganesh Devanarayanan et al. *Background for the Self Consistent Renormalisation (SCR) Theory*. 2021. arXiv: 2108.12683 [cond-mat.str-el].

[14] "II. The Doctor's Dissertation (Text and Translation)**[See Introduction, sect. 2.]" In: *EARLY WORK (1905–1911)*. Ed. by L. Rosenfeld and J. Rud Nielsen. Vol. 1. Niels Bohr Collected Works. Elsevier, 1972, pp. 163–393. DOI: https://doi.org/10.1016/S1876-0503(08)70015-X. URL: https://www.sciencedirect.com/science/article/pii/S187605030870015X.

[15] H.-J. van Leeuwen. "Problèmes de la théorie électronique du magnétisme". In: *Journal de Physique et le Radium* 1051.10 (1921), pp. 361–377.

[16] W. Heisenberg. "Zur Theorie des Ferromagnetismus". In: *Zeitschrift für Physik* (1928).

[17] Edmund Clifton Stoner. "Collective electron ferromagnetism". In: *Proceedings of the Royal Society of London. Series A. Mathematical and Physical Sciences* 165.922 (1938), pp. 372–414.

[18] Takeo Izuyama, Duk-Joo Kim, and Ryogo Kubo. "Band Theoretical Interpretation of Neutron Diffraction Phenomena in Ferromagnetic Metals". In: *Journal of the Physical Society of Japan* 18.7 (1963), pp. 1025–1042. DOI: 10.1143/JPSJ.18.1025. eprint: https://doi.org/10.1143/JPSJ.18.1025. URL: https://doi.org/10.1143/JPSJ.18.1025.

[19] Tôru Moriya and Arisato Kawabata. "Effect of Spin Fluctuations on Itinerant Electron Ferromagnetism. II". In: *Journal of the Physical Society of Japan* 35.3 (1973), pp. 669–676. DOI: 10.1143/JPSJ.35.669. eprint: https://doi.org/10.1143/JPSJ.35.669. URL: https://doi.org/10.1143/JPSJ.35.669.

[20] Toru Moriya. *Spin fluctuations in itinerant electron magnetism*. Vol. 56. Springer Science & Business Media, 2012.

[21] Toru Moriya. "Developments of the theory of spin fluctuations and spin fluctuation-induced superconductivity". In: *Proceedings of the Japan Academy, Series B* 82.1 (2006), pp. 1–16.

[22] P. Hohenberg and W. Kohn. "Inhomogeneous Electron Gas". In: *Phys. Rev.* 136 (3B Nov. 1964), B864–B871. DOI: 10.1103/PhysRev.136.B864. URL: https://link.aps.org/doi/10.1103/PhysRev.136.B864.

[23] L Landau. "On theory of phase transitions". In: *Zh.Eksp.Teor.Fiz* (1937).

[24] David S. Richeson. *Euler's Gem: The Polyhedron Formula and the Birth of Topology*. Princeton University Press, 2008. ISBN: 9780691154572. URL: http://www.jstor.org/stable/j.ctt7sqb7 (visited on 08/13/2024).

[25] S. Pancharatnam. "Generalized theory of interference, and its applications". In: *Proceedings of the Indian Academy of Sciences - Section A* (1956). DOI: https://doi.org/10.1007/BF03046050.

[26] Michael Victor Berry. "Quantal phase factors accompanying adiabatic changes". In: *Proc. R. Soc. Lond. A39245–57* (1984). DOI: https://doi.org/10.1098/rspa.1984.0023.

[27] János K. Asbóth, László Oroszlány, and András Pályi. "The Su-Schrieffer-Heeger (SSH) Model". In: *A Short Course on Topological Insulators: Band Structure and Edge States in One and Two Dimensions*. Cham: Springer International Publishing, 2016, pp. 1–22. ISBN: 978-3-319-25607-8. DOI: 10.1007/978-3-319-25607-8_1. URL: https://doi.org/10.1007/978-3-319-25607-8_1.

[28] J. Zak. "Berry's phase for energy bands in solids". In: *Phys. Rev. Lett.* 62 (23 June 1989), pp. 2747–2750. DOI: 10.1103/PhysRevLett.62.2747. URL: https://link.aps.org/doi/10.1103/PhysRevLett.62.2747.

[29] F. D. M. Haldane. "Model for a Quantum Hall Effect without Landau Levels: Condensed-Matter Realization of the "Parity Anomaly"". In: *Phys. Rev. Lett.* 61 (18 Oct. 1988), pp. 2015–2018. DOI: 10.1103/PhysRevLett.61.2015. URL: https://link.aps.org/doi/10.1103/PhysRevLett.61.2015.

[30] Bo-Hung Chen and Dah-Wei Chiou. "An elementary rigorous proof of bulk-boundary correspondence in the generalized Su-Schrieffer-Heeger model". In: *Physics Letters A* 384.7 (2020), p. 126168. ISSN: 0375-9601. DOI: https://doi.org/10.1016/j.physleta.2019.126168. URL: https://www.sciencedirect.com/science/article/pii/S0375960119311028.

[31] Shimizu, M. "Itinerant electron metamagnetism". In: *J. Phys. France* 43.1 (1982), pp. 155–163. DOI: 10.1051/jphys:01982004301015500. URL: https://doi.org/10.1051/jphys:01982004301015500.

[32] Peter Mohn. *Magnetism in the solid state: an introduction*. Vol. 134. Springer Science & Business Media, 2006.

[33] J. C. Slater. "The Ferromagnetism of Nickel". In: *Phys. Rev.* 49 (7 Apr. 1936), pp. 537–545. DOI: 10.1103/PhysRev.49.537. URL: https://link.aps.org/doi/10.1103/PhysRev.49.537.

[34] Toru Moriya. *Spin Fluctuations in Itinerant Electron Magnetism*. Springer, Berlin, Heidelberg: Springer Series in Solid-State Sciences, 1985.

[35] FR De Boer et al. "Exchange-Enhanced Paramagnetism and Weak Ferromagnetism in the Ni3Al and Ni3Ga Phases; Giant Moment Inducement in Fe-Doped Ni3Ga". In: *Journal of Applied Physics* 40.3 (1969), pp. 1049–1055.

[36] A Fujita et al. "Spin fluctuations in amorphous La(NixAl1-x) alloys consisting of icosahedral clusters". In: *Journal of Physics: Condensed Matter* 7.2 (Jan. 1995), pp. 401–412. DOI: 10.1088/0953-8984/7/2/018. URL: https://doi.org/10.1088/0953-8984/7/2/018.

[37] Tatsumi Hioki and Yoshika Masuda. "Nuclear Magnetic Resonance and Relaxation in Itinerant Electron Ferromagnet Sc3In". In: *Journal of the Physical Society of Japan* 43.4 (1977), pp. 1200–1206.

[38] Y Ishikawa et al. "Paramagnetic spin fluctuations in the weak itinerant-electron ferromagnet MnSi". In: *Physical Review B* 31.9 (1985), p. 5884.

[39] Masaaki Kontani, Tatsumi Hioki, and Yoshika Masuda. "NMR studies on magnetic properties of ZrZn2". In: *Journal of the Physical Society of Japan* 39.3 (1975), pp. 665–671.

[40] Ryou Nakabayashi, Shigeyuki Murayama, et al. "Itinerant electron weak ferromagnetism in Y2Ni7 and YNi3". In: *Journal of the Physical Society of Japan* 61.3 (1992), pp. 774–777.

[41] Hiroyuki Shiba and PA Pincus. "Thermodynamic properties of the one-dimensional half-filled-band Hubbard model". In: *Physical Review B* 5.5 (1972), p. 1966.

[42] Masayuki Shiga et al. "Giant Spin Fluctuations in $Y_{0.97}Sc_{0.03}Mn_2$". In: *Journal of the Physical Society of Japan* 57.9 (1988), pp. 3141–3145. DOI: 10.1143/JPSJ.57.3141. eprint: https://doi.org/10.1143/JPSJ.57.3141. URL: https://doi.org/10.1143/JPSJ.57.3141.

[43] M Shiga. "Magnetism and spin fluctuations of laves phase manganese compounds". In: *Physica B+ C* 149.1-3 (1988), pp. 293–305.

[44] T Shigeoka et al. "Magnetic properties of $LaMn_2Ge_2$ single crystal". In: *Journal of magnetism and magnetic materials* 53.1-2 (1985), pp. 83–86.

[45] Hiroshi Yasuoka et al. "NMR and susceptibility studies of MnSi above Tc". In: *Journal of the Physical Society of Japan* 44.3 (1978), pp. 842–849.

[46] Kazuyoshi Yoshimura et al. "NMR study of weakly itinerant ferromagnetic Y (Co1- xAlx) 2". In: *Journal of the Physical Society of Japan* 56.3 (1987), pp. 1138–1155.

[47] KRA Ziebeck et al. "Observation of spatial magnetic correlations in the paramagnetic phase of chromium using polarised neutrons and polarisation analysis". In: *Zeitschrift für Physik B Condensed Matter* 48.3 (1982), pp. 233–239.

[48] G G Lonzarich and L Taillefer. "Effect of spin fluctuations on the magnetic equation of state of ferromagnetic or nearly ferromagnetic metals". In: *Journal of Physics C: Solid State Physics* 18.22 (Aug. 1985), pp. 4339–4371. DOI: 10.1088/0022-3719/18/22/017. URL: https://doi.org/10.1088/0022-3719/18/22/017.

[49] JR Schrieffer. "Effect of virtual spin waves on the properties of strongly paramagnetic metals". In: *Journal of Applied Physics* 39.2 (1968), pp. 642–648.

[50] N Lundquist and Ho P Myers. "The saturation magnetisation of the monoborides of Mn, Fe and Co". In: *Arkiv for Fysik* 21.5 (1961), pp. 463–471.

[51] H. Wada et al. "Stability of Mn moments and spin fluctuations in RMn2 (R: Rare earth)". In: *Journal of Magnetism and Magnetic Materials* 70.1 (1987), pp. 134–136. ISSN: 0304-8853. DOI: https://doi.org/10.1016/0304-8853(87)90380-5. URL: https://www.sciencedirect.com/science/article/pii/0304885387903805.

[52] M. Shiga. "Magnetism and spin fluctuations of laves phase manganese compounds". In: *Physica B+C* 149.1 (1988), pp. 293–305. ISSN: 0378-4363. DOI: https://doi.org/10.1016/0378-4363(88)90256-2. URL: https://www.sciencedirect.com/science/article/pii/0378436388902562.

[53] Conyers Herring and Charles Kittel. "On the Theory of Spin Waves in Ferromagnetic Media". In: *Phys. Rev.* 81 (5 Mar. 1951), pp. 869–880. DOI: 10.1103/PhysRev.81.869. URL: https://link.aps.org/doi/10.1103/PhysRev.81.869.

[54] C Herring. *Magnetism, ed. GT Rado and H. Suhl.* 1966.

[55] Yoshinori Takahashi. "On the Origin of the Curie-Weiss Law of the Magnetic Susceptibility in Itinerant Electron Ferromagnetism". In: *Journal of the Physical Society of Japan* 55.10 (1986), pp. 3553–3573. DOI: 10.1143/JPSJ.55.3553. eprint: https://doi.org/10.1143/JPSJ.55.3553. URL: https://doi.org/10.1143/JPSJ.55.3553.

[56] Y Takahashi. "Quantum spin fluctuation theory of the magnetic equation of state of weak itinerant-electron ferromagnets". In: *Journal of Physics: Condensed Matter* 13.29 (July 2001), pp. 6323–6358. DOI: 10.1088/0953-8984/13/29/305. URL: https://doi.org/10.1088/0953-8984/13/29/305.

[57] Yoshinori Takahashi and Tôru Moriya. "On the Spin Fluctuations in Weak Itinerant Ferromagnets". In: *Journal of the Physical Society of Japan* 52.12 (1983), pp. 4342–4348. DOI: 10.1143/JPSJ.52.4342. eprint: https://doi.org/10.1143/JPSJ.52.4342. URL: https://doi.org/10.1143/JPSJ.52.4342.

[58] Tôru Moriya. "Ferro- and Antiferromagnetism of Transition Metals and Alloys". In: *Progress of Theoretical Physics* 33.2 (Feb. 1965), pp. 157–183. ISSN: 0033-068X. DOI: 10.1143/PTP.33.157. eprint: https://academic.oup.com/ptp/article-pdf/33/2/157/5293278/33-2-157.pdf. URL: https://doi.org/10.1143/PTP.33.157.

[59] Hideo Hasegawa and Toru Moriya. "Effect of Spin Fluctuations on Itinerant Electron Antiferromagnetism". In: *Journal of the Physical Society of Japan* 36.6 (1974), pp. 1542–1553. DOI: 10.1143/JPSJ.36.1542.

[60] Yoshinori Takahashi. "Theoretical Development in Itinerant Electron Ferromagnetism". In: *Journal of Physics: Conference Series* 868 (June 2017), p. 012002. DOI: 10.1088/1742-6596/868/1/012002. URL: https://doi.org/10.1088/1742-6596/868/1/012002.

[61] V. Yushankhai, P. Thalmeier, and T. Takimoto. "Self-consistent renormalization theory of spin fluctuations in paramagnetic spinel LiV_2O_4". In: *Phys. Rev. B* 77 (12 Mar. 2008), p. 125126. DOI: 10.1103/PhysRevB.77.125126. URL: https://link.aps.org/doi/10.1103/PhysRevB.77.125126.

[62] P Coleman et al. "How do Fermi liquids get heavy and die?". In: *Journal of Physics: Condensed Matter* 13.35 (Aug. 2001), R723–R738. DOI: 10.1088/0953-8984/13/35/202. URL: https://doi.org/10.1088/0953-8984/13/35/202.

[63] Philipp Gegenwart, Qimiao Si, and Frank Steglich. "Quantum criticality in heavy-fermion metals". In: *nature physics* 4.3 (2008), pp. 186–197.

[64] L. Steinke et al. "$CaMn_2Al_{10}$: Itinerant Mn magnetism on the verge of magnetic order". In: *Phys. Rev. B* 92 (2 July 2015), p. 020413. DOI: 10.1103/PhysRevB.92.020413. URL: https://link.aps.org/doi/10.1103/PhysRevB.92.020413.

[65] S Doniach and S Engelsberg. "Low-temperature properties of nearly ferromagnetic Fermi liquids". In: *Physical Review Letters* 17.14 (1966), p. 750.

[66] P Rhodes and Eo P Wohlfarth. "The effective Curie-Weiss constant of ferromagnetic metals and alloys". In: *Proceedings of the Royal Society of London. Series A. Mathematical and Physical Sciences* 273.1353 (1963), pp. 247–258.

[67] J. W. Simonson et al. "Magnetic and structural phase diagram of $CaMn_2Sb_2$". In: *Phys. Rev. B* 86 (18 Nov. 2012), p. 184430. DOI: 10.1103/PhysRevB.86.184430. URL: https://link.aps.org/doi/10.1103/PhysRevB.86.184430.

[68] D. E. McNally et al. "Origin of the charge gap in LaMnPO". In: *Phys. Rev. B* 90 (18 Nov. 2014), p. 180403. DOI: 10.1103/PhysRevB.90.180403. URL: https://link.aps.org/doi/10.1103/PhysRevB.90.180403.

[69] JW Simonson et al. "From antiferromagnetic insulator to correlated metal in pressurized and doped LaMnPO". In: *Proceedings of the National Academy of Sciences* 109.27 (2012), E1815–E1819.

[70] D. C. Johnston et al. "Magnetic exchange interactions in $BaMn_2As_2$: A case study of the J_1-J_2-J_c Heisenberg model". In: *Phys. Rev. B* 84 (9 Sept. 2011), p. 094445. DOI: 10.1103/PhysRevB.84.094445. URL: https://link.aps.org/doi/10.1103/PhysRevB.84.094445.

[71] E. E. Huber and D. H. Ridgley. "Magnetic Properties of a Single Crystal of Manganese Phosphide". In: *Phys. Rev.* 135 (4A Aug. 1964), A1033–A1040. DOI: 10.1103/PhysRev.135.A1033. URL: https://link.aps.org/doi/10.1103/PhysRev.135.A1033.

[72] R. R. Heikes. "Magnetic Transformation in MnBi". In: *Phys. Rev.* 99 (2 July 1955), pp. 446–447. DOI: 10.1103/PhysRev.99.446. URL: https://link.aps.org/doi/10.1103/PhysRev.99.446.

[73] K Ahlborn, K Bärner, and W Schröter. "Magnetic properties of alloys in the system MnSb–MnBi". In: *physica status solidi (a)* 30.1 (1975), pp. 251–261.

[74] Shigeru Okada et al. "Crystal growth and some properties of $REMn_2Si_2$ (RE=Er, Tm, Yb, Lu) compounds". In: *Journal of Crystal Growth* 244.3 (2002), pp. 267–273. ISSN: 0022-0248. DOI: https://doi.org/10.1016/S0022-0248(02)01689-5. URL: https://www.sciencedirect.com/science/article/pii/S0022024802016895.

[75] C. Marques et al. "$HfFeGa_2$ and $HfMnGa_2$: Transition-metal-based itinerant ferromagnets with low Curie temperatures". In: *Phys. Rev. B* 83 (18 May 2011), p. 184435. DOI: 10.1103/PhysRevB.83.184435. URL: https://link.aps.org/doi/10.1103/PhysRevB.83.184435.

[76] Abhishek Pandey et al. "Correlations and incipient antiferromagnetic order within the linear Mn chains of metallic Ti_4MnBi_2". In: *Phys. Rev. B* 102 (1 July 2020), p. 014406. DOI: 10.1103/PhysRevB.102.014406. URL: https://link.aps.org/doi/10.1103/PhysRevB.102.014406.

[77] Paolo Giannozzi et al. "QUANTUM ESPRESSO: a modular and open-source software project for quantum simulations of materials". In: *Journal of Physics: Condensed Matter* 21.39 (Sept. 2009), p. 395502. DOI: 10.1088/0953-8984/21/39/395502. URL: https://doi.org/10.1088/0953-8984/21/39/395502.

[78] S. L. Dudarev et al. "Electron-energy-loss spectra and the structural stability of nickel oxide: An LSDA+U study". In: *Phys. Rev. B* 57 (3 Jan. 1998), pp. 1505–1509. DOI: 10.1103/PhysRevB.57.1505. URL: https://link.aps.org/doi/10.1103/PhysRevB.57.1505.

[79] John P. Perdew, Kieron Burke, and Matthias Ernzerhof. "Generalized Gradient Approximation Made Simple". In: *Phys. Rev. Lett.* 77 (18 Oct. 1996), pp. 3865–3868. DOI: 10.1103/PhysRevLett.77.3865. URL: https://link.aps.org/doi/10.1103/PhysRevLett.77.3865.

[80] Qing-Miao Hu, Levente Vitos, and Rui Yang. "Theoretical investigation of the ω-related phases in TiAl – Nb/Mo alloys". In: *Phys. Rev. B* 90 (5 Aug. 2014), p. 054109. DOI: 10.1103/PhysRevB.90.054109. URL: https://link.aps.org/doi/10.1103/PhysRevB.90.054109.

[81] Alexei Kitaev. "Periodic table for topological insulators and superconductors". In: *AIP Conference Proceedings* 1134.1 (May 2009), pp. 22–30. ISSN: 0094-243X. DOI: 10.1063/1.3149495. eprint: https://pubs.aip.org/aip/acp/article-pdf/1134/1/22/11584243/22_1_online.pdf. URL: https://doi.org/10.1063/1.3149495.

[82] Elliott H. Lieb. "Two theorems on the Hubbard model". In: *Phys. Rev. Lett.* 62 (10 Mar. 1989), pp. 1201–1204. DOI: 10.1103/PhysRevLett.62.1201. URL: https://link.aps.org/doi/10.1103/PhysRevLett.62.1201.

[83] Allen Hatcher. *Algebraic topology*. Cambridge: Cambridge Univ. Press, 2000. URL: https://cds.cern.ch/record/478079.

[84] Yuval Gefen, Benoit B. Mandelbrot, and Amnon Aharony. "Critical Phenomena on Fractal Lattices". In: *Phys. Rev. Lett.* 45 (11 Sept. 1980), pp. 855–858. DOI: 10.1103/PhysRevLett.45.855. URL: https://link.aps.org/doi/10.1103/PhysRevLett.45.855.

[85] Lang-Tao Huang and Dung-Hai Lee. "Topological insulators on a Mobius strip". In: *Phys. Rev. B* 84 (19 Nov. 2011), p. 193106. DOI: 10.1103/PhysRevB.84.193106. URL: https://link.aps.org/doi/10.1103/PhysRevB.84.193106.

[86] Li Chen et al. "The impossibility of exactly flat non-trivial Chern bands in strictly local periodic tight binding models". In: *Journal of Physics A: Mathematical and Theoretical* 47.15 (Mar. 2014), p. 152001. DOI: 10.1088/1751-8113/47/15/152001. URL: https://dx.doi.org/10.1088/1751-8113/47/15/152001.

[87] Jun-Won Rhim and Bohm-Jung Yang. "Singular flat bands". In: *Advances in Physics: X* 6.1 (2021), p. 1901606. DOI: 10.1080/23746149.2021.1901606. eprint: https://doi.org/10.1080/23746149.2021.1901606. URL: https://doi.org/10.1080/23746149.2021.1901606.

[88] and and. "Exotic electronic states in the world of flat bands: From theory to material". In: *Chinese Physics B* 23.7 (May 2014), p. 077308. DOI: 10.1088/1674-1056/23/7/077308. URL: https://dx.doi.org/10.1088/1674-1056/23/7/077308.

[89] A Mielke. "Ferromagnetic ground states for the Hubbard model on line graphs". In: *Journal of Physics A: Mathematical and General* 24.2 (Jan. 1991), p. L73. DOI: 10.1088/0305-4470/24/2/005. URL: https://dx.doi.org/10.1088/0305-4470/24/2/005.

[90] Congjun Wu et al. "Flat Bands and Wigner Crystallization in the Honeycomb Optical Lattice". In: *Phys. Rev. Lett.* 99 (7 Aug. 2007), p. 070401. DOI: 10.1103/PhysRevLett.99.070401. URL: https://link.aps.org/doi/10.1103/PhysRevLett.99.070401.

[91] Si Min Chan, B. Grémaud, and G. G. Batrouni. "Designer flat bands: Topology and enhancement of superconductivity". In: *Phys. Rev. B* 106 (10 Sept. 2022), p. 104514. DOI: 10.1103/PhysRevB.106.104514. URL: https://link.aps.org/doi/10.1103/PhysRevB.106.104514.

[92] R. G. Dias and J. D. Gouveia. "Origami rules for the construction of localized eigenstates of the Hubbard model in decorated lattices". In: *Scientific Reports* 5.1 (Nov. 2015), p. 16852. ISSN: 2045-2322. DOI: 10.1038/srep16852. URL: https://doi.org/10.1038/srep16852.

[93] Mit H. Naik and Manish Jain. "Ultraflatbands and Shear Solitons in Moiré Patterns of Twisted Bilayer Transition Metal Dichalcogenides". In: *Phys. Rev. Lett.* 121 (26 Dec. 2018), p. 266401. DOI: 10.1103/PhysRevLett.121.266401. URL: https://link.aps.org/doi/10.1103/PhysRevLett.121.266401.

[94] Johannes Knebel, Philipp M. Geiger, and Erwin Frey. "Topological Phase Transition in Coupled Rock-Paper-Scissors Cycles". In: *Phys. Rev. Lett.* 125 (25 Dec. 2020), p. 258301. DOI: 10.1103/PhysRevLett.125.258301. URL: https://link.aps.org/doi/10.1103/PhysRevLett.125.258301.

[95] Narasimha Raju Chebrolu, Bheema Lingam Chittari, and Jeil Jung. "Flat bands in twisted double bilayer graphene". In: *Phys. Rev. B* 99 (23 June 2019), p. 235417. DOI: 10.1103/PhysRevB.99.235417. URL: https://link.aps.org/doi/10.1103/PhysRevB.99.235417.

[96] Thomas Bilitewski and Roderich Moessner. "Disordered flat bands on the kagome lattice". In: *Phys. Rev. B* 98 (23 Dec. 2018), p. 235109. DOI: 10.1103/PhysRevB.98.235109. URL: https://link.aps.org/doi/10.1103/PhysRevB.98.235109.

[97] Ville A. J. Pyykkönen, Sebastiano Peotta, and Päivi Törmä. "Suppression of Nonequilibrium Quasiparticle Transport in Flat-Band Superconductors". In: *Phys. Rev. Lett.* 130 (21 May 2023), p. 216003. DOI: 10.1103/PhysRevLett.130.216003. URL: https://link.aps.org/doi/10.1103/PhysRevLett.130.216003.

[98] Md Nurul Huda, Shawulienu Kezilebieke, and Peter Liljeroth. "Designer flat bands in quasi-one-dimensional atomic lattices". In: *Phys. Rev. Res.* 2 (4 Dec. 2020), p. 043426. DOI: 10.1103/PhysRevResearch.2.043426. URL: https://link.aps.org/doi/10.1103/PhysRevResearch.2.043426.

[99] Feng Liu and Katsunori Wakabayashi. "Novel Topological Phase with a Zero Berry Curvature". In: *Phys. Rev. Lett.* 118 (7 Feb. 2017), p. 076803. DOI: 10.1103/PhysRevLett.118.076803. URL: https://link.aps.org/doi/10.1103/PhysRevLett.118.076803.

[100] Wladimir A. Benalcazar, B. Andrei Bernevig, and Taylor L. Hughes. "Quantized electric multipole insulators". In: *Science* 357.6346 (2017), pp. 61–66. DOI: 10.1126/science.aah6442. eprint: https://www.science.org/doi/pdf/10.1126/science.aah6442. URL: https://www.science.org/doi/abs/10.1126/science.aah6442.

[101] Wladimir A. Benalcazar, B. Andrei Bernevig, and Taylor L. Hughes. "Electric multipole moments, topological multipole moment pumping, and chiral hinge states in crystalline insulators". In: *Phys. Rev. B* 96 (24 Dec. 2017), p. 245115. DOI: 10.1103/PhysRevB.96.245115. URL: https://link.aps.org/doi/10.1103/PhysRevB.96.245115.

[102] V. M. Martinez Alvarez and M. D. Coutinho-Filho. "Edge states in trimer lattices". In: *Phys. Rev. A* 99 (1 Jan. 2019), p. 013833. DOI: 10.1103/PhysRevA.99.013833. URL: https://link.aps.org/doi/10.1103/PhysRevA.99.013833.

[103] Yiqi Zhang et al. "Topological states in the super-SSH model". In: *Opt. Express* 29.26 (Dec. 2021), pp. 42827–42836. DOI: 10.1364/OE.445301. URL: https://opg.optica.org/oe/abstract.cfm?URI=oe-29-26-42827.

[104] Chen-Shen Lee, Iao-Fai Io, and Hsien-chung Kao. "Winding number and Zak phase in multi-band SSH models". In: *Chinese Journal of Physics* 78 (2022), pp. 96–110. ISSN: 0577-9073. DOI: https://doi.org/10.1016/j.cjph.2022.05.007. URL: https://www.sciencedirect.com/science/article/pii/S0577907322001381.

[105] Juan Zurita, Charles Creffield, and Gloria Platero. "Tunable zero modes and quantum interferences in flat-band topological insulators". In: *Quantum* 5 (Nov. 2021), p. 591. ISSN: 2521-327X. DOI: 10.22331/q-2021-11-25-591. URL: https://doi.org/10.22331/q-2021-11-25-591.

[106] Shao-Liang Zhang and Qi Zhou. "Two-leg Su-Schrieffer-Heeger chain with glide reflection symmetry". In: *Phys. Rev. A* 95 (6 June 2017), p. 061601. DOI: 10.1103/PhysRevA.95.061601. URL: https://link.aps.org/doi/10.1103/PhysRevA.95.061601.

[107] Beatriz Pérez-González et al. "Interplay between long-range hopping and disorder in topological systems". In: *Phys. Rev. B* 99 (3 Jan. 2019), p. 035146. DOI: 10.1103/PhysRevB.99.035146. URL: https://link.aps.org/doi/10.1103/PhysRevB.99.035146.

[108] Chao Li and Andrey E. Miroshnichenko. "Extended SSH Model: Non-Local Couplings and Non-Monotonous Edge States". In: *Physics* 1.1 (2019), pp. 2–16. ISSN: 2624-8174. DOI: 10.3390/physics1010002. URL: https://www.mdpi.com/2624-8174/1/1/2.

[109] Chuanhao Yin et al. "Geometrical meaning of winding number and its characterization of topological phases in one-dimensional chiral non-Hermitian systems". In: *Phys. Rev. A* 97 (5 May 2018), p. 052115. DOI: 10.1103/PhysRevA.97.052115. URL: https://link.aps.org/doi/10.1103/PhysRevA.97.052115.

[110] O.V. Ogloblya, H.M. Kuznietsova, and Y.M. Strzhemechny. "Effects of coulomb repulsion on conductivity of heterojunction carbon nanotube quantum dots with spin-orbital coupling and interacting leads". In: *Physica B: Condensed Matter* 504 (2017), pp. 96–102. ISSN: 0921-4526. DOI: https://doi.org/10.1016/j.physb.2016.10.018. URL: https://www.sciencedirect.com/science/article/pii/S0921452616304793.

[111] O.V. Ogloblya et al. "Linear polarizability of carbon nanotubes bonded to maleimide derivative and fluorescent probe Nile red". In: *Computational Materials Science* 46.1 (2009), pp. 112–114. ISSN: 0927-0256. DOI: https://doi.org/10.1016/j.commatsci.2009.02.010. URL: https://www.sciencedirect.com/science/article/pii/S0927025609000676.

[112] Bo Xing et al. "Attractive Su-Schrieffer-Heeger-Hubbard model on a square lattice away from half-filling". In: *Phys. Rev. B* 108 (16 Oct. 2023), p. L161103. DOI: 10.1103/PhysRevB.108.L161103. URL: https://link.aps.org/doi/10.1103/PhysRevB.108.L161103.

[113] C. A. Downing and A. J. Toghill. "Quantum topology in the ultrastrong coupling regime". In: *Scientific Reports* 12.1 (July 2022), p. 11630. ISSN: 2045-2322. DOI: 10.1038/s41598-022-15735-0. URL: https://doi.org/10.1038/s41598-022-15735-0.

[114] M. Kiczynski et al. "Engineering topological states in atom-based semiconductor quantum dots". In: *Nature* 606.7915 (June 2022), pp. 694–699. ISSN: 1476-4687. DOI: 10.1038/s41586-022-04706-0. URL: https://doi.org/10.1038/s41586-022-04706-0.

[115] P. W. Anderson. "Absence of Diffusion in Certain Random Lattices". In: *Phys. Rev.* 109 (5 Mar. 1958), pp. 1492–1505. DOI: 10.1103/PhysRev.109.1492. URL: https://link.aps.org/doi/10.1103/PhysRev.109.1492.

[116] Muralidhar Aaina et al. "Risk Factors and Treatment Outcome Analysis Associated with Second-Line Drug-Resistant Tuberculosis". In: *Journal of Respiration* 2.1 (2022), pp. 1–12. ISSN: 2673-527X. DOI: 10.3390/jor2010001. URL: https://www.mdpi.com/2673-527X/2/1/1.

[117] Muralidhar Aaina et al. "Risk Factors and Treatment Outcome Analysis Associated with Second-Line Drug-Resistant Tuberculosis". In: *Journal of Respiration* 2.1 (2022), pp. 1–12. ISSN: 2673-527X. DOI: 10.3390/jor2010001. URL: https://www.mdpi.com/2673-527X/2/1/1.

[118] Usharani Brammachary et al. “Mechanisms and Action of Drug Resistance on Mycobacterium tuberculosis”. In: (2022). Ed. by Dr. Ghulam Mustafa and Prof. Shailendra K. Saxena. DOI: 10.5772/intechopen.108943. URL: https://doi.org/10.5772/intechopen.108943.

[119] Venkateswari Ramachandra et al. “Assess the Diagnostic Accuracy of GeneXpert to Detect Mycobacterium tuberculosis and Rifampicin-Resistant Tuberculosis among Presumptive Tuberculosis and Presumptive Drug Resistant Tuberculosis Patients”. In: *Microbiology Research* 15.1 (2024), pp. 91–108. ISSN: 2036-7481. DOI: 10.3390/microbiolres15010006. URL: https://www.mdpi.com/2036-7481/15/1/6.

[120] J. C. Woicik et al. “Hybridization and Bond-Orbital Components in Site-Specific X-Ray Photoelectron Spectra of Rutile $\mathbf{TiO_2}$”. In: *Phys. Rev. Lett.* 89 (7 July 2002), p. 077401. DOI: 10.1103/PhysRevLett.89.077401. URL: https://link.aps.org/doi/10.1103/PhysRevLett.89.077401.

yato vāco nivartante | aprāpya manasā saha |
ānandaṃ brahmaṇo vidvān | na bibheti kutaścaneti ||
taittirīya upaniṣad

"He who knows the bliss of Brahman, whence (all) words recede,
as well as mind, without reaching, he is not afraid of any one whatsoever."